ABSTRACT

Title of dissertation: HIGH ELASTIC MODULUS NANOPOWDER REINFORCED RESIN COMPOSITES FOR DENTAL APPLICATIONS

Yijun Wang, Doctor of Philosophy, 2007

Dissertation directed by: Associate Professor Isabel K. Lloyd

Department of Material Science and Engineering

Dental restorations account for more than $3 billion dollars a year on the market. Among them, all-ceramic dental crowns draw more and more attention and their popularity has risen because of their superior aesthetics and biocompatibility. However, their relatively high failure rate and labor-intensive fabrication procedure still limit their application.

In this thesis, a new family of high elastic modulus nanopowder reinforced resin composites and their mechanical properties are studied. Materials with higher elastic modulus, such as alumina and diamond, are used to replace the routine filler material,

silica, in dental resin composites to achieve the desired properties. This class of composites is developed to serve (1) as a high stiffness support to all-ceramic crowns and (2) as a means of joining independently fabricated crown core and veneer layers. Most of the work focuses on nano-sized Al_2O_3 (average particle size 47 nm) reinforcement in a polymeric matrix with 50:50 Bisphenol A glycidyl methacrylate (Bis-GMA): triethylene glycol dimethacrylate (TEGDMA) monomers. Surfactants, silanizing agents and primers are examined to obtain higher filler levels and enhance the bonding between filler and matrix. Silane agents work best. The elastic modulus of a 57.5 vol% alumina/resin composite is 31.5 GPa compared to current commercial resin composites with elastic modulus <15 GPa. Chemical additives can also effectively raise the hardness to as much as 1.34 GPa. Besides alumina, diamond/resin composites are studied. An elastic modulus of about 45 GPa is obtained for a 57 vol% diamond/resin composite. Our results indicate that with a generally monodispersed nano-sized high modulus filler, relatively high elastic modulus resin-based composite cements are possible. Time-dependent behavior of our resin composites is also investigated. This is valuable for understanding the behavior of our material and possible fatigue testing in the future. Our results indicate that with effective coupling agents and higher filler loading, viscous flow can be greatly decreased due to the attenuation of mobility of polymer chains. Complementary studies indicate that our resin composites are promising for the proposed applications as a stiff support to all-ceramic crowns.

HIGH ELASTIC MODULUS NANOPOWDER REINFORCED RESIN COMPOSITES FOR DENTAL APPLICATIONS

by

Yijun Wang

Dissertation submitted to the Faculty of the Graduate School of the
University of Maryland, College Park in partial fulfillment
of the requirements for the degree of
Doctor of Philosophy
2007

Advisory Committee:

Associate Professor Isabel K. Lloyd, Chair/Advisor
Professor Van P. Thompson
Assistant Professor Srinivasa R. Raghavan
Associate Professor Luz Martinez-Miranda
Professor Sandra C. Greer

DEDICATION

To my father Xinmin Wang, my mother Qinque Gao, and my wife Ying Tang

ACKNOWLEDGEMENTS

I would first sincerely thank Professor Isabel Lloyd for giving me the chance to work in an area I really like. As my advisor, she has been a source of direction and encouragement. Besides research study, her mother-like care is my best support for the campus life.

I would like to specially acknowledge Dr. Brian Lawn and his group, Dr. Yu Zhang, Dr. Yan Deng, Dr. Sanjit Bhowmick and Dr. Yeon-Gil Jung at the National Institute of Standards and Technology (NIST) for their helpful discussions and use of their equipment.

I also like to thank my colleague, James Lee, for all the cooperation, discussion, help and friendship throughout my whole graduate study. Special thanks to Patrick Stahl for his wonderful work concerning measurement of degree of conversion. I would like to thank Mey Saied for her help in resolving some lab issues as well.

My sincere gratitude goes to Dr. Robert Cook at NIST for his tremendous support by providing the use of nanoindentation machine. I hereby would like to thank him for his precious time out of his tight schedule to discuss and instruct me. My appreciation goes to Ms. Lin-Sien Lum for instructing me to operate the machine and perform calibration.

There are so many people to whom I am indebted for their support and encouragement. Prof. Otto Wilson, at the Catholic University of America has been very

kind in teaching me organic chemistry. The helpful discussion concerning polymer chemistry with Prof. Srinivasa Raghavan and his graduates, Bani Cipriano and Shih-Huang Tung at Department of Chemical and Biomolecular Engineering at University of Maryland, College Park, was highly appreciated. Prof. Marc Rosenblum at University of Medicine and Dentistry of New Jersey helped me to initialize my experiments. Prof. Wole Soboyejo and Dr. Zong Zong at Princeton University assisted me with indentation experiments.

Financial support from NIDCR grant (P01 DE10976) is gratefully acknowledged. The principal investigators, Drs. Dianne Rekow and Van Thompson at New York University are very supportive and always bring fresh ideas to the discussion table.

I would also like to thank ESSTECH for donating BisGMA and Degussa for donating the silica powder OX-50 for these initial materials studies.

Finally, I am deeply grateful to my parents for giving me life-long education and supporting me with their encouragement and optimism. I also like to thank my uncle who helped me build the first interest of doing scientific research. The support from my wife, Ying Tang is always the most precious.

TABLE OF CONTENTS

LIST OF TALBLES

LIST OF FIGURES

CHAPTER 1 INTRODUCTION

Dental caries, also described as tooth decay, is a common chronic disease that causes pain, tooth loss, infection, disability, and even death across all age groups throughout the world. Once decay occurs, various treatments are needed to restore tooth structure and function depending on the extent of tooth destruction, i.e. dental fillings and dental crowns. Various materials serve as dental restorations including dental amalgam, resin composites, porcelain, and gold etc. In dentistry, resin composites consisting of inorganic fillers, such as radiopaque glass, quartz, or ceramic particles, and an organic resin matrix based on a mixture of dimethacrylates, are frequently used as filling materials when the aesthetics of restoration are a concern. However, they are not as strong as dental amalgam and gold, limiting their application in posterior areas. Dental crowns, often made of gold, porcelain, or porcelain fused to metal, are needed when the dental caries are too extensive. Nowadays, ceramics are replacing metals as materials for dental crowns. All-ceramic crowns, made from layered structure of porcelain veneer fused to a ceramic core, have become a compelling choice because of their superior aesthetics and biocompatibility. However, they have a higher failure rate based on experience in clinical trials. In addition, the fabrication of an all-ceramic crown is complicated by the different firing temperatures for core and veneer and the need to match their coefficients of thermal expansion (CTE) of porcelain and ceramics. In addition, their fabrication is very labor intensive. An alternative method is raised in our

project to optimize the fabrication of all-ceramic crowns by strongly adhering the porcelain veneer onto the ceramic core with resin composites at ambient temperatures instead of fusing them in an oven, to avoid the need to fire veneers on the core and match the CTEs. To adapt resin composites to this application, strict demands in structural aspects and in mechanical properties, especially high elastic modulus, *E*, mean that current dental resin composites are not qualified. Thus, a new class of resin composites is needed.

The main propose of this thesis is to develop a new resin composite with much higher elastic modulus, hardness and resistance to fatigue. However, the mechanical properties of the composite also need to be tested under appropriate conditions, especially with respect to sample size and configuration. From a materials perspective, in order to achieve higher elastic modulus in composites, either a resin matrix with higher *E*, or a filler with higher *E*, or both have to be employed. Because the composites are used in the human mouth, a standard, FDA approved dental resin system is used in our work and just various filler materials with much higher *E* are examined. Because our resin composites have to serve in a very small structures where the composite cross-section is expected to vary from about 5~100 μm, nano-sized alumina and sub-micro-sized diamond are explored to provide uniform properties across the thin composite region. The use of nano-sized alumina and sub-micro-sized diamond as filler materials in dental resin composites is novel.

The organization of this thesis is as follows. Chapter 2 presents a general background for biomaterials and polymer composites. Then, background for dental crowns will be introduced and requirements of the new resin composites will be discussed based on the analysis of layer structure of simplified flat model of dental crown. In chapter 3, the materials selection, preparation, fabrication and testing methods are described. A special mixing apparatus developed in the lab to deal with the high viscosity of highly loaded nano-filled composite pastes and the surface treatments necessary to incorporate them into a viscous matrix are included. The protocols and testing procedures for the nanoindentation studies used to test mechanical properties in very small samples are also described in this chapter.

In chapter 4, the microstructures and mechanical properties of our resin composites are discussed. The effect of filler loading and additives on the degree of conversion is investigated by FT-IR. The relationship between mechanical properties, i.e. elastic modulus, E, and hardness, H, and microstructures, i.e. filler type, filler loading, filler size and additives is explored thoroughly by nanoindentation. In addition, several models for modulus prediction are applied to our resin composites. Because of the high modulus mismatch of filler and matrix in our composites, the effectiveness of the models is investigated. Time dependent behaviors using nanoindentation of the resin composites are explored in chapter 5. By analyzing the load-displacement behaviors subject to a triangular loading-unloading cycle under different time scales, the elastic, plastic and viscous deformations are presented quantitatively. The effect of filler

loading and additives on viscous flow of the composites and mechanisms are also discussed. In addition, the application of a model used to predict the load-displacement behavior in terms of time scales of instrumented indentation is presented. Chapter 6 is a summary of our results and conclusions and Chapter 7 proposes future work.

CHAPTER 2 BACKGROUND AND LITERATURE REVIEW

2.1 Biomaterials and Dental Restorations

2.1.1 Biomaterials

Biomaterials are natural or synthetic materials that are used to supplement or replace the entity or function of any living tissues and organs of the human body. The utilization of such materials to reconstruct missing or defective parts of the body can be traced back to ancient times. Artificial organs such as eyes, teeth and noses were found on Egyptian mummies [1, 2]. Before human beings could make synthetic materials, natural materials were used to serve as biomaterials. Nowadays, biological artificial materials are widely implemented to improve the quality of life for patients in many ways. Biomaterials are rarely used on their own but are more commonly integrated into devices or implants. With the development of synthetic materials and surgical techniques, more and more types of implants such as heart valves, joint replacements, ligaments, and dental crowns are widely used to restore degenerated organs or tissue. The market for biomaterials was estimated to be around $12 billion per year in 1995 and growing at 7~12% annually [2]. Dental restorations account for a large portion of the biomedical materials on the market, about $1 billion of revenues for dental implants each year with a growth rate of 18 percent per year and $2 billion for dental crowns [3].

In the early days, besides natural materials such as wood and stone, manufactured materials such as metal or glass were used as biomaterials as well [4]. The host response was examined by trial and error. Some of materials were rejected by the body, whereas some were accepted by the body. Those materials accepted by the body were termed biomaterials. The term, "biocompatibility,' is used to indicate the acceptance of biomaterials by the body. According to Williams' definition, biocompatibility is the ability of a material to perform with an appropriate host response in a specific application [4]. In other words, it consists of two parts: surface and structural compatibility of an implant [5]. Surface biocompatibility indicates the ability of materials to be compatible with host tissues chemically and biologically. For instance, implants having toxic or injurious effects on biological systems are not biocompatible. Being structurally biocompatible means the mechanical behavior of implants has been adapted to that of host tissue. Generally, it refers to the mechanical properties of the implant materials, i.e. elastic modulus, E, hardness, H, strength and so forth. Therefore, the implants can support the activity of the body. All in all, only when these two requirements are met, can implant materials be called "biocompatible."

Biomaterials can be cataloged into metals, ceramics, polymers. and composites (any combination of them). A large number of materials are widely used as biomaterials for different applications. Metals have great mechanical properties. However, the low biocompatibility and corrosion really hold back their application. Ceramics are great choice for prostheses because of their biocompatibility and aesthetics but the brittleness

and low fracture strength and toughness largely limit their applications as well. Composites can combine the advantages of various materials. For instant, a large number of polymer composites are able to serve as biomaterials in various applications by changing the composition and adding additives [2]. The shortcomings of polymer composites include that they are too weak to meet the mechanical demands under some circumstances, that there can occur swelling and leaching of some undesired products such as plasticizer, filler, and monomers.

Tissues are of two categories: soft tissues including skin, blood vessels, cartilage and ligaments, and hard tissues including bone and tooth. For hard tissues, polymer composite materials can generally be used in dental restorations, bone fracture repair, and joint replacements. For soft tissues, polymer composites have applications in bulk space fillers, encapsulants and carriers and other functional load-carrying and supporting implants, such as tendons and ligaments. The major applications of polymer composites are shown in the Fig. 2.1 [2, 6].

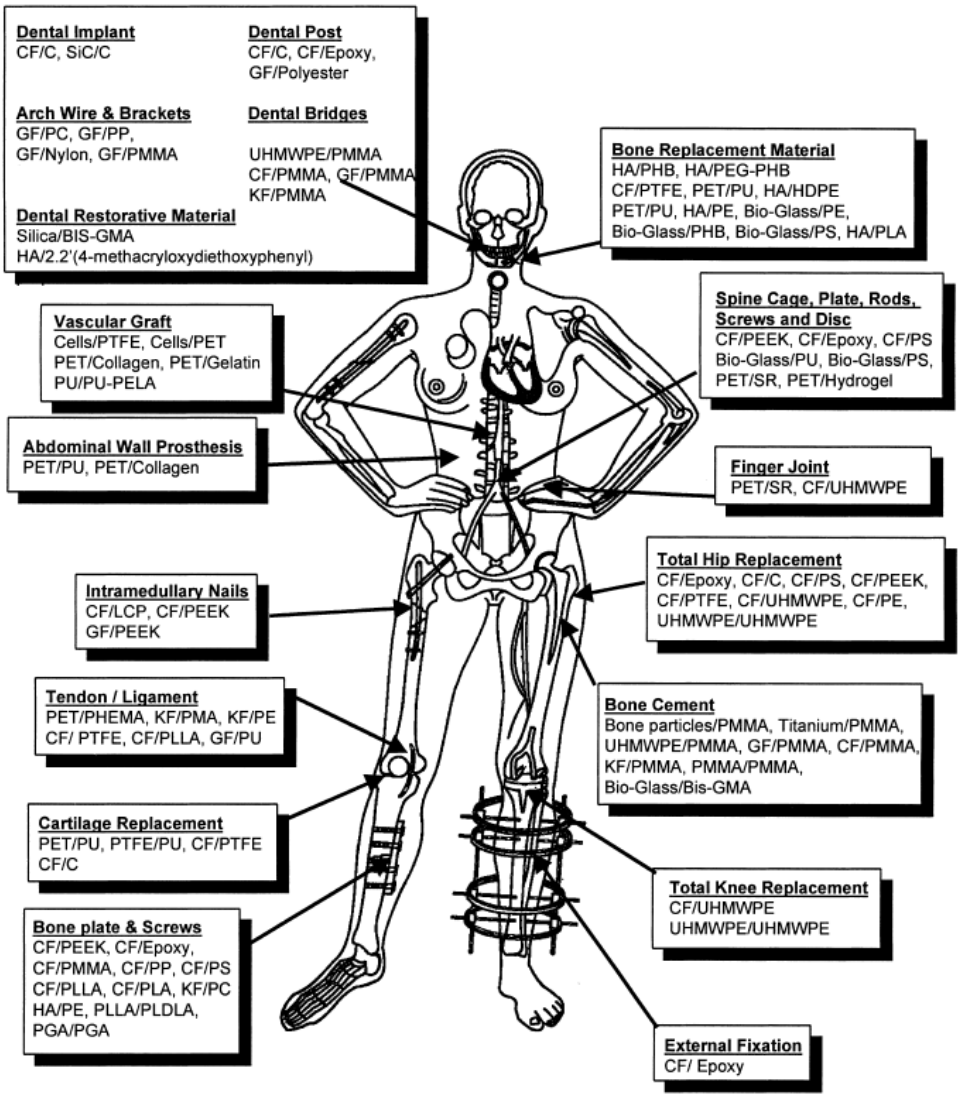

Figure 2.1 Various applications of different polymer composite biomaterials [2].

2.1.2 Tooth and dental restorations

A section of tooth structure is shown in Fig. 2.2 (a). An individual tooth consists of an exposed crown and a root, buried in the gum and jaw. The crown is usually at least partly covered by an outer layer of a hard and aesthetic substance called enamel. Beneath the enamel is an intermediate layer of material called dentine. Dentin surrounds an inner pulp cavity filled with pulp (a living, vascular and well innervated tissue). Blood vessels and nerves reach the pulp cavity through a channel, the root canal, which penetrates the root. An additional layer of bony material, cementum, usually surrounds the root. The dentin structure is shielded by enamel and sometimes exposed to the surface if the enamel is missing or worn away, as shown in Fig. 2.2 (b). Thus, the enamel not only provides the tooth with the function of chewing and biting, but protects the soft, organic tissue beneath it. Enamel has a very high mineral (97%) and low organic (1%) content. Its mechanical properties have been investigated by nanoindentation [7]. Fig. 2.3 shows the result of nanoindentation to map out the properties of dental enamel over the axial cross-section of a maxillary second molar by hardness, H, and elastic modulus, E, from cross sections. The average values of E and H decrease from the enamel surface to the enamel-dentin junction, as illustrated by the color changes: H decreases from 4.6 to 3.4 GPa and E from 91.1 to 66.2 GPa. The gradual change of mechanical properties in teeth provides a cushion function to distribute the stress and decrease the impact from biting and chewing.

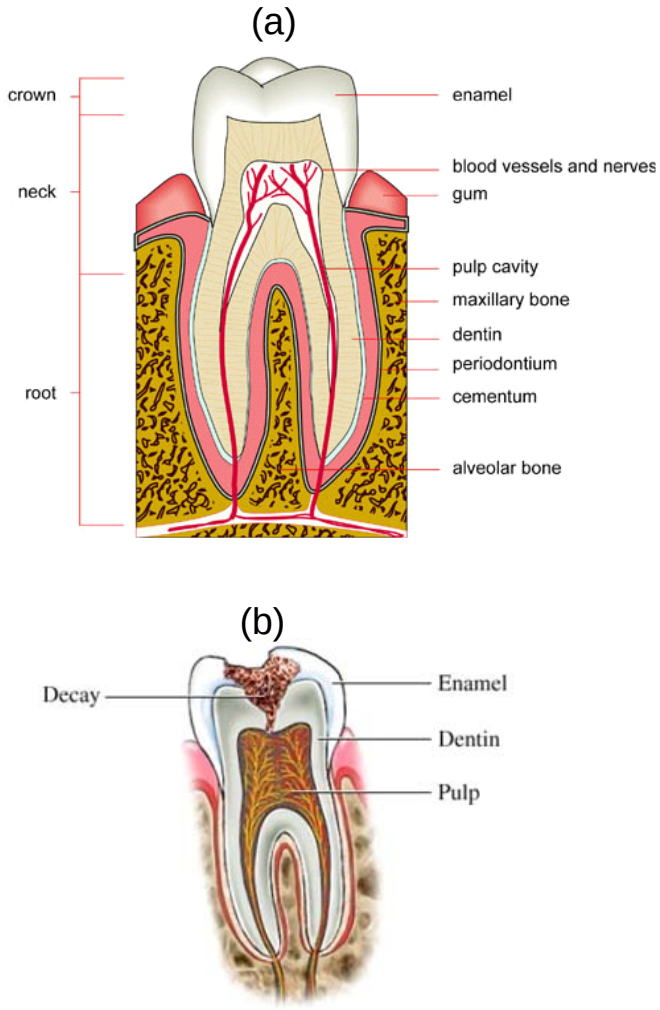

Figure 2.2 (a) Tooth, section of molar (http://www.infovisual.info); (b) tooth decay (http://www.nucleusinc.com).

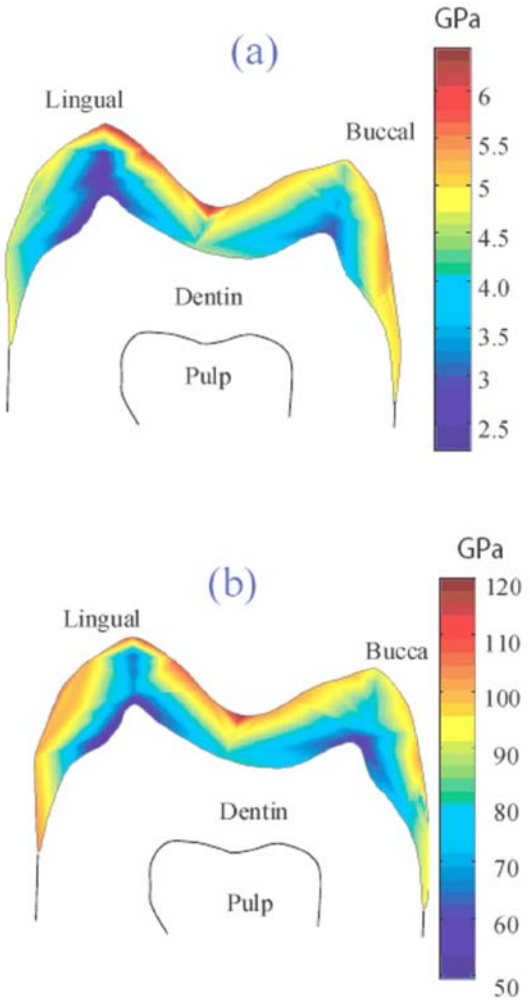

Figure 2.3 Nanoindentation mapping of (a) hardness and (b) elastic modulus in natural teeth [7].

A dental restoration is a material that has been placed in or onto a tooth to restore function and shape when tooth structure has been lost due to decay or fracture (generally because of extensive caries which weaken the cusps or external trauma), or to improve the esthetics of the tooth. Amalgam, gypsum, gold, ceramics, resin composites and glass ionomer cement are commonly used for restoring decayed teeth [8].

If the enamel and dentin have been invaded by acid-producing bacteria or damaged for other reasons, the decayed hard tissue has to be removed. The resulting cavities must be filled in order to restore structural integrity and mechanical solidity of the tooth. The filling materials could be amalgam, resin composites, glass ionomer or gold. Amalgam is an alloy that contains mercury. In dentistry, amalgam refers to a specific result of mixing a silver-based alloy, in the form of small particles, with mercury into a paste which then sets hard [8]. Amalgam and gold are mainly used in the restoration of the posterior teeth, and not preferred for anterior teeth for cosmetic reasons. Presently, dental resin composite is a common type of filling material. It is a mixture of ceramic powder including quartz, barium glass, and colloidal silica as fillers, and a resin such as Bisphenol A glycidyl methacrylate (Bis-GMA) as the polymer matrix [9-12]. One of the advantages of resin composites is that their refractive index can match the appearance of the natural tooth. So they are commonly used to restore posterior teeth as well as anterior teeth. Moreover, the preparation of composite fillings requires less removal of tooth structure to achieve adequate strength than amalgam. Glass ionomer cement is another type of dental material used as dental filling. Its advantages include

minimal shrinkage, microleakage, and release of fluoride, but it is not as strong and aesthetic as resin composites.

2.2 Dental Resin Composites

Generally, composite materials are engineered materials made from two or more constituent materials with different physical or chemical properties that remain separate and distinct within the finished structure. The matrix and reinforcement are the major constituent materials in composites. Commonly, the polymers function as matrix materials, which enclose and bond the reinforcement materials. In this section, the general polymer-based ceramic-reinforced composites will be introduced and then the dental resin composites will be specified in detail.

2.2.1 Polymer-based ceramic-reinforced composites

Composite materials are widely used commercial materials with applications in autos, aircraft, electrical insulators, biomaterials, and so forth [13, 14]. Polymer systems have desirable properties, most notably their ability to be adhesive and easily formed into complex shapes. However, pure resin systems have limited use for the manufacture on their own due to their poor mechanical properties. Some materials, like glass or ceramics, have significantly higher mechanical properties, such as stiffness and strength. But the shortcomings of being brittle and lacking toughness impede their usage when subject to cyclic loading. By combining these two types of materials together, the resin

systems are significantly reinforced mechanically. Moreover, the fillers can also improve the properties of resin systems in other aspects: such as electronic, optical or thermal properties [13-18]. Overall, the properties of the composite are determined by:

i. The properties of the fillers and the resin;
ii. The ratio of fillers to resin in the composite (filler volume fraction);
iii. The geometry, dimensions, and orientation of the filler (non equi-axed fillers);
iv. The interface between fillers and matrices.

Different types of polymers are used depending on the application and working environment. The requirements for polymers include good mechanical properties, especially toughness, and good resistance to environmental degradation. The most common polymers include polyamide, polypropylene, polyethylene, epoxy, rubber, and so forth. The properties of fillers are key factors in determining the properties of the polymer composites. Fibers are one of the most widely used fillers. Fiber-reinforced-composites have their applications in cases where large tensile strength is needed. The polymer matrix spreads the load applied to the composites to each fiber, which not only protects fibers from damage but also makes the composites undergo large tensile load without breaking. By adding equi-axed fillers, the composites increase the yield stress, the tensile strength, and the Young's modulus compared to pure polymer [19]. A volume faction of only 0.04 mica-type silicates in epoxy increases the modulus below

the glass transition temperature by 58 % and the modulus in the rubbery region by 450 % compared to unfilled epoxy [20].

2.2.2 Dental resin composites

Dental resin composites are a class of polymer composites with specifications related to the oral environment, i.e. biocompatibility, resistance to water and substances in mouth, and excellent mechanical properties and fatigue resistance. They consist of three materials, monomer systems consisting of monomers and other chemicals that assist reaction, fillers, and coupling agents that help dispersion of fillers and establish chemical bonds between fillers and matrix.

Dental resin monomers

Methylmethacrylate was introduced to dentistry during the 1930s [8]. When it could be cured by light, it was possible to apply it directly into an oral cavity for restoration. However, its application was limited by the tremendous shrinkage of monomers during curing, which is as much as 7% linearly [8]. By using prepolymerized methylmethacrylate beads mixed with monomer, the shrinkage was reduced down to around 3.5% linearly, which is, however, still beyond the tolerance for a reliable dental material. The excessive shrinkage creates contraction stresses in the dental resin and internal stress and deformation in the surrounding tooth structure. Bowen, therefore, produced a dimethacrylate that is called Bis-GMA or “Bowen’s resin”

[21]. The chemical structure of methylmethacrylate and Bis-GMA are shown in Fig. 2.4 (a) and (b), respectively. The advantage of Bis-GMA is its smaller polymerization shrinkage. The stiff central backbone structure and the pendant OH groups make this monomer quite viscous. In order to decrease the viscosity and improve the workability, low viscosity liquids such as triethylene glycol dimethacrylate (TEGDMA) are used to lower the viscosity (chemical structure in Fig 2.4 (c)).

In our research, a Bis-GMA and TEGDMA mixture is used as the resin system. Various ratios of these two are investigated to reveal the effect of the monomers on the mechanical properties of resin composites. With higher ratio of Bis-GMA, the resin system would be stiffer, resulting in a slightly higher elastic modulus of resin composites after curing. Moreover, the advantage with increased viscosity is that the paste retains its shape better and that filler particles do not sediment as fast as in a less viscous liquid. However, the resultant higher viscosity makes the monomer less workable, i.e. more difficult to incorporate filler particles into the monomer and work it in the mouth. With higher ratio of TEGDMA, the viscosity is reduced and it is easier to add particles into the resin. However, the cured resin is not as stiff as one with less TEGDMA due to its intrinsically weaker chemical structure. More importantly, low molecular weight monomers show higher polymerization shrinkage than high molecular weight monomers. Therefore, adding too much TEGDMA might increase the polymerization shrinkage, which in turn causes the formation of margin gaps in the restoration. Here a margin gap is formed due to the loss of adhesion between restoration and remaining tooth structure.

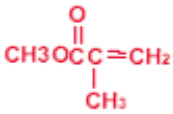

(a)

(b)

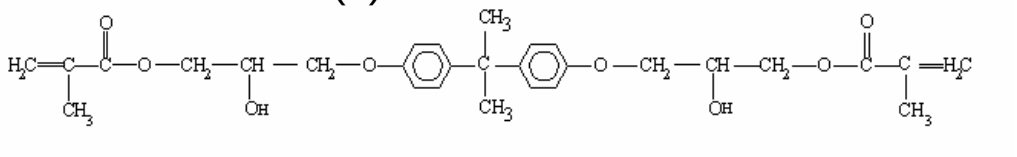

(c)

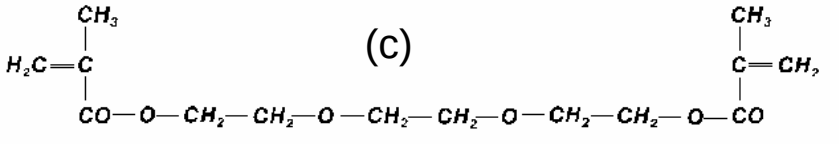

Figure 2.4 Chemical structures of (a) methylmethacrylate, (b) Bis-GMA, and (c) TEGDMA [8].

Filler materials used in dentistry

Reduction of the polymerization shrinkage is always a problem in using resins as dental materials, since shrinkage compromises the adhesion of the restorative composite to the tooth structure. An alternative means is to add filler materials into the resin. Since the ceramic particles have no shrinkage at all, the shrinkage of the resin composites can be considerably reduced depending on the volume fraction of fillers. The properties of composite restoratives are greatly influenced by incorporating filler in terms of elastic modulus, hardness, toughness, wear resistance, and thermal coefficient of expansion. Usually, by employing a larger volume fraction of fillers, dental composites become stiffer and stronger. However, adding too much filler can cause: (1) higher viscosity; (2) lower polymerization degree; (3) low toughness. Thus, there is a compromise between the filler loading and desired properties of the resin composites.

Since the monomer systems do not change much from case to case, composite restoratives have been commonly classified according to the types of filler added [22]. Macrofillers are larger ground quartz or glass particles. The filler particles that were used in the first dental composites had diameters ranging from 20-40 μm and consisted most often of quartz [8]. Due to its high hardness, it is difficult to grind it into fine particles.

Those macrofilled composites are now used less frequently because of aesthetic concerns and the difficulty of achieving smooth surface. Recent composites contain ground particles that are in the one-micron particle size range or even smaller, such as

pyrogenic silica. Pyrogenic silica is made by burning $SiCl_4$, H_2 and O_2. During the reaction that occurs in the flame, HCl is formed as well as SiO_2. The SiO_2 is in small equi-axed particles with diameter of 30~40 nm. One gram of this filler has an enormous surface area, about 50 m^2/g. Some other particles are formed by sol-gel process [8]. These particles are mostly of equi-axed shape with an average size of 5~100 nm. In this thesis, the particles below 100 nm are termed as "nanofiller." Pyrogenic or fumed silica fillers are routinely used as filler materials in dental resin composites. Because it is difficult to achieve high filler fraction using nanofiller alone (due to excessive large surface area), hybrid composites are usually employed, which contain a mixture of microfiller (about 1 μm diameter) and nanofiller. Such composites provide the relatively smooth surface and better mechanical properties, due to the higher filler loading achieved [23].

One of the most important issues brought up by fine particles is the very large surface area, causing a very strong thickening effect. In other words, the viscosity of paste of such composites is much higher than that of those filled with larger particles at the same filling level, as shown in Fig. 2.5 [8]. To make the paste workable for dentists, the volume fraction of filler has to be lower. However, it can be expected that the elastic modulus and strength would be reduced and the shrinkage would be increased, raising the failure rate or making it unsuitable for posterior restorations. In addition, we can expect that there would be more agglomeration between fine particles.

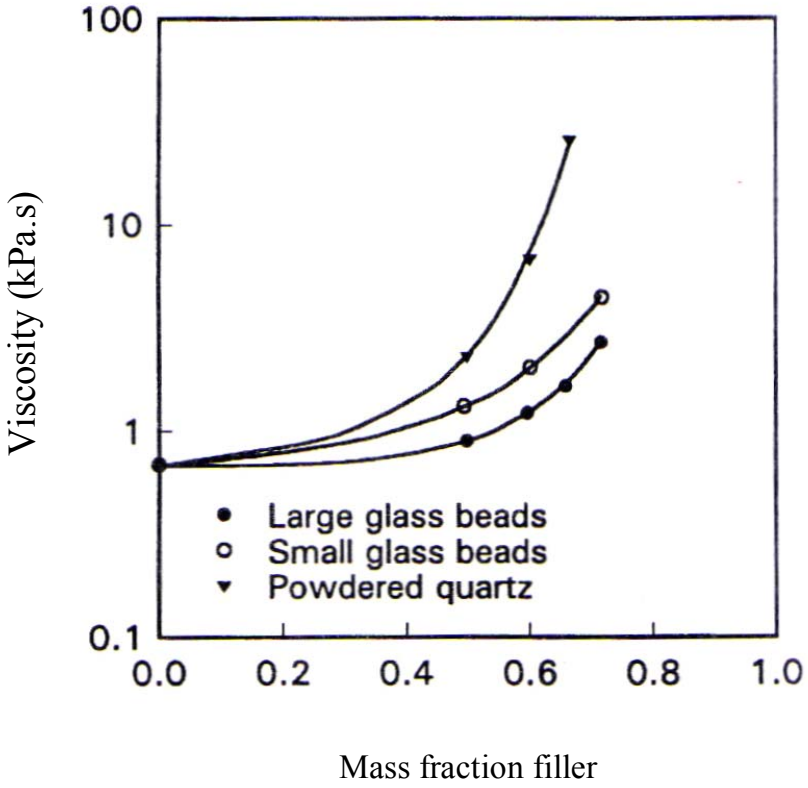

Figure 2.5 The effect of filler size and specific surface area on the viscosity (log scale) of the uncured resin matrix [8].

To overcome the problems associated with high viscosity related to high loading levels, three things can be done. First, reduce agglomeration by modifying the grinding approach, including using higher powered equipments and dispersants. With this approach, higher volume fractions of powder can be incorporated into resin and at the same time, any agglomerated mass can be broken up. Second, use hybrid size distributions of fillers to allow packing more particles into the unit volume by filling fine ones into the gaps of bigger ones. Third, add plasticizers to reduce viscosity.

An alternative way to reinforce the dental composites without increasing filler loading and viscosity is to turn to another type of filler. The filler material made of silica glass is of low elastic modulus intrinsically, around 70 GPa. Based on the law of mixtures, the elastic modulus of both fillers and matrix determine the overall elastic modulus of composites [8, 24, 25]. If we use the filler particles with higher elastic modulus, such as aluminum oxide (370 GPa) or diamond (925 GPa), then the elastic modulus and strength of composites can be increased with relatively low volume fractions compared to the counterparts reinforced with silica glass. Some modeling work on the modulus of elasticity of the composites will be discussed in Chapter 4.

A few studies have been published with respect to the alumina/Bis-GMA composites for bone cement applications, in which the size of alumina powder is about 10 μm [26, 27]. In comparison with conventional bone cement material, PMMA mixed with hydroxyapatite powder, alumina/Bis-GMA composites exhibit superior mechanical properties and osteoconductivity. Shinzato et al. also compared the silica/Bis-GMA

composites and alumina/Bis-GMA composites, the latter of which have better osteoconductivity, characteristic of the much more bone formed directly apposed to the composite surface. This shows that alumina has excellent biocompatibility [27].

Coupling agents and interfaces

To achieve a strong polymer-ceramic dental composite that will be less subject to swelling in an aqueous environment, filler particles must be chemically bonded to the resin. This is achieved using a chemical, termed a "coupling agent" in this thesis. Why is this so important? An example is shown in Fig. 2.6 (a) and (b). Under tension, the unbonded filler detaches from the matrix. As a result, the filler does little to help to improve the composites in stiffness [8]. Moreover, the overall strength and toughness of composites are reduced because the filler particles act more like voids in the composites. The transferring of stress between reinforcement and matrix only occurs in the presence of effective bonding between them. Fig. 2.7 (a) and (b) show scanning electron microscope images of filler particles with and without good bonding in the dental composites, respectively. The techniques for using coupling agents in dentistry have been well developed. Most of the coupling agents have similar chemical structures, based on a molecular with bifunctional groups $YRSiX_3$. This type of molecule is capable of reacting to the silanol groups of glass or ceramic fillers via its silane functional group (-SiX3) to form Si-O-Si- bonds to filler surfaces, and also to the resin matrix by grafting copolymerization via its -Y functional group, usually a methacrylic vinyl group.

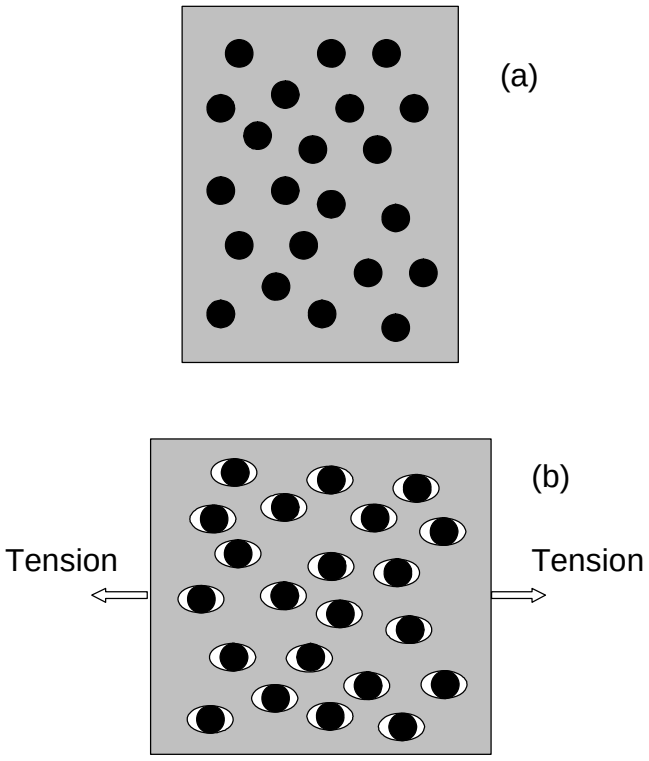

Figure 2.6 Under tension, unbonded filler provides negligible constraint to deformation and therefore little improvement subject to tension [8].

(a)

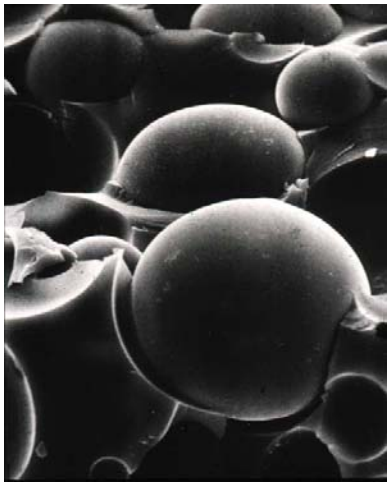

(b)

Figure 2.7 SEM images of (a) filler bonded to matrix and (b) filler not bonded to matrix (http://nersp.nerdc.ufl.edu/~soderho/E05.htm).

This type of bonding between filler and matrix is much stronger than by any other attractive mechanism, such as hydrogen bonding or van de Waals force. For particles other than silica, similar silanizing agents are used as well. Ash et al. show that a strong bonding between alumina and PMMA can effectively influence the thermal behavior of alumina/PMMA nanocomposites, characterized by a change in the glass transition temperature [28, 29].

In composites, there is a region called the interfacial region, which "begins at the point in the filler at which the properties differ from those of the bulk filler and ends at the point in the matrix at which the properties become equal to those of the bulk matrix" [30]. In traditional composites, this is a small region but critical to control the properties of composites, such as chemistry of bonding, polymer chain mobility, degree of conversion, and crystallinity. This region can reach up to 2-9 nm thickness around the particles [31]. Recently, with the tendency to employ finer fillers, this interfacial region is even more critical because its relative volume increases dramatically with increasing surface area for the finer fillers. Our calculations as shown in Fig. 2.8 (a) and (b) indicate how the surface area per unit volume increases as a particle size decreases and how inter-particle distance decreases as the volume fraction for spherical particles increases. It illustrates why incorporating nanoparticles into the matrix is so different from adding microparticle or mixed-sized particles. It also reveals that even a small volume of nanofiller in the composites can change the properties of the whole piece significantly by altering the more extended interfacial region [20].

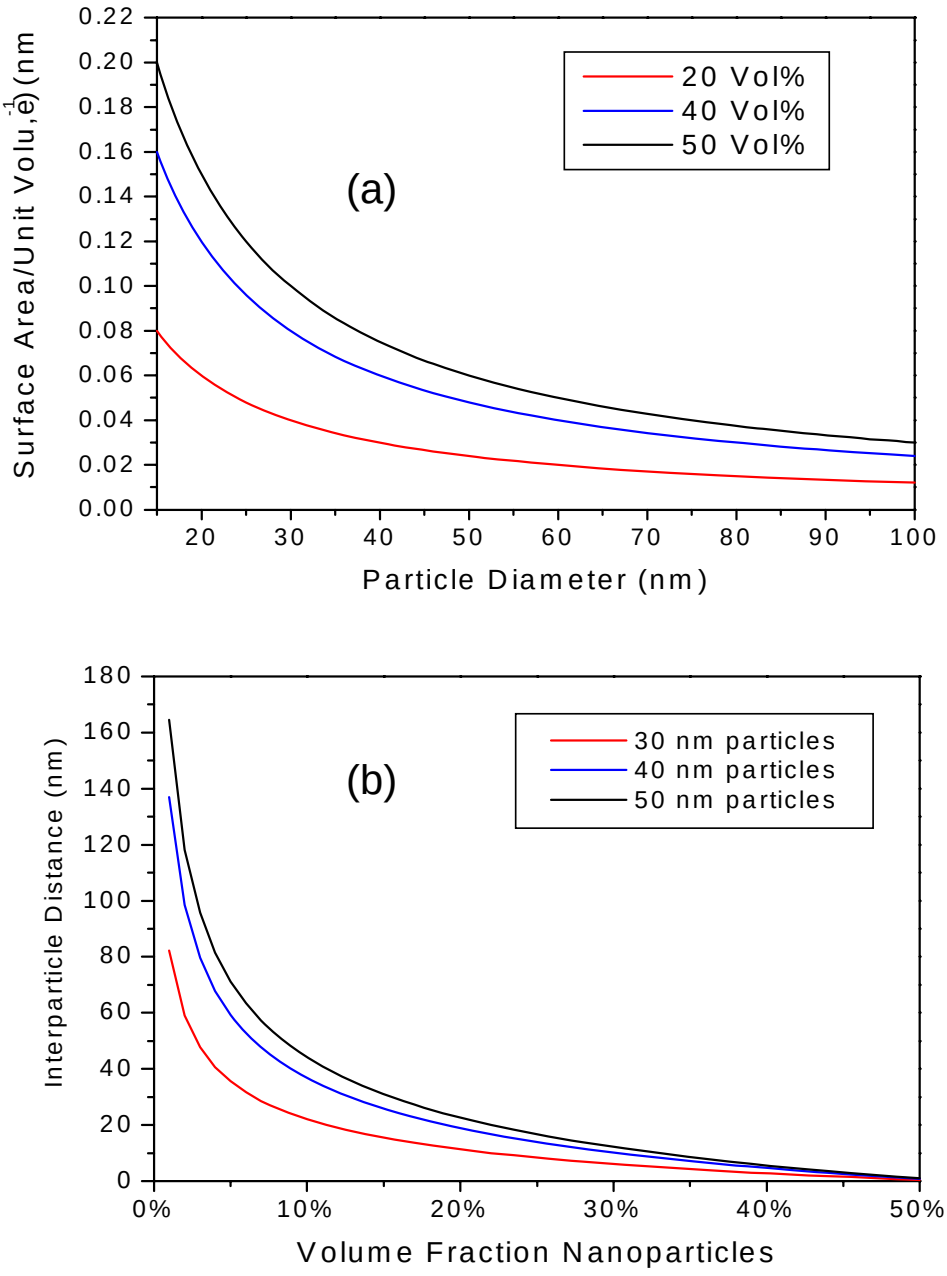

Figure 2.8 (a) Surface area per unit volume vs. particle size for spherical particles that are ideally dispersed, and (b) interparticle distance for spherical particles that are ideally dispersed.

2.3 All-ceramic Dental Crowns and Layered Structures

2.3.1 Dental crowns

Dental crowns are a type of dental restoration which, when cemented into place, fully covers the portion of a tooth lying at or above the gum line to add strength, durability, tooth stability and cosmetic appearance. Modern aesthetic restorations have a porcelain veneer layer that matches the coloration and translucency of natural teeth. Typical crowns have an underlying core layer, either ceramic such as alumina (InCeram) or, more conventionally, metal (in porcelain fused to metal (PFM) crowns), to provide essential structural support [32]. Recently, crown design has focused on layered structures with the retention of porcelain as an aesthetic veneer but with much stronger alumina or zirconia ceramics as core materials, termed as all-ceramic crowns [32]. All-ceramic crowns have superior aesthetics, but their lifetimes in posterior restorations remain problematic [3]. Clinical research shows that about 18% of Dicor® glass-ceramic dental restorations cemented with resin fail within the first 5 years of service in the oral cavity, and their failure rate differs from case to case, depending on the gender, age and service positions [33]. For posterior crowns and bridges where stresses are greatest and for male patients, the failure rate is highest [3, 34]. The factors that cause the crowns to fail are multiplex, influenced by mechanical properties of selected materials, engineering design, fabrication operations, environmental conditions, and even the clinical operations [3, 35].

In this manuscript, the efforts to improve the fabrication of all-ceramic crowns are demonstrated. Fig. 2.9 shows two illustrational images of the current fabrication procedure of all-ceramic crowns. Due to the difference in firing temperatures, cores and veneers are fabricated sequentially. The core is fabricated first, as shown in Fig. 2.9 (a). In order to cover the core with porcelain veneer, an aqueous slurry of porcelain particles is applied by hand with a brush and then it is sintered at a temperature above the softening point of porcelain at which the glassy matrix melts and powder particles coalesce. The porcelain veneer is added layer by layer by repeating this procedure, as shown in Fig 2.9 (b). Then, the biting surface of the crown needs to be adjusted by dental technicians with dental drills, which takes lots of effort and possibly causes damage to the materials [3].

The current method of fabrication limits the optimization of the properties of both materials, and problems are brought by differences in firing temperature and hand fabrication. In addition, a certain degree of porosity in porcelain veneer is induced by this manual manufacturing. Moreover, the fabrication of all-ceramic crowns is very labor-intensive and time-consuming.

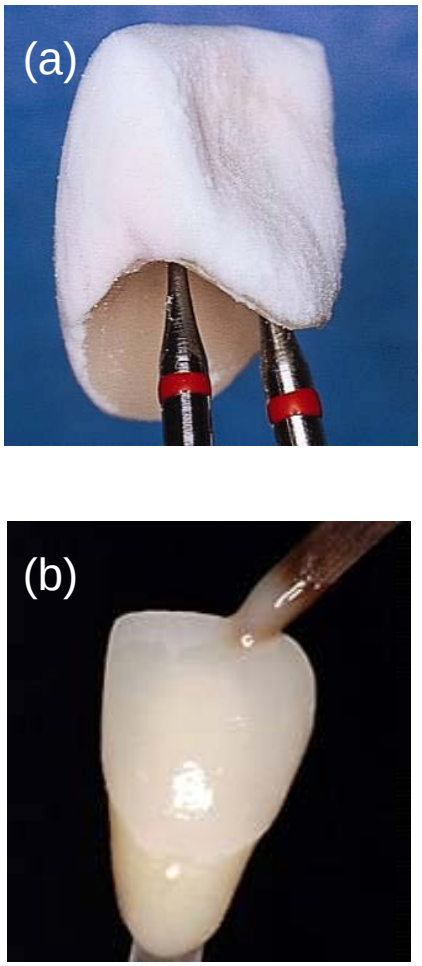

Figure 2.9 Fabrication of all-ceramic crowns: (a) ceramic core is fabricated first and (b) porcelain powder slurry is applied onto the core by hand with brush layer by layer (Private/Personal Communication with Mariano A. Polack, DDS, MS).

If both layers were fabricated independently and then reliably joined, new materials and fabrication techniques could be utilized and both layers could be optimized. The key here is to find an adhesive to bond two layers that will still perform well mechanically. Two methods are being investigated in our project, glassy joins or resin composite joins. This manuscript is focused on exploring approaches to create a high modulus resin-composite adhesive that could be used for (1) attaching a crown to a tooth while providing a stiffer supporting interlayer between the tooth and crown and (2) effectively joining independently fabricated crown layers without delamination. A simple flat layer model is sketched in Fig. 2.10 (a) consisting of a top porcelain layer, a strong ceramic core layer, and an in-house-developed resin-composite join. The performance of the resin composites has been investigated in the flat layer model [36], and our ultimate aim is to test the composites in the dental crowns with real geometry, as shown in Fig. 2.10 (b).

2.3.2 Effect of interlayers

Dental resin composites are routinely used as restorative materials. Historically, the elastic modulus of these materials has not been thought to be of as much importance as the other properties, i.e. adhesion. However, recent clinical results by Malament suggest that the mechanical properties of adhesive cement influence failure rates of all-ceramic crowns [33, 37].

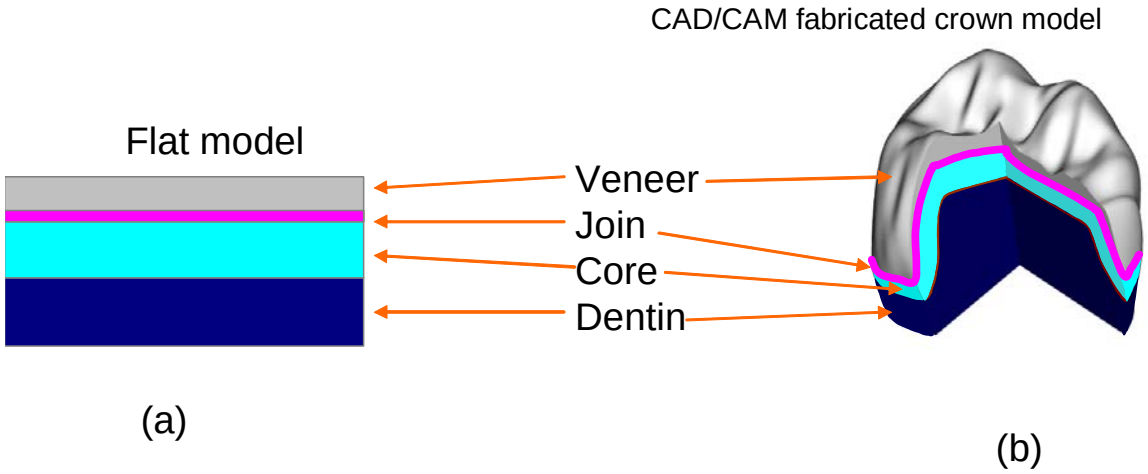

Figure 2.10 (a) Simplified flat model of dental crown and (b) CAD/CAM fabricated crown model with real geometry (Private/Personal Communication with Prof. Guangming Zhang, University of Maryland, College Park).

Thompson and Rekow note that the elastic modulus of the supporting structure and of luting cement and its thickness is critical in flexural fracture [3, 38]. In parallel, Lawn and co-workers have shown that the modulus of the supporting cement can influence the magnitude of the force needed to initiate fracture in the tensile fields of core-veneer bilayer ceramic structures on compliant substrates (like tooth dentin) [35, 39]. Thin, high modulus adhesive layers would improve the performance of all-ceramic crowns. Here the interlayer is defined as the cement layer, which is used to adhere dental crown onto dentin, or the joining layer, which is used to join independently fabricated dental core and veneer layers together. The stiffness of interlayer plays a critical role when the component on the top is subject to large load from chewing.

A heuristic and analogous work has been done by Kim [39]. In his work, the significance of the elastic modulus and thickness of adhesive are evaluated based on experiments using flat specimens of glass/adhesive/silicon layers in terms of critical load for radial crack initiation. His work suggests that the critical load for radial fracture rises with increasing elastic modulus of various adhesives but drops with increasing thickness of the same adhesives. Directly related work by Lee et al. shows the effect of the adhesive interlayer on the mechanical performance of sandwich structures [36]. The sandwich structure as shown in Fig. 2.11 is used to model the core-composite-veneer of dental crown structure.

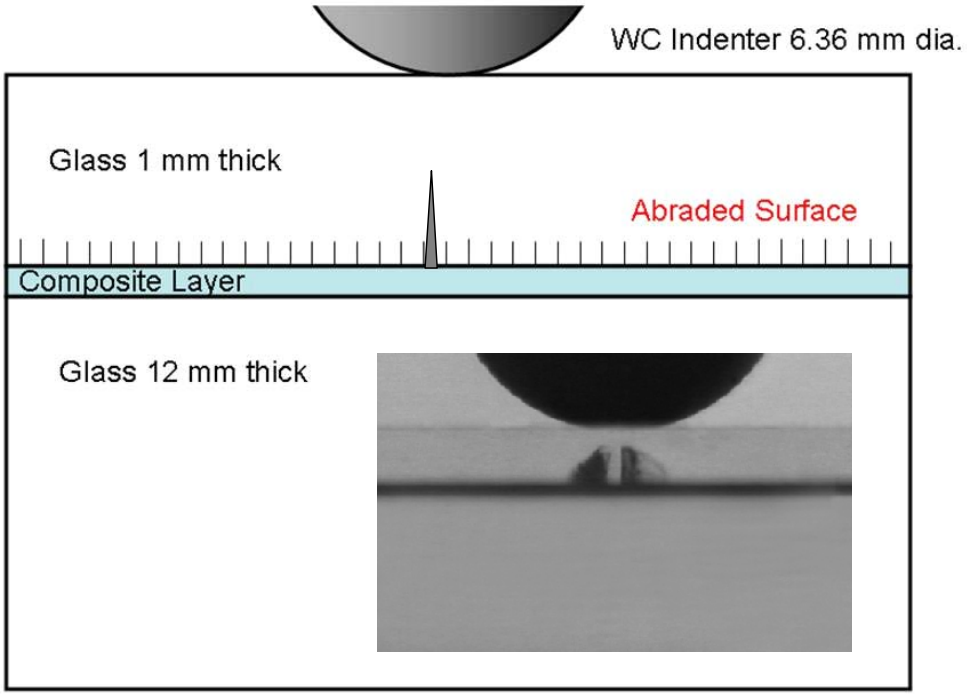

Figure 2.11 Schematic of glass/adhesive/glass layer system in contact loading, showing key variables; at bottom right corner, a typical snapshot of side view when radical fracture occurs, crack visible as elliptical shadow [36].

The top glass layer is bonded to the substrate with adhesive (either epoxy or in-house-made composite) and then loaded with a hard sphere. The size-controlled flaws are prepared at the veneer glass undersurface before loading. The critical loads for fracture (the fracture image at bottom right corner) are able to be tested, observed and recorded by Hertzian indentation and a video system. Fig. 2.12 shows that both modulus and thickness of interlayer determine the critical loads leading to failure of veneer glass. With certain thickness of interlayer, the adhesive with higher elastic modulus offers the prospect of improved resistance to veneer failure [36].

Besides the elastic modulus, other properties also influence the performance of the adhesive, i.e. creep and environment. Because viscous flow during cyclic loading at oral temperatures is inevitable for polymeric materials, permanent dimensional change is likely to occur. Once it happens, it might lead to excessive stress on the tensile surface of the top layer that relies on the support of the composites.

Huang et al. have presented a combined experimental and computational work of the contact fatigue mechanisms of sandwich structures, which is similar to the layer model in Lawn and co-workers' study [40, 41]. It shows that stress build-up could be "due to viscous deformation of the composite join layers, plastic deformation in dental cement due to ratcheting and subcritical crack growth in the ceramic layer." Although the results from a finite element model suggest that viscous deformation alone is not sufficient to cause cracking in the top layer, it does put extra stress onto the structure [41].

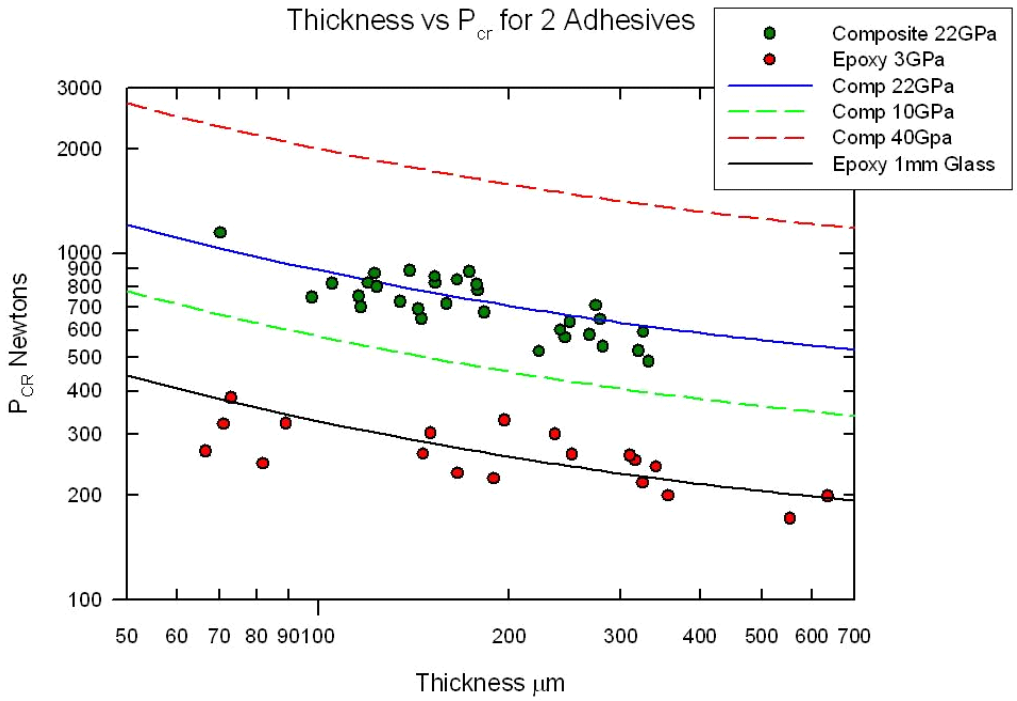

Figure 2.12 Two plots of critical load (PCR) versus join thickness *h* in logarithmic coordinates for glass veneer of thickness *d* = 1.0 mm bonded to glass substrate with adhesive of modulus *Ei* = 2.3 GPa (epoxy) and 20.4 GPa (composite). Data points with error bars at *h* = 150 mm are means and standard deviations for minimum of 6 specimens each. Dashed lines are for hypothetical adhesives of *Ei* = 10 GPa and 40 GPa [36].

In addition, viscous flow is sensitively related to temperature, circumstance, and rate and frequency of loading [42, 43]. A static test at room temperature at dry condition is not sufficient to explain all cases. The resistance to fatigue subject to cyclic loading is a very important factor to assess the composites. Moreover, the wet environment and changing temperatures in the mouth also bring challenges for our resin composites.

2.3.3 Other high modulus dental resin composites

In current dental resin composites, because the fillers are typically silicates and silicate glasses, which have a relatively low elastic modulus (<100 GPa), the extent of improvement in elastic modulus of composite is limited. The elastic modulus of commercially available resin composite adhesive systems is < 15 GPa [39].

Fiber-matrix composites are more likely to be utilized in the fields of polymer composites for structural applications including athletic gear, high tech components, and so forth. In dental applications, short glass fibers have been used as filler, producing limited improvements in composite mechanical properties [44]. Hockin Xu has further improved fiber type filler reinforced resin composites by introducing ceramic whiskers into dental resin composites to explore them as large stress-bearing crowns. The whiskers used were single-crystalline silicon nitride with diameters ranging from 0.1 μm to 1.5 μm (mean = 0.4 μm) and length ranging from 2 μm to 20 μm (mean = 5 μm) [11, 45-48]. To facilitate silanization, silica glass was fused on the whiskers. His whisker

composites demonstrated flexural strength and fracture toughness nearly 2 times those of currently available dental composites and had a much higher indentation modulus (see Section 3.4), around 29 GPa for the specimens with 80 weight percent filler loading [45-47].

However, the micro-sized fillers used in Xu's systems are not appropriate for applications with very small cross-sections. For our application, it is very important to maintain strength and elastic modulus in the thin areas of the join (~ 10 μm) as well as the thicker regions (~ 50-100 μm). In real crowns the complex geometry and manufacturing considerations mean that the joins will be of variable thickness and the thinnest area could be 1-10 μm. Thus, the utilization of sub-micro-sized fillers is necessary to get uniform mechanical properties by having hundreds of particles across the section for most of the area.

CHAPTER 3 EXPERIMENTAL PROCEDURES

3.1 Introduction

In this chapter, the materials selection, preparation, fabrication, and testing methods are described. The raw materials include inorganic fillers, resin monomers, and chemical additives. Since incorporating high filler loading significantly increases the viscosity of the paste, a special mixing apparatus has been developed. The methods of mechanical testing are an essential part of characterizing the novel resin composites. Nanoindentation is mainly used to obtain the elastic modulus, hardness, and viscoelastic properties of the crosslinked composites. The testing procedures and protocols are introduced in detail in this chapter. Thermo Gravimetric Analysis (TGA), Differential Thermal Analysis (DTA), Fourier Transform Infrared (FT-IR) spectrometry, Environmental Scanning Electron Microscope (ESEM), Brunauer-Emmett-Teller (BET) specific surface area (SSA) analysis, and Transmission Electron Microscope (TEM), are used to characterize the microstructures and physical properties of the resin composites and inorganic fillers.

3.2 Materials Selection and Preparation

3.2.1 Fillers

Table 3.1 List of filler materials and their properties

Materials	Average particle size (nm)	Morphology	SSA (m^2/g)	Density (g/cc)	*E* (GPa)
Silicon oxide (Aerosil® OX 50)	40	Equi-axed	50	2.18	68~70
Alumina oxide (NanoTek®)	47	Equi-axed	35	3.60	370~400
Buehler Alumina (Micropolish II)	3000	Irregular	N/a	3.96	370~400
Diamond (Advanced Abrasives)	375	irregular	7.47	3.2 ~ 3.5	800 ~ 924

Nano-sized fused silica (Aerosil-OX50, Degussa Co., Mobile, AL) is used as a control subject because most of current dental resin composites are reinforced with silica particles for facilitating the silanization and optical properties. The elastic modulus of fused silica is about 68~70 GPa. Nano-sized alumina (NanoTek® Aluminum Oxide, Nanophase Technologies Corporation, Romeoville, IL) is used as the primary filler material. The manufacturer's specification sheet indicates an equi-axed powder with an average particle diameter of 47 nm and a density of 3.6 g/cc. Both the manufacturer's

specifications and our measurements indicate a specific surface area (from BET) of about 35 m^2/g. Three-micron alumina polishing powder (Buehler Ltd., Lake Bluff, IL) is used as a micro-sized filler material. The elastic modulus of alumina oxide is about 370~400 GPa depending on phases (α-alumina or γ-alumina). Metal bond diamond powder (Advanced Abrasives Corporation, Pennsauken, NJ) is used to reinforce resin composites as well. Diamond is used because of its high stiffness, about 800~924 GPa. The diamond particles are of irregular shapes.

3.2.2 Dental resin monomers

Bisphenol A glycidyl methacrylate (Bis-GMA, Esstech, Essington, PA) and triethylene glycol dimethacrylate (TEGDMA, Sigma-Aldrich Inc., St. Louis, MO), are mixed in a 49.0 wt% Bis-GMA and 49.0 wt% TEGDMA, to form the resin system. 2.0 wt% benzoyl peroxide (an aqueous solution of 75% benzoyl peroxide (BPO, Fisher Scientific) is dissolved in the above monomer system as the initiator of polymerization. Their chemical structures are shown in Fig. 2.5 in Chapter 2.

3.2.3 Surfactants, coupling agents and their applications

Surfactant

Phosphate based surfactants (Dow Chemical Midland, MI 48674) are used to aid mixing and increase the maximum filler loading. The surfactants are mainly used with alumina fillers and diamond fillers. Their names and properties are listed in Table 3.2.

Table 3.2 Brand names and compositions of surfactants

Product name (Triton®)	Major component (%W/W_{total})	Water amount (%W/ W_{total})
XQS-20	Polyethylene glycol mono(octylphenyl) ether phosphate (>60%), phosphoric acid (<9%)	<31%
QS-44	Polyethylene glycol mono(octylphenyl) ether phosphate (>65%), phosphoric acid (<13%)	<21%
H-55	Phosphate ester potassium salt (50%)	50%
H-66	Phosphate ester potassium salt (42%), Dipotassium hydrogen phosphate (7%)	50%

There are two ways to apply surfactants. One way is to add surfactants directly into the paste during compounding (mixing) and then the maximum filler fraction of alumina can be increased from about 72 wt% to up to 80 wt%. The same method is applied to diamond filler. The amount of surfactant is about 3 wt% of total weight of paste in order to get about 80 wt% of filler loading. The other way is to pretreat the surface of filler particles before compounding. The powder is added into acetone with an amount of surfactant that is about 2% of the weight of dry powder. Then the mixture is exposed in the hood to evaporate the solvent for 24 hours. The dried powder is then directly added into the monomer paste.

Thione primers

MetalPrimer II (MEPS thiophosphoric methacrylate, GC America, Inc., Alsip, IL) and Metaltite (Tokuyama Corp., Tokyo, Japan) are dental primers used to improve the adhesion between resins and precious metals such as gold, titanium, semi-precious metals and many other dental alloys. Metaltite contains 6-methacryloyloxyhexyl 2-thiouracil-5-carboxylate (MTU-6) in ethanol solution. The usage of the primers is similar to the surfactants except that they are expected to help bond the fillers to the resin.

Silanizing coupling agents

The routine silanizing agent, 3-methacryloxypropylteimethoxysilane (MPTMS, Sigma-Aldrich, St. Louis, MO) is used to provide a chemical bond between filler, both alumina and fused silica, and organic matrix. The chemical structure is shown in Fig. 2.5 in Chapter 2. The filler is silanized by being mixed with MPTMS in cyclohexane with n-propylamine as a catalyst in a rotary evaporator in a 90 ^{o}C water bath until dry [46]. Then the dried powder is directly added into monomer.

Organotitanates and zirconates coupling agents

Three types of organotitanate and zirconate coupling agents (Kenrich Petrochemicals, Inc., Bayonne, NJ) are used to treat the surface of alumina to explore if they chemically bridge the filler and organic matrix. The way to apply these coupling agents is the same as the pretreating procedure for the surfactants. Typically 0.02~0.03

of mass fraction of the coupling agents are mixed with alumina powder. With addition of titanate and zirconate coupling agents, a maximum of about 80 wt% of alumina filler fraction can be achieved.

Table 3.3 Chemical names and structures of organotitanates and zirconates coupling agents

Product name	Chemical name	Chemical structure
KR 33	Titanium IV, tris(2-methyl)-2-propenoato-O, methoxydiglycolylato	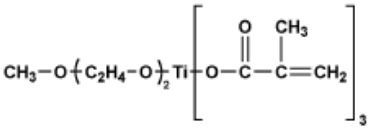
KR 55	Titanium IV tetrakis(bis 2-propenolato methyl)-1-butanolato adduct 2 moles (di-tridecyl)hydrogen phosphite	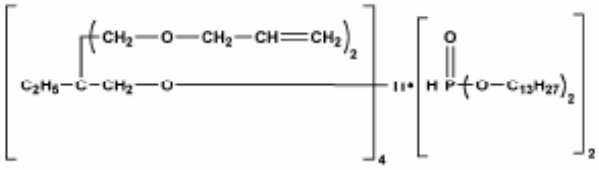
NZ 33	Zirconium IV 2,2(bis-2-propenolatomethyl)butanolato, tris 2-methyl-2-propenoato-O	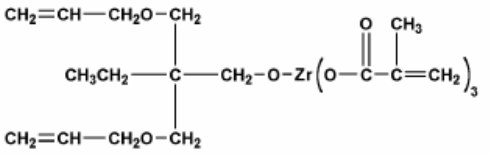

3.3 Mixing Apparatus and Fabrication Procedures

One of the difficult technical problems is how to compound this high viscosity paste. The viscosity increases dramatically as filler is added, due to the increasing friction between particles and between particles and monomer. It is a particular problem with the addition of large volumes of filler. Since the nano-sized filler has higher specific surface area than conventional micro-sized filler, the viscosity of nanofiller reinforced composites is even higher than the micro-sized counterpart at the same filler loading. There are several well established inorganic/polymer mixing techniques, i.e. direct mixing, solution mixing and in-situ particle processing [49]. Considering the environmental requirements of the application of the composites, we choose direct mixing as our processing method for compounding. We developed our own method to mix composites since the traditional two-roll mill and twin screw extruder are not available. In addition, these two methods have their own limitations when dealing with high filler loading samples [19].

3.3.1 Mixing apparatus

The mixing apparatus consists of two main parts, a vibration table and an electronic drill loaded with PTFE coated spatula. The mixing cup is mounted onto the vibration platform to help mixing. The PTFE coating on the spatula is to prevent reaction with the monomers. The spatula utilizes shear force in addition to the vibration

from the table to push the particles into the monomer matrix and break up the possible agglomeration of particles. Fig. 3.1 shows the setup of the mixing apparatus. The conventional dental plate-and-spatula method is also employed when preparing a small amount of specimen. The monomer precursor is placed on the dental glass plate and the filler is added step by step via repeatedly kneading, spreading and folding the paste until it is mixed. A PTFE coated spatula is used to compound precursor and fillers.

3.3.2 Fabrication procedure

The specimens are fabricated by following the procedure illustrated in Fig. 3.2. Filler is added progressively to the resin system with our mixing apparatus. For nano-sized alumina powder, our technique allows the addition of up to about 72 wt% without additives. In order to raise the maximum filler fraction, it is necessary to add a surfactant or to treat the surface of filler with a surfactant or coupling agent before compounding. With chemical additives, filler loadings up to 80 wt% are achievable. For some silanized fillers, the composites can be loaded up to 82 wt%. To prepare bulk samples for characterization including indentation tests, composite pastes are packed into glass tubes of 15 mm in diameter and 45 mm long and compacted by centrifugation at 9000 rpm (above 15,000G). Centrifuging is used to increase the composite density and provide a regular shape for testing. Sometimes, a glass rod is used to push and compact samples as well. Each specimen is cured via thermal crosslinking in oven at 120 ^{o}C for about 6~9 hours and then removed from the mold.

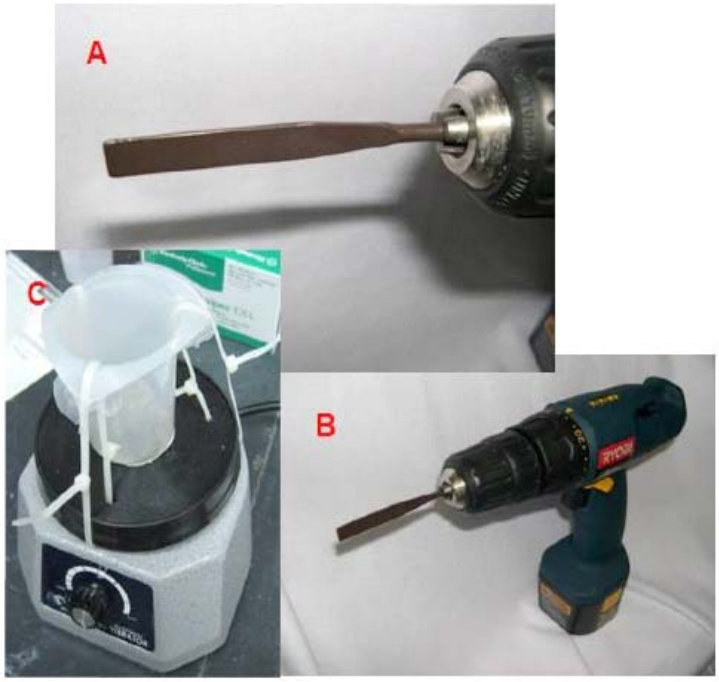

Figure 3.1 Mixing apparatus. A) PTFE coated spatula; B) Electronic drill with spatula mounted; C) Mixing cup mounted on a vibration table.

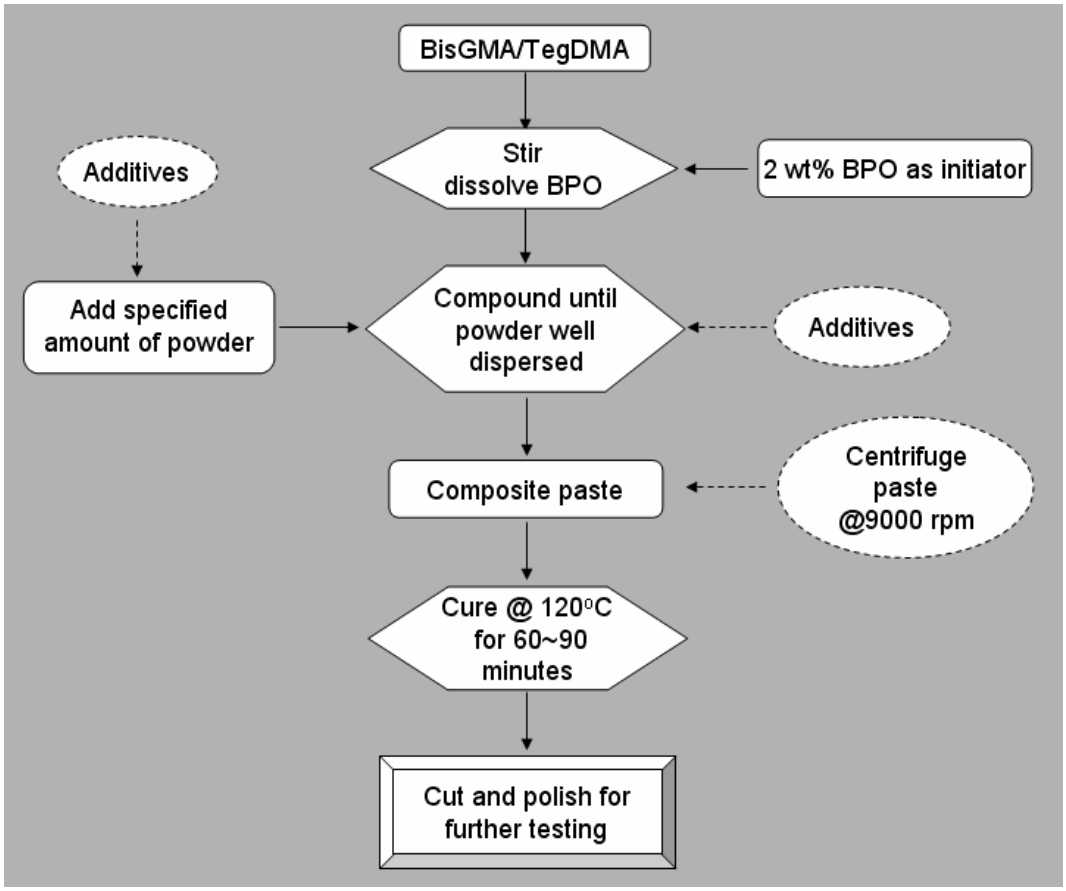

Figure 3.2 Procedure of fabrication of resin composites.

3.4 Nanoindentation

Nanoindentation is the primary mechanical testing method in our study. The working theory and protocol of nanoindentation will be introduced in detail since they are necessary to explain and understand the results. Nanoindentation is a convenient means of measuring elastic modulus and hardness of the bulk composite and joined samples, and even the viscous flow of the resin composites. Before the appearance of nanoindentation, a bending test was widely used to measure the elastic modulus of materials. However, it is not applicable to small size samples or thin films. Nanoindentation is uniquely suited to measure the elastic modulus of thin films and small volumes.

3.4.1 Background

The indentation test is one of the most used methods for testing the mechanical properties of materials of all kinds [50]. The basic testing procedure is to press a hard tip of various shapes into the sample materials, control the load, and measure the residual indents upon removing the load. The theory defines the hardness, H, of materials by

$$H=P/A_r \tag{3.1}$$

where P is maximum load and A_r is the area of residual indents. In fact, this is the working principal of microhardness testing as well. Nanoindentation differs from a microhardness test not only by the shape and size of indenter tips but also by the

procedure, which includes an in-situ depth-sensing component. Basically, nanoindentation refers to an indentation testing machine which can record the in-situ load and displacement of the tiny tip with very high accuracy and precision. After testing, computer software interprets and analyzes the recorded data to give out the results, i.e. elastic modulus, hardness, and other mechanical properties. One of the most attractive attributes of nanoindentation is providing elastic modulus measurement for small samples.

3.4.2 Testing principles

The most widespread model of nanoindentation is one which assumes the unloading data arise from a purely elastic contact. This approach was developed over 40 years ago [50-52]. Several important assumptions were first developed by workers at the Baikov Institute of Metallurgy in Moscow during the 1970's (Bulychev and Alekhin in Russian) [53, 54]. They include

1) Deformation upon unloading is purely elastic.
2) The combination of moduli of tip and sample can be expressed as springs in series

$$\frac{1}{E_r} = \frac{1-\nu_i^2}{E_i} + \frac{1-\nu_s^2}{E_s} \tag{3.2}$$

where E_r is the reduced modulus, accounting for deformation of both the indenter and the sample, E is the Young modulus, ν is the Poisson ratio and i and s refer to the indenter and sample, respectively.

3) The contact area and indenter can be connected with Equation 3.3 in the case of indenter tip of a homogeneous isotropic elastic half space.

$$S = \frac{2\sqrt{A}}{\sqrt{\pi}} E_r \tag{3.3}$$

where S is the contact stiffness and A the contact area.

Another breakthrough was the development of data analysis by Doerner and Nix (D&N), who related the load-contact depth data to contact area [52]. If the change in contact area is small during unloading, the indenter can be treated as a flat punch. Then the material in contact with the indenter undergoes plastic deformation and elastic deformation occurs at the outside surface only. Fig. 3.3 shows the schematic plot of the D&N model. They define h_c as the contact depth, which is the distance that is in contact with the sample material along the indenter axis. So the slope S of the loading at the maximum load P_{max} yields h_c, which is also defined as the maximum contact stiffness.

Sneddon's research predicted that the unloading data for an elastic contact follows a power law for many simple indenter geometries [51]

$$P = \alpha (h - h_f)^m \tag{3.4}$$

where P is the indenter load, h is penetration depth, h_f is the final unloading depth, α contains geometric constants, and m is a power law exponent that is related to the geometry of indenter; for a flat-ended cylindrical punch, $m=1$, for a paraboloid of revolution, $m=1.5$, and for a cone, $m=2$ [51, 55].

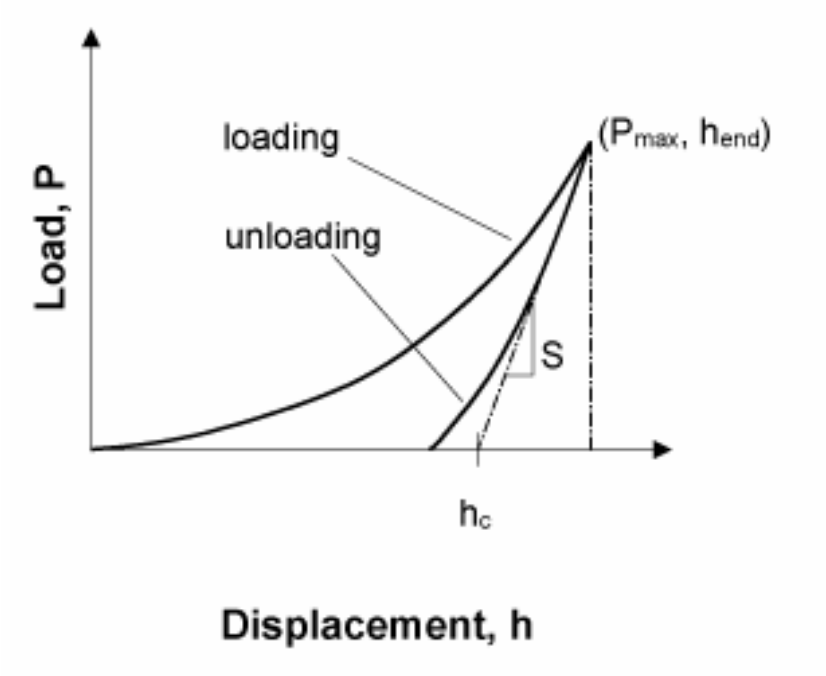

Figure 3.3 Schematic plot of the Doerner and Nix model showing various quantities used in analysis [52].

Oliver and Pharr (O&P) made a critical improvement by formulating a new equation to determine the contact area at maximum load and also pointed out the contact area should change during unloading. In Fig. 3.4, the indentation load-displacement curve is illustrated along with several important parameters used in the O&P analysis [50]. The stiffness, *S*, is the slope of the tangent line to the unloading curve at the maximum loading point [50, 55]

$$S = \left(\frac{dP}{dh}\right)_{(h_{\max}, P_{\max})} = \alpha m (h_{\max} - h_f)^{m-1} \tag{3.5}$$

After removal of the load-frame compliance, the displacement of the load frame is removed so that *h* represents only the displacement of the tip in the sample. The contact area, *A*, the stiffness, *S*, and the reduced modulus can be related by Equation 3.3. In Fig. 3.5, $h_c = h_{max} - h_s$, where h_s is defined as the elastic displacement of the surface, which can be calculated for specific geometries using displacement equations from Sneddon's analyses [51]

$$h_s = \theta \frac{P_{\max}}{S} \tag{3.6}$$

where θ = 0.72, 0.75 and 1, for cone-, sphere- and flat-punch-geometry respectively. Thus,

$$h_c = h_{\max} - \theta \frac{P_{\max}}{S} \tag{3.7}$$

O&P significantly improved the method proposed by D&N. The contact stiffness can be derived as the function of slope at the maximum loading. In addition, the slope is also used to determine the actual contact depth depending on the geometry.

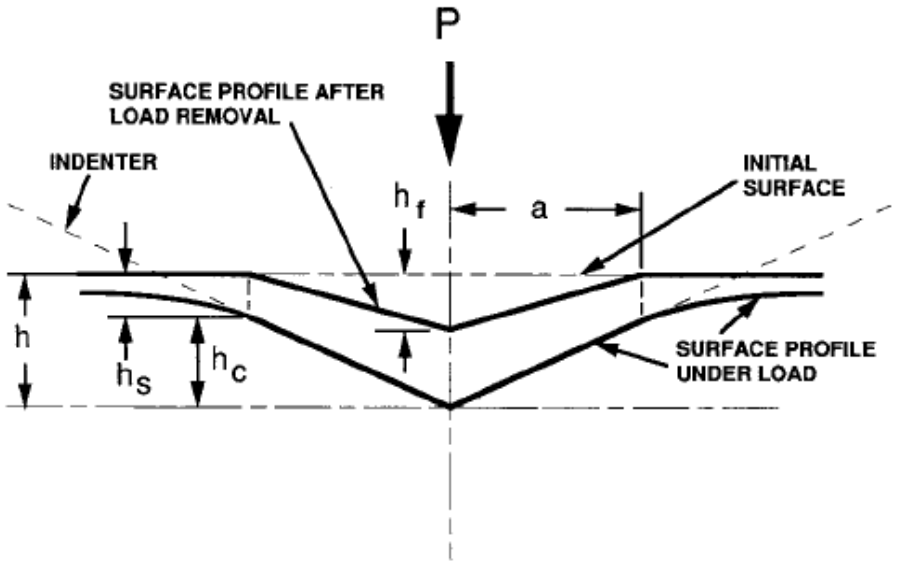

Figure 3.4 A schematic representation of a section through an indentation showing various quantities used in analysis [50].

3.4.3 Testing protocols and sample preparation

A Nano Indenter XP (MTS Nano Instruments, Oak Ridge, TN 37830) with a standard Berkovich diamond tip is used for the nanoindentation tests. The testing method we use is called CSM mode (continuous stiffness measurement), which is accomplished by applying a small oscillation to the force signal at a relatively high frequency. All the tests for each composition are done on a single sample to minimize effects from minor processing variations. Tests have also been repeated on different samples made from the same recipe to verify the results. Typically 2~3 additional samples are measured for each composition. The crosslinked composites are cut, then ground and polished down to 1 μm to provide a flat and parallel surface for indentations. Indents are made at the center of the specimens far enough apart (larger than 300 μm) to not interact with each other. Note the triangular indents with medians of about 50 μm. Nine indents are made on each sample. To have confidence that the measurements are representative of the entire sample rather than just the local composition and microstructure, the maximum load, P_{max}, is about 2 N, which results in the size of indents, 50 mm, much larger than size of filler. The elastic modulus, E, and hardness, H, vs. penetration depth, h, of materials are directly taken from the software analysis by the machine.

The measurement of viscous flow uses a different testing protocol. The same Berkovich indenter is used with load-control mode. A triangle-wave loading-unloading

cycle is applied on the surfaces of samples, which are polished down to 0.5 μm, as shown in Fig. 3.5. Loading and uploading equally divide the testing time, either 30, 100 or 300 seconds. The peak load, P_{max}, is 300 mN fixed for all three tests. The load-displacement traces are recorded for further analysis (Chapter 5).

3.5 Microhardness

The microhardness values of some resin composites are measured using an Instron Tukon® 2100 Indentation Hardness Tester (Instron Wilson Instruments, Canton, MA). Nine points are taken for each sample to allow comparison of hardness values from nanoindentation and microindentation measurements.

3.6 Microstructural Characterization

3.6.1 BET, TEM and filler particles

Brunauer-Emmett-Teller (BET) basically is a gas sorption analyzer (Nova-1200, Quantachrome Corp., Boynton Beach, FL). By calculating the amount of gas absorbed onto the surface of the sample, the surface area is obtained. Prior to gas adsorption, the powder sample is degassed and dried in a vacuum at elevated temperatures to desorb gases and moisture from the powder surface. After degassing, the sample is placed in a nitrogen atmosphere to allow absorption. The mean particle size is calculated by comparing the weight difference through absorption.

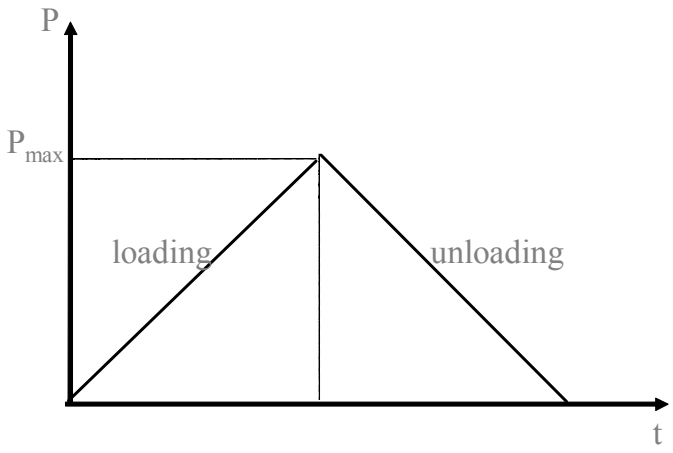

Figure 3.5 A schematic plot of triangle-wave of loading-unloading with maximum load, P_{max}.

Besides mean particle size from BET, TEM (JEOL 2100F, Tokyo, Japan) is also used to examine the filler particles in terms of size, shape, and agglomeration.

3.6.2 TGA and DTA

Thermo Gravimetric Analysis (TGA-50, Shimadzu, Kyoto, Japan) is used to determine the weight fraction of fillers and absorbed water on the filler surface. The crosslinked sample is ground to powder to decrease the likelihood of polymer residue during heating. About 10~20 mg of sample (ground composite or filler powder) is put in a small alumina crucible and heated up to 900 °C at heating rate of 5 °C/min with gas flow (compressed air) of 20 ml/min. The internal optical scale records the in-situ weight during heating. Some samples have been tested twice, however there is no apparent evidence showing that there is a polymer residue after the first heating, which is possibly due to our relatively slow heating rate.

Differential Thermal Analysis (DTA-50, Shimadzu, Kyoto, Japan) is used to find the temperature of polymerization. A small amount of sample (about 2 mg) is put in an alumina crucible and covered with a platinum lid. The temperatures of the sample and reference substance rise at a constant rate. The thermally inert reference substance (air or alumina powder) keeps rising in temperature at a constant rate. When an endothermic change (such as fusion) takes place in the sample on the other hand, heat energy supplied from the exterior is consumed by the change so that the temperature stops rising. Therefore, when the change is complete, a substantial difference will result

between the sample and the reference temperatures. This causes a large amount of heat energy to be transferred to the samples, resulting in a sharp rise in the sample temperature signal. The temperature difference ΔT is detected and amplified to be recorded as a peak. Polymerization is an exothermic reaction, so an upward peak is shown. Both uncrosslinked paste and crosslinked sample with the same composition are tested separately. By comparing them, the polymerization temperature is determined.

3.6.3 Degree of conversion and FT-IR

More detailed discussion concerning the degree of conversion and FT-IR is presented in Section 4.3. For powder samples, 5 or 10 wt % of samples are mixed with KBr powder and put into a sample holder for testing. For uncured paste samples, a thin film, which is less than 1 mm, is smeared on a KCl IR card (International Crystal Laboratories, Garfield, NJ) and then covered by another piece of IR cover. Each sample is measured by FT-IR spectroscopy five times on different spots. Then the whole sandwich sample is put in the furnace to get crosslinked. After crosslinking, the same measurement is taken to get the absorption spectrum.

3.6.4 Fracture surface and ESEM

SEM images are taken by environmental scanning electron microscopy (ESEM, Philips ElectroScan E3 environmental SEM) on fracture surfaces to look for porosity and nanopowder agglomeration, and evaluate the adhesion effect of coupling agents.

3.6.5 Immersion density and open porosity

Immersion density is determined using an adaptation of ASTM D792 and ASTM C373 standards for density and open porosity measurements via water immersion Archimedes measurements. Density is measured on crosslinked samples that are cut into cylindrical disks. Open porosity is estimated using the saturated and suspended weights method.

CHAPTER 4 MODULUS OF PARTICLE REINFORCED COMPOSITES

4.1 Introduction

In this chapter, the microstructures and mechanical properties of particle reinforced composites are discussed. Since the filler loading fraction and the curing temperature have a strong impact on the mechanical properties of the resin composites we develop, they are examined by TGA and DTA, respectively. The effect of filler loading and additives on the degree of conversion is investigated by FT-IR as well. A good dispersion of filler is desired for obtaining uniform mechanical properties of the composites. SEM is used to observe fracture surfaces of composites to investigate dispersion of filler particles and possible effects of coupling agents. The elastic modulus (E) and hardness (H) are two critical parameters for optimizing performance of layered structures for dental crowns. Due to the fact that we need to probe the mechanical properties of composites in a very small area, nanoindentation is the major method to obtain elastic modulus and hardness of composites. Explicit relationships of the elastic modulus and filler associate with types and loading will be thoroughly investigated. The predictive models for elastic modulus of composites are also described to verify and help understanding the mechanism of reinforcement.

4.2 Microstructure

4.2.1 Filler particles

Three types of filler particles are used in the research: equi-axed alumina with mean diameter of 47 nm, equi-axed silica with mean diameter of 40 nm and diamond particles of irregular shape with mean diameter of 375 nm. The properties of filler particles directly affect the overall properties of composites as discussed in Chapter 2. In this section, these nanoparticles are characterized by various methods with respect to the size, shape, and surface.

The alumina powder received from Nanophase Technologies Corporation is analyzed by TGA and FT-IR, which allows calculation of the desired coupling agent concentration. The TGA of the as-received particles is presented in Fig. 4.1 (a). It shows an immediate mass loss as heating begins from room temperature. This is attributed to the physisorbed water on the alumina surface [56, 57]. The curve (b) in Fig. 4.1 shows the TGA of dried particles. These particles are dried in the TGA furnace by being kept at 200 $^{\circ}$C with blowing compressed air to remove the evaporated moisture for 2 hours. This curve shows a relative plateau through around 200 $^{\circ}$C, which indicates that the water content on the alumina surface has been effectively removed. Then curve (b) parallels curve (a) up to 900 $^{\circ}$C. The decrease in mass exhibited by these two curves above 200 $^{\circ}$C does not stop until around 500 $^{\circ}$C.

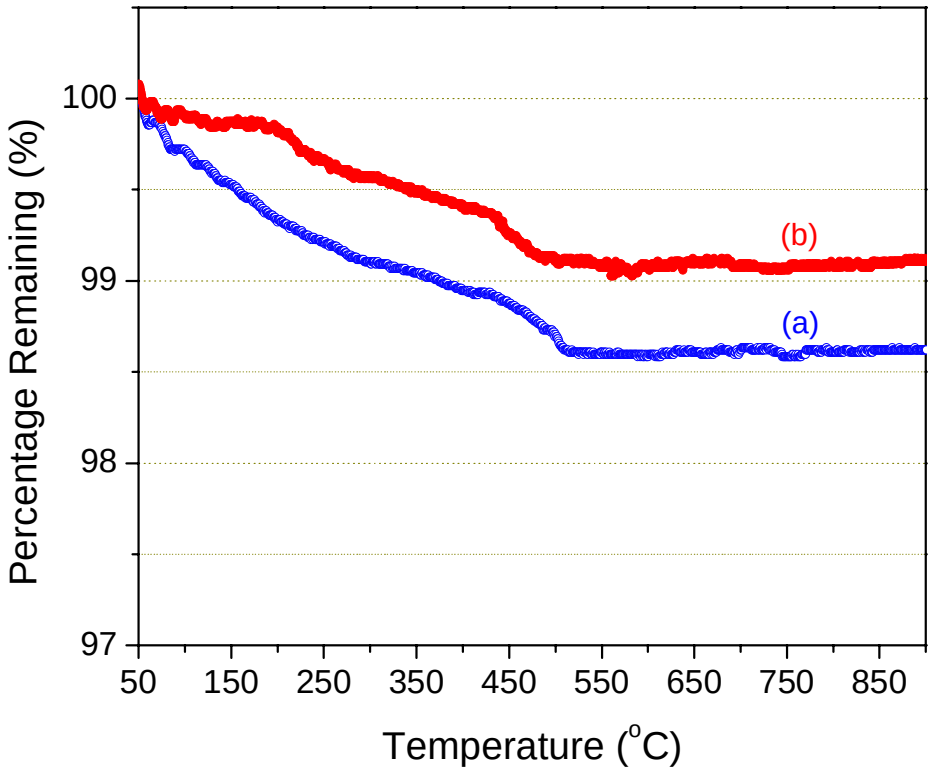

Figure 4.1 TGA of (a) as-received NanoTek® Al_2O_3 nanoparticles and (b) nanoparticles with drying at 200°C for 2 hours.

As described in Abboud's research, there are three domains in the thermograms obtained for pristine powders: 100-400 °C, 400-800 °C and 800-1100 °C [57]. In the first region, the main weight loss is assigned to the desorption of physisorbed water. In the second region, the weight loss is attributed to the combination of adjacent OH groups on the surface. Between 800 and 1000 °C, the isolated hydroxyl groups migrate on the surface and are consumed via the same reaction. In Fig. 4.1, there is no apparent weight loss after 500 °C possibly because the TGA-50 is not sensitive enough to detect that tiny weight loss.

By calculating the mass difference between two curves at 200 °C, the physisorbed water coverage can be derived based on specific surface area in Table 3.1. Equation 4.1 shows how to calculate the mole of physisorbed water per unit area on the surface.

$$mol_w = \frac{m_w / u_w}{SSA \times m_p} \tag{4.1}$$

where mol_w is moles of water per m^2, m_w is weight of physisorbed water, u_w is the atomic mass unit of water, SSA is specific surface area and m_p is the weight of powder. For alumina powder from Nanophase, the calculated physisorbed water coverage is about 7.8 μmol/m^2. Similarly, the hydroxyl group (-OH) on the surface following drying can be calculated from curve (b) and (a) of Fig. 4.1, which gives the value of about 17.5 μmol/m^2. However, this method is not very reliable for quantitative analysis for the following reasons. The drying process can not remove all the absorbed water on the

surface. After drying, the powder exposed in air will rapidly regain some moisture, which further misleads the estimation. Usually, the result as described is an overestimation of OH density. It is still informative for estimating the amount of coupling agents necessary to provide surface coverage. Other fillers are not tested by TGA since they are unstable at high temperature.

The NanoTek® alumina is analyzed by FT-IR as well. The FT-IR spectrum (Fig 4.2) reveals the presence of hydroxyl groups, as indicated by the large OH stretching bands at ~3500 and 1630 cm^{-1} [28]. Those hydroxyl groups provide the potential sites for the hydrolysis reaction with coupling agents.

4.2.2 TEM and SEM

TEM images of fillers

The shapes and sizes of particles play important roles in mixing and performance after curing. They affect powder flow, viscosity, and mechanical, thermal and optical properties. Because of the very small sizes and agglomeration of nanoparticles, the Transmission Electron Microscope is used for characterization. A small amount of powder is immersed into acetone. In order to break the possible agglomeration between particles, the suspension is sonicated for 20 minutes. After 3 days of sedimentation, a drop of suspension from the top is extracted and put on a copper mesh grid (Tedpella, Redding, CA).

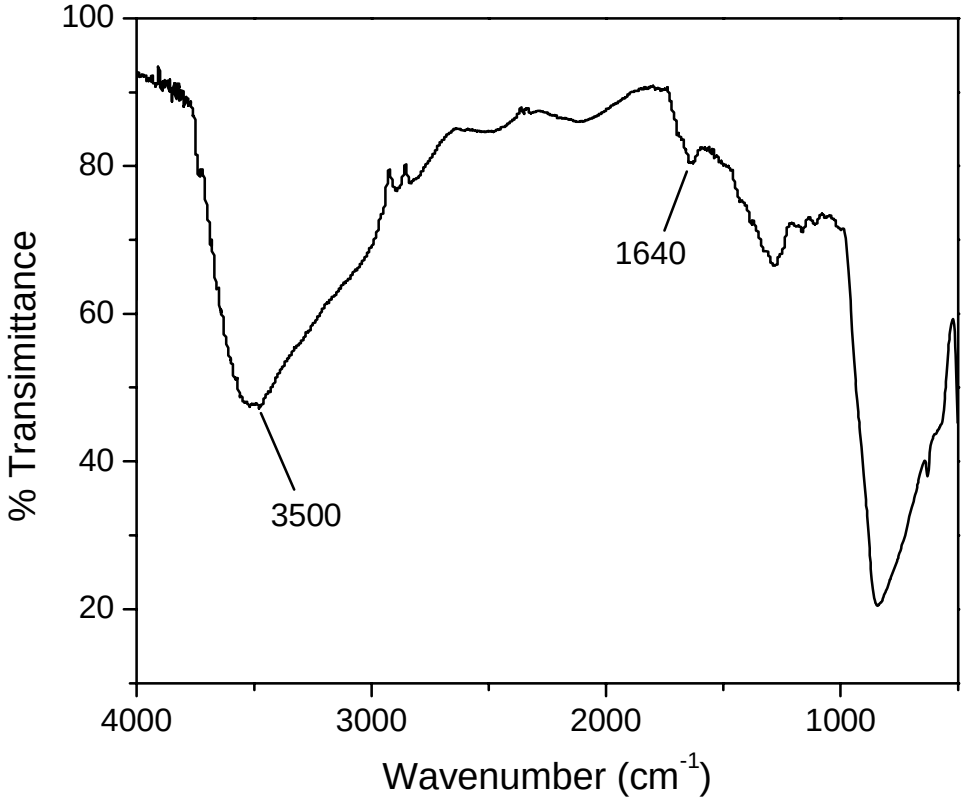

Figure 4.2 FT-IR spectra of as-received NanoTek® alumina.

Typical TEM images of alumina nanoparticles are given in Fig. 4.3 (a) and (b), respectively. In Fig. 4.3 (a), we find the distribution of particle sizes is quite uniform. The Fig. 4.3 (b) shows a single particle, which is not of perfect equi-axed shape. The striped pattern of this particle is attributed to polycrystalline structure of alumina. The OX 50 silica particles are also examined by TEM, as shown in Fig 4.4 (a) and (b). The particles are very spherical, but many are agglomerated in chains. Some have also sintered to form oval particles. This irregularity makes the mixing even more difficult than with nano-alumina. The TEM image of MDP 0.375 diamond particles is shown in Fig. 4.5. The particles are of more irregular shapes and are agglomerated. Their size is hard to estimate from the TEM images. The average of 375 nm diameter is obtained from the supplier's datasheet.

SEM images of resin composites

Two resin composite specimens are observed: 80 wt% Al_2O_3 powder with Bis-GMA/TEGDMA monomers (ALBT80) and 80 wt% Al_2O_3 powder with pure TEGDMA (ALT80). SEM images of fracture surface of ALBT80 and ALT80 are shown in Fig. 4.6 (a) and (b), respectively. Note that the features in Fig. 4.6 (a) are roughly the size expected for 50 nm particles, indicating that agglomeration was limited in ALBT80 samples, while 0.5-1 μm agglomerates are evident in the ALT80 samples in Fig. 4.6 (b). The arrows in Fig. 4.6 highlight a few pores.

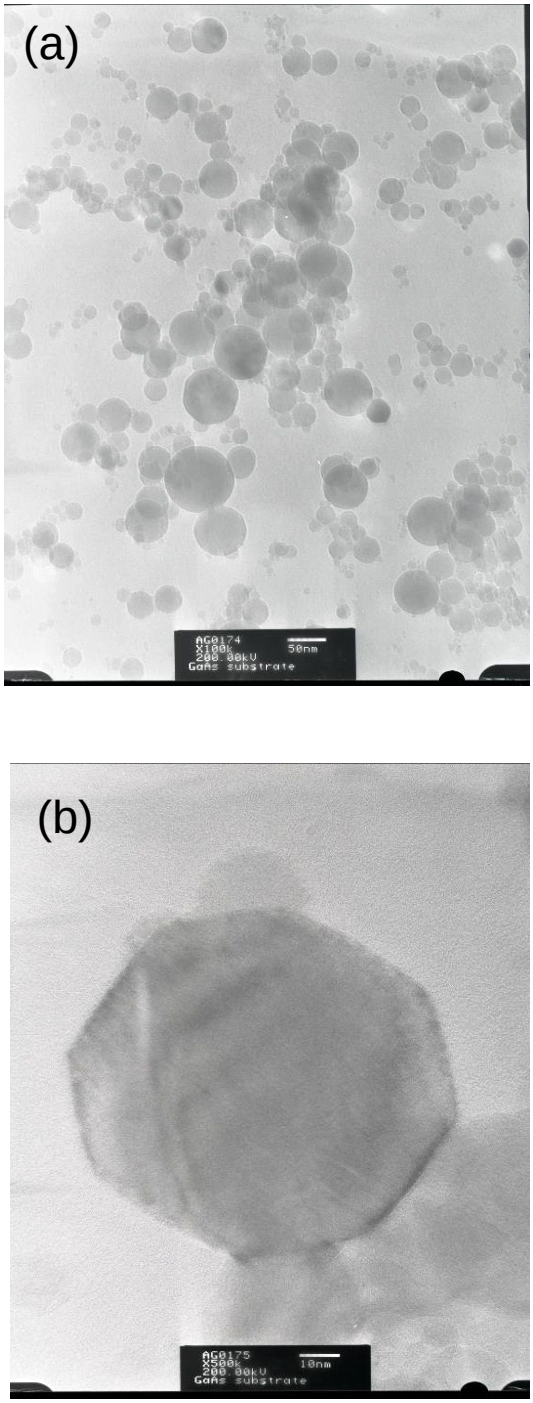

Figure 4.3 TEM images of NanoTek® Al_2O_3 nanoparticles. Scales in both images are 50 nm.

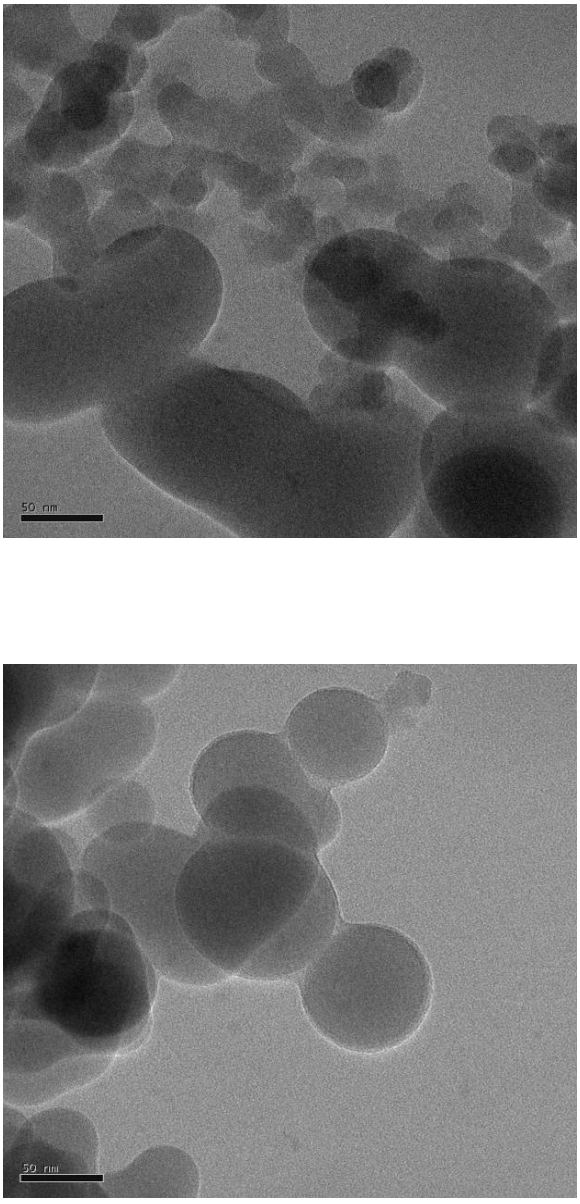

Figure 4.4 TEM images of Aerosil® OX 50 silica nanoparticle. Scales in both images are 50 nm.

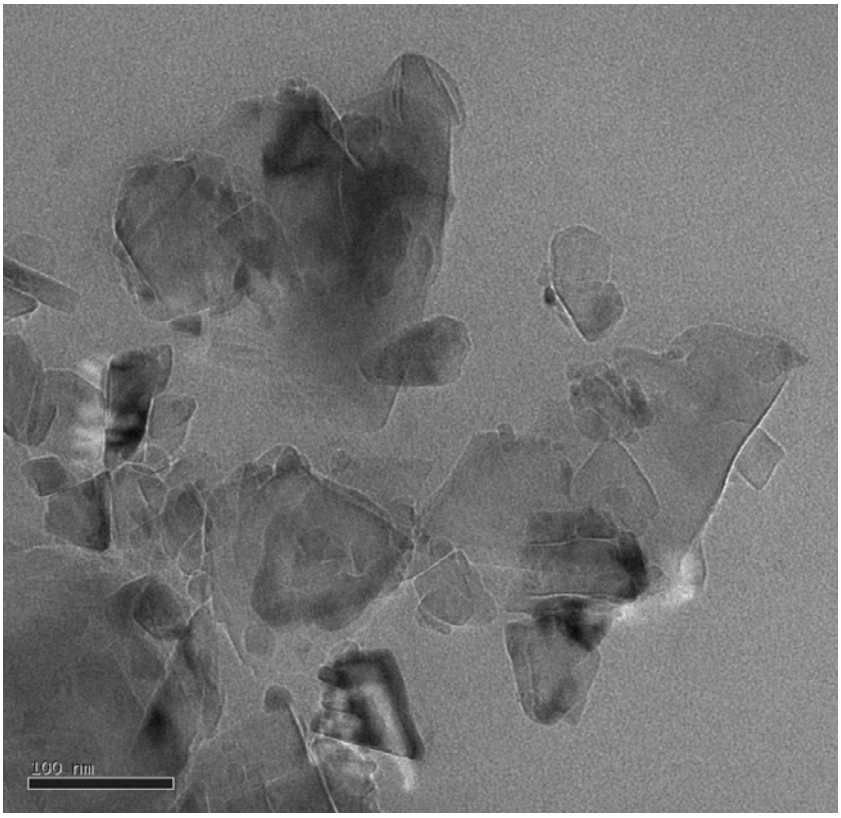

Figure 4.5 TEM image of diamond particles of MDP 0.375. Scale is 100 nm.

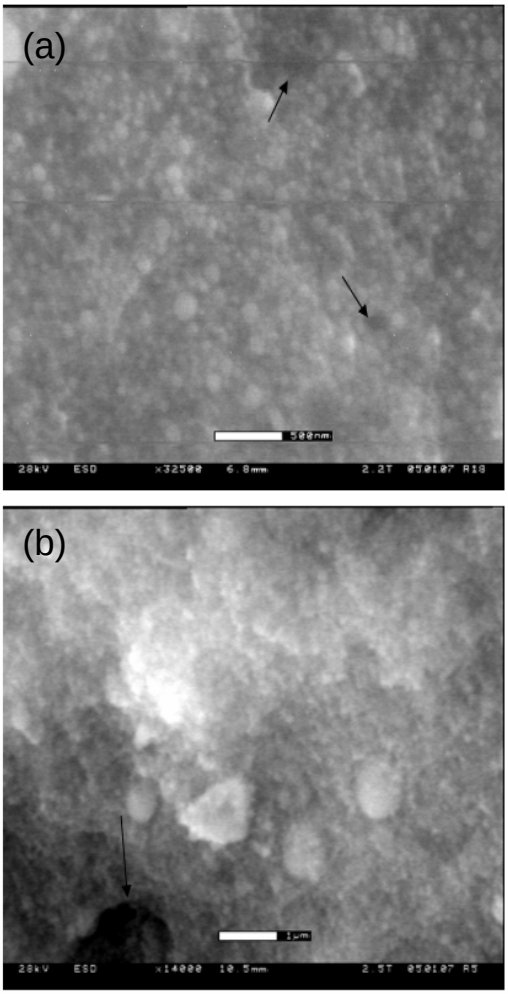

Figure 4.6 The SEM images show the fracture surface of (a) ALBT80 and (b) ALT80. Scale in (a) is 500 nm and in (b) is 1 μm.

In addition, note that the samples have limited porosity, confirming the immersion density measurements (Fig. 4.7). All of the composites measured have less than 1.5% open porosity. Optical microscopy results (not shown) indicate that there are a few large pores within the samples, with more porosity in the ALT samples than the ALBT samples. We believe that the low viscosity of the pure TEGDMA system is less likely to hold the filler and matrix together, making it easier to incorporate porosity into composites.

Fig. 4.8 (a) and (b) show the fracture surfaces of (a) ALBT74 without coupling agents and (b) ALBT80 with silanizing agents. For polymer composites, there are several mechanisms of crack propagation and failure [58, 59]. Cracks may pass through particles if fillers are weak. More likely, failure may occur along the interface of filler and matrix by debonding them or inside the matrix by cohesive failure of matrix. Fig. 4.8 (a) shows a largely smooth fracture surface, indicative of brittle fracture with little resistance to crack propagation. It is not surprising that the brittleness of polymer composites is increased by the addition of rigid fillers. In contrast, the coupled composite, ALBT80, shows a less brittle fracture surface. The rougher and raft-like features in Fig. 4.8 (b) indicate that bonding between particles and matrix can improve the toughness of composites. Several researchers have reported this behavior [58, 60]. However, this effect is less noticeable in our composites due to the effect of much higher filler volume fraction.

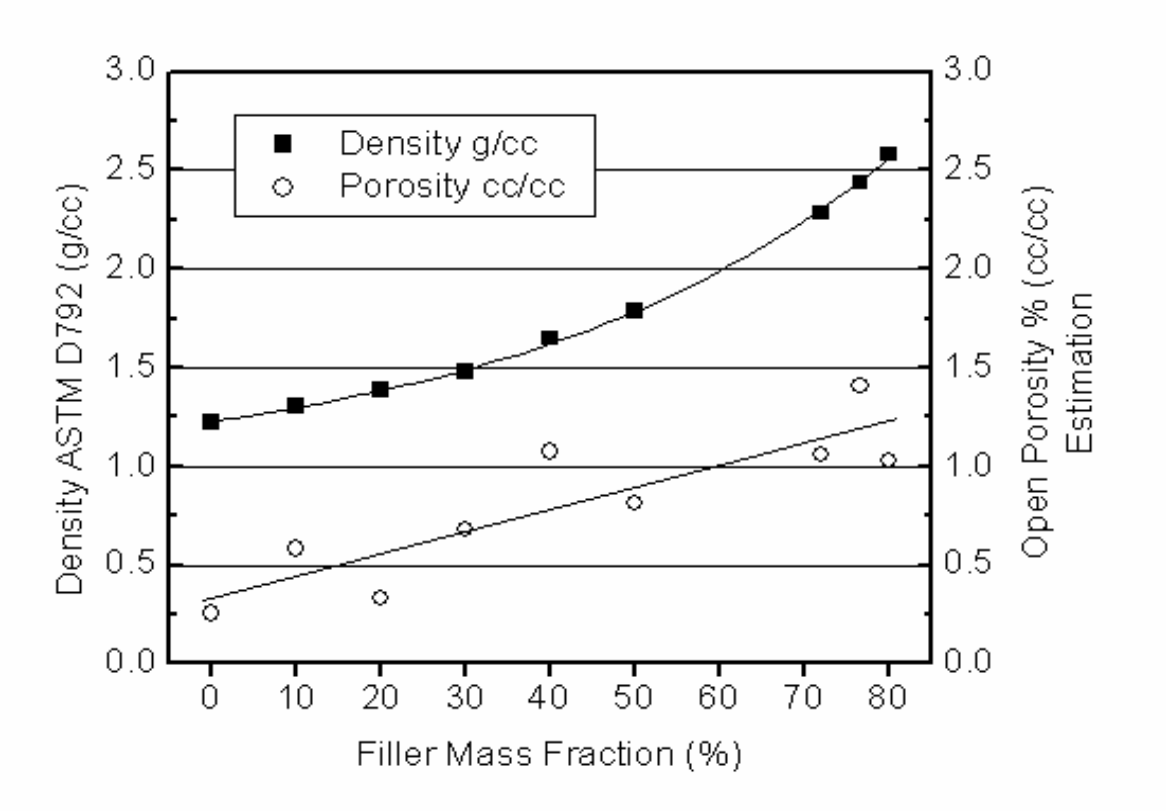

Figure 4.7 The immersion density and open porosity of the ALBT series of specimens. Density and porosity of specimens were indicated by open squares and filled squares, respectively.

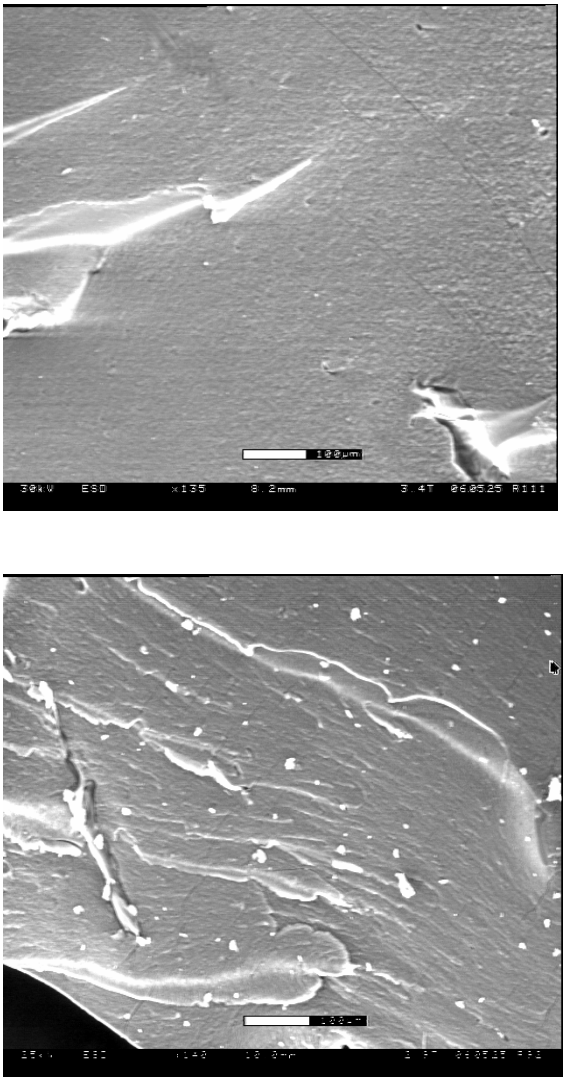

Figure 4.8 Fracture surfaces of resin composites (a) without coupling agents treated filler (brittle fracture with smooth surface) and (b) with silanized filler having rough surface texture.

4.3 Filler Loading and Degree of Conversion

Ideally, a dental resin composite will convert all of its monomer into a crosslinked network during polymerization to optimize its mechanical properties and performance. However, not every carbon double bond joins the reaction, so there is always a significant concentration of unreacted carbon double bonds (varying from 25% to 50%) remaining within resin [61, 62]. This is mainly due to the limitations on the mobility of reactive groups imposed by the rapid formation of a crosslinked polymeric network. In addition, the rigid backbone of high molecular-weight monomers used in dentistry further increases the possibility of unreacted double bonds.

The degree of double bond conversion (DC) is determined using an FT-IR spectrometer. As noted in Chapter 3, our technique is based on prior work that examined the effect of intensity and time span of exposure of light curing [62]. In our study, the DCs are measured as a function of filler loading. Moreover, the effect of temperature during thermal curing is investigated.

The conversion analysis by infrared methods relies upon calculation of the ratio of the aliphatic C=C absorption at 1640 cm^{-1} to the aromatic C-C absorption at 1608 cm^{-1} or the C=O bond at 1720 cm-1 depending on which one functions as an internal standard, as shown in Fig. 4.9. The DC is calculated using Equation 4.2.

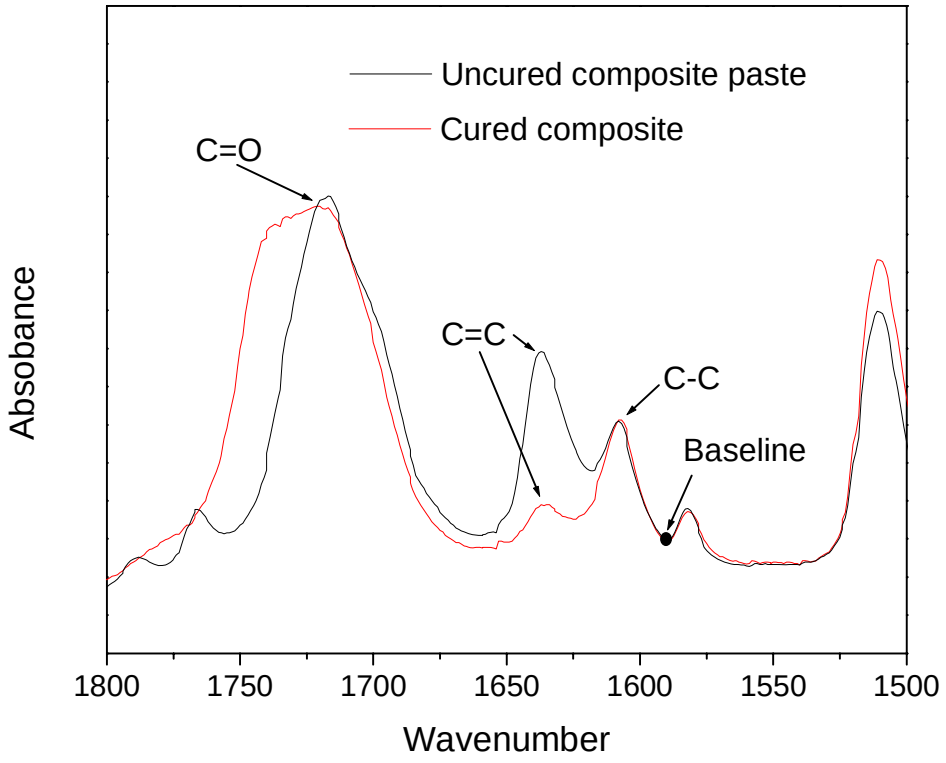

Figure 4.9 FT-IR graph of uncured and cured composite with labels on the interesting peaks.

$$DC = 1 - \frac{[A(\mathrm{C=C}) / A(\mathrm{C\text{-}C})]_{cured\_sample}}{[A(\mathrm{C=C}) / A(\mathrm{C\text{-}C})]_{uncured\_paste}} \tag{4.2}$$

4.3.1 Effect of filler loading

Resin composites with 0%, 10%, 20%, 40%, 60%, and 70% weight of Nanotek® alumina powder are prepared to investigate the relationship between DC and filler loading. Sandwich IR cards are made of these specimens and measured with FT-IR before and after curing for 6 hours at 120 ºC. The degrees of conversion are calculated according to Equation 4.2 with baseline correction by choosing the baseline to be the minimum found to the right of the C-C peak.

The results are shown in Fig. 4.10. The DCs increase from the samples of low filler loading to a maximum at the 20 wt% sample. Then it decreases with increasing filler loading. Unless we coat the surface of fillers with a coupling agent, the filler can not join into the polymerization. The presence of filler impedes polymerization by both decreasing the mobility of monomers and decreasing the contact area between monomers. Thus, theoretically, the increase of filler loading would decrease the DC of composites by above mechanisms.

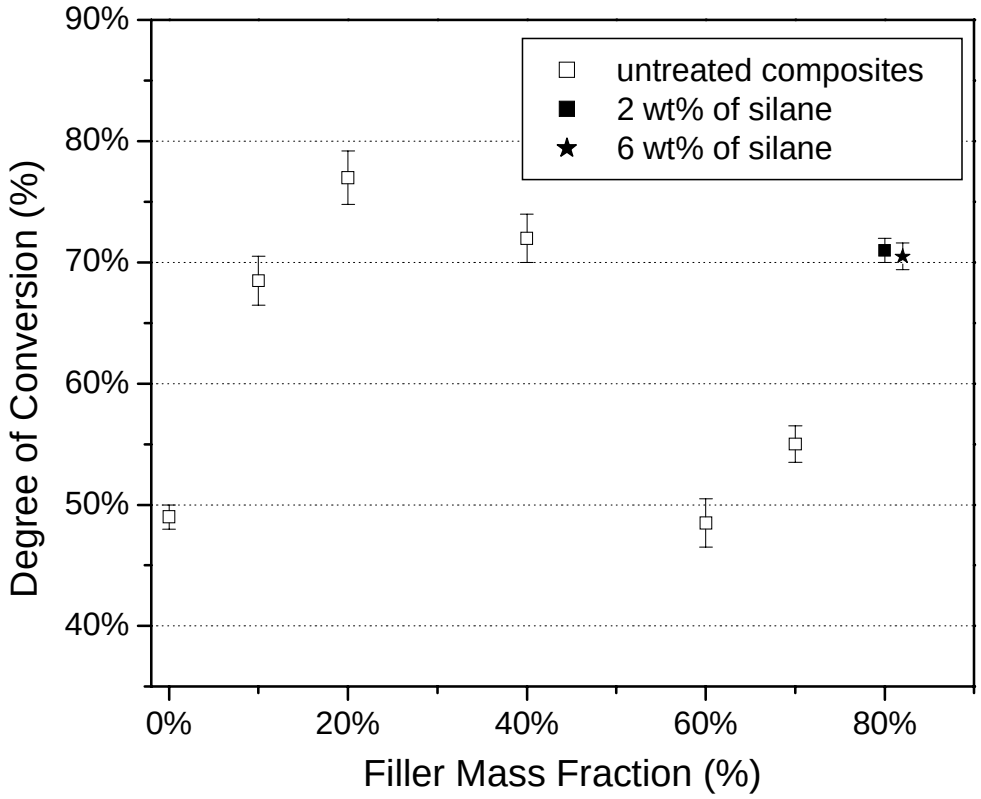

Figure 4.10 Average and standard deviation of degree of conversion vs. filler loading.

The cause of the unexpected phenomenon of lower DC for 0 and 10 wt% has not been discussed. It is possibly attributable to the ultra-thin film in the sample sandwiches. Because of the very low viscosity of lightly filled uncured paste, the paste tends to spread on the KCl IR cards and becomes very thin, i.e. less than 50 μm. The spreading of the pure resin and paste indicates the attractive interaction between the surface of IR cards and uncured samples. A similar situation is discussed in the literature, where an attractive interface for thermoplastic thin film increases the glass transition temperature (T_g) by decreasing the mobility of polymer chains [63, 64]. Thus, the attractive boundary between cards and the paste possibly decreases the mobility of monomers in our case. Therefore, the decrease in mobility of monomer in turn drops the DC of the composites for the lightly filled samples. For samples with above 20 wt% loading, the thicker paste films can be obtained. As a result, the DC of resin composites decreases as the filler loading increases except for the sample with 60 wt%.

4.3.2 Effect of silanization

As addressed above, unless the surface of the filler is coated with coupling agents, the filler can not join into polymerization. If the filler is coated with coupling agent, it is expected that the coupling agent would have an effect on the reaction by tangling itself into the matrix. The mechanism of polymerization within the bound polymer layer that is "stuck" to a particle surface is not very clear. The Nanotek® alumina particles is silanized with 3-methacryloxypropyltrimethoxysilane (MPTMS).

Two samples are measured: one with 2 wt% and the other with 6 wt% of MPTMS. Note that the weight percentage of MPTMS refers to the weight of powder and the weight fractions of powder are around 80. Each of them has an average degree of conversion of 70%, which is about 15% higher than the sample of 70 wt% filler loading without coupling agents. Therefore, the silanizing agents MPTMS influence reaction of polymerization and increase the DC. There are two possible mechanisms involved. One is that by adding coupling agents, the mobility of monomers increases. The other is that coupling agents provide a large number of reactive sites that make polymerization continue at surface of fillers. We believe that the latter is at least partially operative since the rougher fracture surfaces indicate that the filler is at least weakly bound to the matrix (Section 4.2.2).

4.3.3 Effect of curing temperature

Curing the composite at lower temperatures is desirable to minimize the thermal expansion mismatch between the composite and ceramic restoration layers. The study of the effect of curing temperature on DC is carried out on 40 wt% samples. The average degrees of conversion for the samples cured at 120 ºC, 100 ºC, and 80 ºC are 72 %, 62 %, and 56 %, respectively, and are shown in Fig. 4.11.

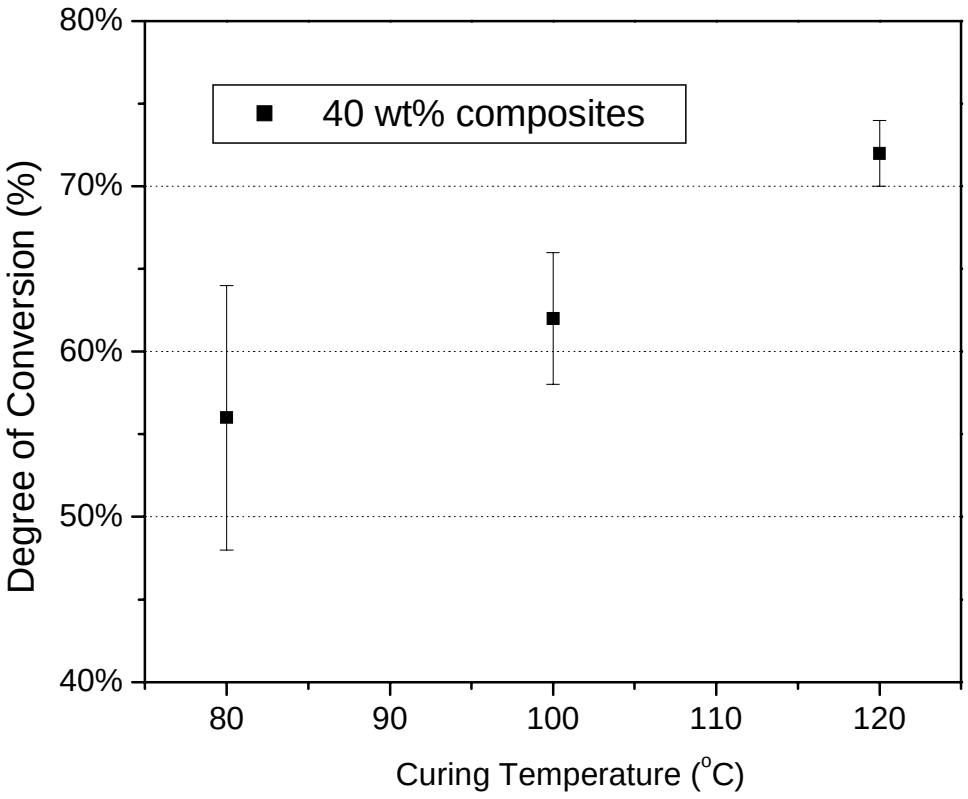

Figure 4.11 Average and standard deviation of degree of conversion in the function of curing temperature.

In addition, the standard deviations are found to be broader for the lower curing temperatures, which indicates that polymerization has already started at as low as 80 ºC during a 6 hour curing. However, the reaction does not occur uniformly across all the samples. At lower temperature, some areas are cured more than others, causing the broader deviation in DC.

Fig. 4.12 shows two DTA tests conducted on both (a) cured polymer and (b) uncured polymer. The exothermic peaks are not present for the cured polymer, indicating that the polymerization reaction occurs around 90~120 ºC. It seems contradictory to the result in Fig. 4.11, where the DC is about 56% for curing at 80 ºC. In fact, the polymerization does occur at lower temperatures, but at a much lower rate. The reason that the exothermic peak does not appear until about 90 ºC in DTA test is that the reaction is too slow at low temperatures to appear in a DTA analysis with the temperature rising at 10 ºC/minute. This information is useful for the process of compounding. If the paste is overheated, even much lower than 90 ºC, polymerization can take place. When polymerization occurs partially, compounding becomes more difficult because of the longer chains of polymer appearing in the matrix. They tangle together to increase the viscosity of the paste.

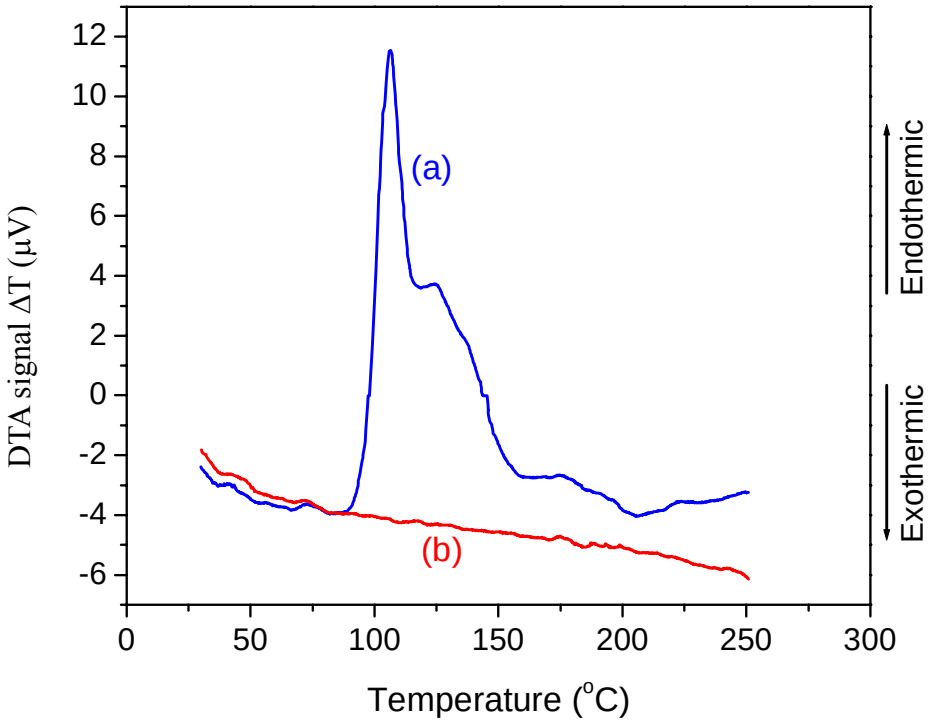

Figure 4.12 DTA curves of (a) uncured Bis-GMA/TEGDMA paste and (b) cured Bis-GMA/TEGDMA resin.

4.4 Mechanical Characterization from Nanoindentation

Most mechanical studies of dental resin composites have been focused on flexural properties to examine flexure and fracture of bulk materials. This is appropriate when the composites are used in bulk applications, such as construction materials and some sport equipment. Recently, indentation modulus and hardness studies have become popular since they provide information that may be more relevant to applications that involve localized, non-uniform deformation or point contacts or very small parts such as those used in dentistry. They have been used to examine the mechanical properties of dental restorative materials [65-68]. They also provide a measure of stiffness as well as hardness and do not require specific sample shapes or elaborate specimen preparation. In addition, indentation methods are especially useful when specimen dimensions are limited, as in the case of measuring elastic modulus in thin joins in our sandwich structures.

In our studies, we examine aluminum oxide (E~370 GPa depending on its structure) and diamond (E~900-1200 GPa) as high modulus fillers. Silicon oxide (E~70 GPa) is used as a benchmark since it is widely used in dentistry. We expect that, with the same volume fraction of fillers, the resin composites filled with higher modulus materials will possess significantly higher elastic modulus. In order to make compounding (uniformly mixing the filler into the resin matrix) easier, which allows higher filler loading for the same effort, multimodal fillers are examined as well.

The interface between fillers and matrix is important. We have explored several surfactants and coupling agents to make mixing the composite easier and/or improve the bonding between filler and matrix. For silica, well-accepted silanizing agents are used to modify the powder. For alumina, the same silanizing agents are examined. In addition, commercial phosphate based surfactants and thion primers are examined as well. Besides, organotitanates and zirconates coupling agents are tested. However, while diamond has a much higher elastic modulus than alumina, surface treatment remains an issue due to the relatively inert surface of diamond. The adoption of a surface treatment effectively increases the maximum diamond filler loading, but chemical bonding between diamond and organic matrix is not readily achievable. Unlike the surface of alumina and silica, the diamond surface contains a C-H bond. In order to get the functional groups for chemical reactions, further treatments are necessary, i.e. UV-irradiation or plasma modification. These methods are not tried in our study for practical reasons [69].

4.4.1 Nano-sized aluminum oxide as filler

Elastic modulus and hardness of untreated resin composites

Two resin composite systems with untreated powder are made: Al_2O_3 powder with Bis-GMA/TEGDMA monomers (ALBT) and Al_2O_3 powder with pure TEGDMA (ALT). In the ALBT system, the resin monomer in most samples consists of 49.0 wt%

Bis-GMA, 49.0 wt% triethylene glycol dimethacrylate and 2.0 wt% benzoyl peroxide (BPO) solution. The effect of Bis-GMA/TEGDMA ratio will be discussed later.

The other system ALT is explored since its viscosity is much lower than ALBT system. It consists of TEGDMA with 2 wt% BPO. In both systems BPO acts as an initiator for crosslinking. The powder is directly added into monomer solution and compounded with the electronic mixing apparatus described in Chapter 3. The weight percentage of filler loading is confirmed by TGA test. The errors do not exceed 0.5 wt%. Without any additives, the maximum filler loading is around 72 wt% (46.6 vol%) for ALBT systems.

The elastic modulus of the composites is obtained from nanoindentation testing. All the tests presented in the figures for each composition are obtained from a single sample to minimize effects from minor processing variations. Multiple samples (at least 2~3 different samples) with the same composition have been tested in order to examine the repeatability of mechanical properties of the resin composites. Due to the inevitable variation in the manual processing, slight differences in weight fractions exist. However, the elastic modulus and hardness values all follow similar trends and the variations between samples are no more than 1~3 %. As noted in Chapter 3, the measurements are made on ground and polished crosslinked composites with indents far enough apart (300 μm) to not interact with each other. The elastic modulus values measured by nanoindentation are shown in Fig. 4.13.

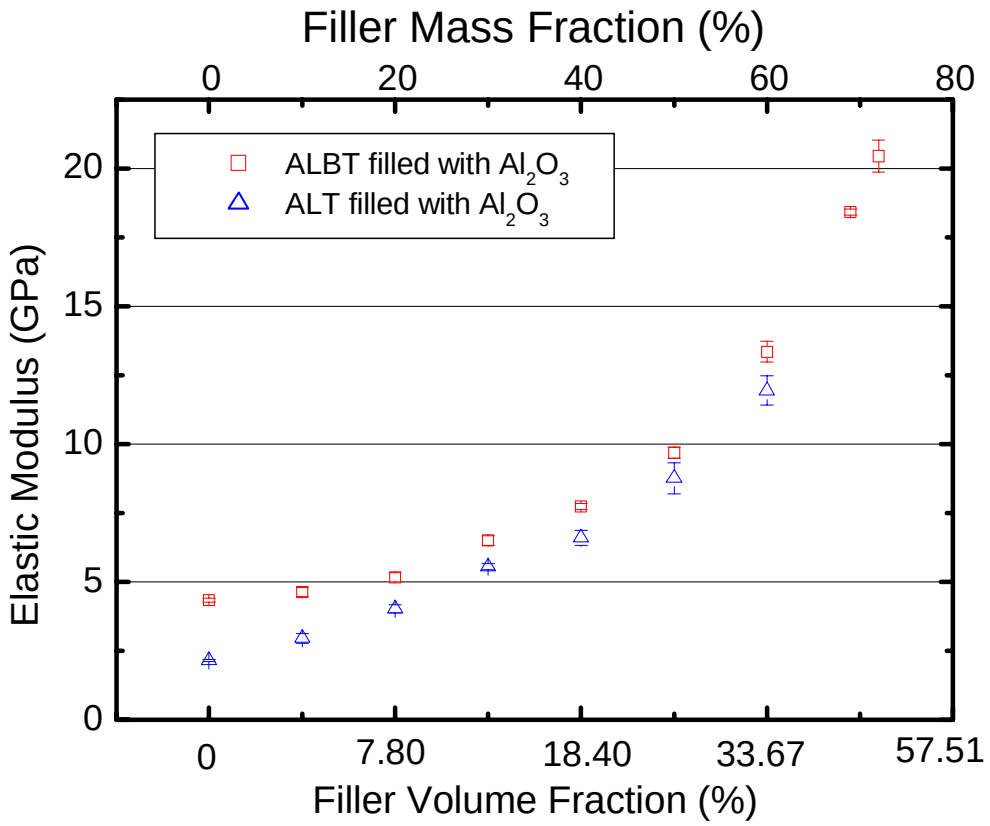

Figure 4.13 Elastic modulus of composites measured using nanoindentation. Values of ALBT and ALT systems are shown with red squares and blue triangles, respectively. Bottom coordinate and top coordinate are indexed by volume and weight percent, respectively.

The elastic modulus for ALBT systems increases from 4.6±0.1 GPa (0 wt% filler) to 20.4±0.6 GPa (72 wt% filler). While the elastic modulus for ALT systems increases from 2.1±0.0 GPa (0 wt% filler) to 11.9±0.5 GPa (60 wt% filler), the loading level of Al_2O_3 has significant effects on composite properties. The ALT system has a lower elastic modulus than the ALBT system for all alumina additions, but the ALT system displays a similar trend with respect to the increase in elastic modulus with increasing amounts of nano-alumina filler.

Since our composite can be described as a two-phase entity, the modulus trend observed is not unexpected. In the low filler weight percent region, the modulus of the composite is mainly dominated by the resin matrix since the filler particles are not networked. In this case, the effect of filler modulus is small. However, at higher filler loadings, the particles are more likely to be in contact, eventually forming a network. Then, their inherent mechanical properties play a much larger role in the stiffness of the composite.

The loading level of Al_2O_3 has significant effects on composite properties even without effective bonding between particles and matrix. It is not a contradiction with what has been stated in Section 2.2.2. Polymers have a much higher (20-30 times) thermal expansion than mineral fillers and thus, in a well-dispersed composites, there will be an intimate interaction between matrix and filler, which results from the compressive stress from matrix on filler developed on cooling and shrinkage [70]. This type of interaction at the very least is mechanical and probably weak compared to chemical

bonding. However, it is sufficient to transfer a certain amount of stress from matrix to filler, especially when subject to a compressive load. Our results show that with a reasonably monodispersed nano-sized high modulus filler, relatively high elastic modulus resin based composite adhesives are possible.

The properties of the matrix itself also play an important role in determining the overall properties of resin composites. ALT composites with a relatively softer matrix system possess lower elastic modulus and hardness compared to those ALBT composites with the same filler loading level. But the gap between ALT and ALBT composites for the same filler loading decreases as filler fraction increases. This can be assigned to the fact that the proportion of matrix decreases as more filler is added and the matrix plays less of a role in determining the mechanical properties of the composites. The effect of weight ratio of Bis-GMA and TEGDMA on elastic modulus of cured composites is also investigated.

Fig. 4.14 shows resin composites with four matrix systems with different ratios of Bis-GMA/TEGDMA, which are 50/50, 60/40, 70/30 and 80/20, respectively. Except for the 50:50 composites, the composites are filled with 0, 20, 40, 60 and 72 weight percent filler. For pure polymer, the resin with the highest portion of Bis-GMA possesses the highest elastic modulus because of the higher portion of stiffer Bis-GMA.

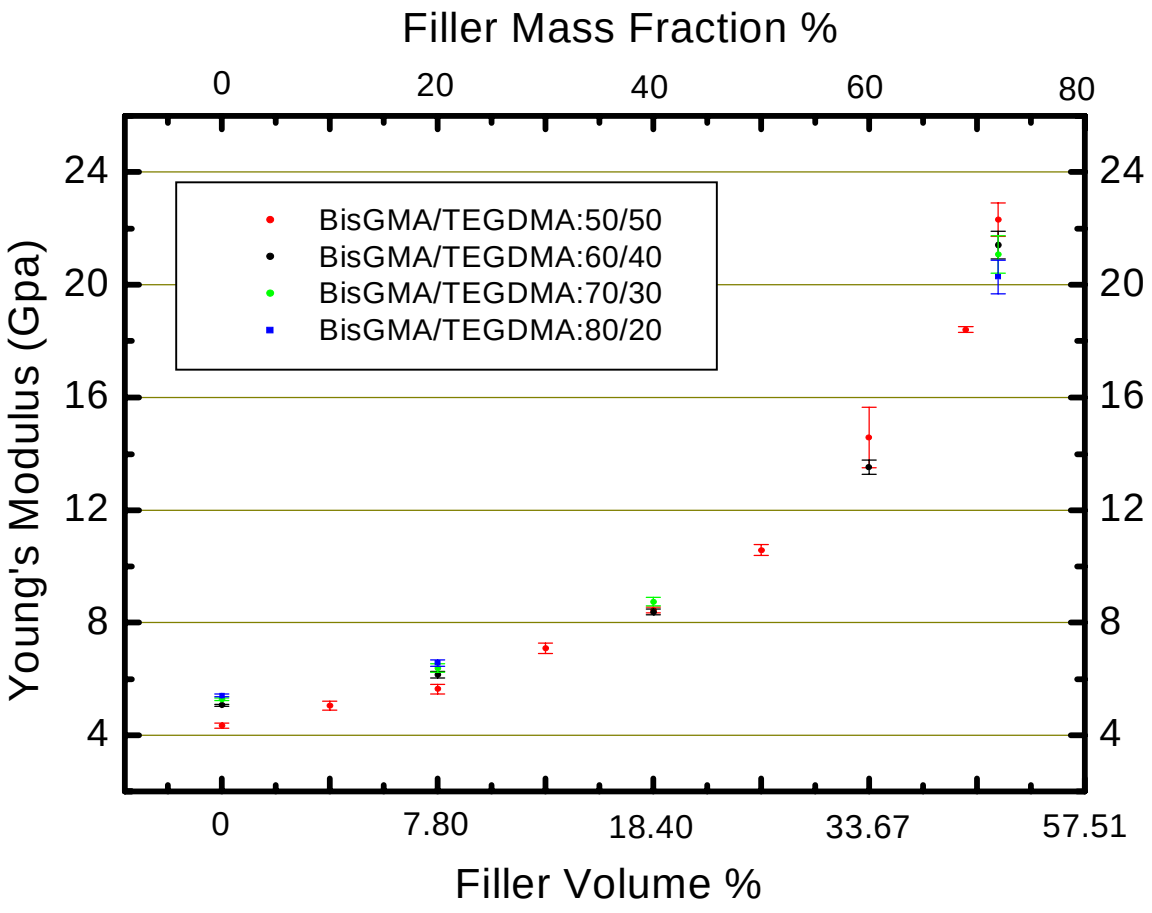

Figure 4.14 Elastic modulus of composites with various ratios of Bis-GMA/TEGDMA at various filler loading.

For composites with high filler loading, the 80:20 Bis-GMA/TEGDMA has the lowest elastic modulus with higher standard deviations. This phenomenon is due to the much higher viscosity of the paste associated with both the higher portion of Bis-GMA and the higher filler loading. When it is too high, it impedes the movement and rotation of reactive monomers. Thus, it in turn decreases the possibility for monomers to find their reactive neighbors. So, the degree of conversion will be decreased by this mechanism. Decreasing the DC drops the elastic modulus of 80:20 Bis-GMA/TEGDMA composites compared to counterparts with a lower portion of Bis-GMA at the same filler loading.

The hardness data are shown in Fig. 4.15. They are obtained from the same measurements as elastic modulus. Just like elastic modulus, hardness increases as the proportion of filler increases. However, the increase in hardness is more nearly linear as compared to the modulus. ALBT hardness increases from 243±7 MPa (0 % filler) to 753±50 MPa (72 wt% filler) and ALT hardness increases from 93±2 MPa (0 % filler) to 531±22 MPa (60 wt% filler).

The degree of uniformity in mechanical properties and achievable dimensional tolerance are major concerns for nanocomposites in dental applications. Vickers hardness data are measured for the ALBT system for comparison with the nanohardness data to ascertain bulk mechanical properties. The filled squares in green in Fig. 4.15 show that the microhardness data are generally comparable to the nanohardness data in terms of the magnitude and the trend with increasing filler loading.

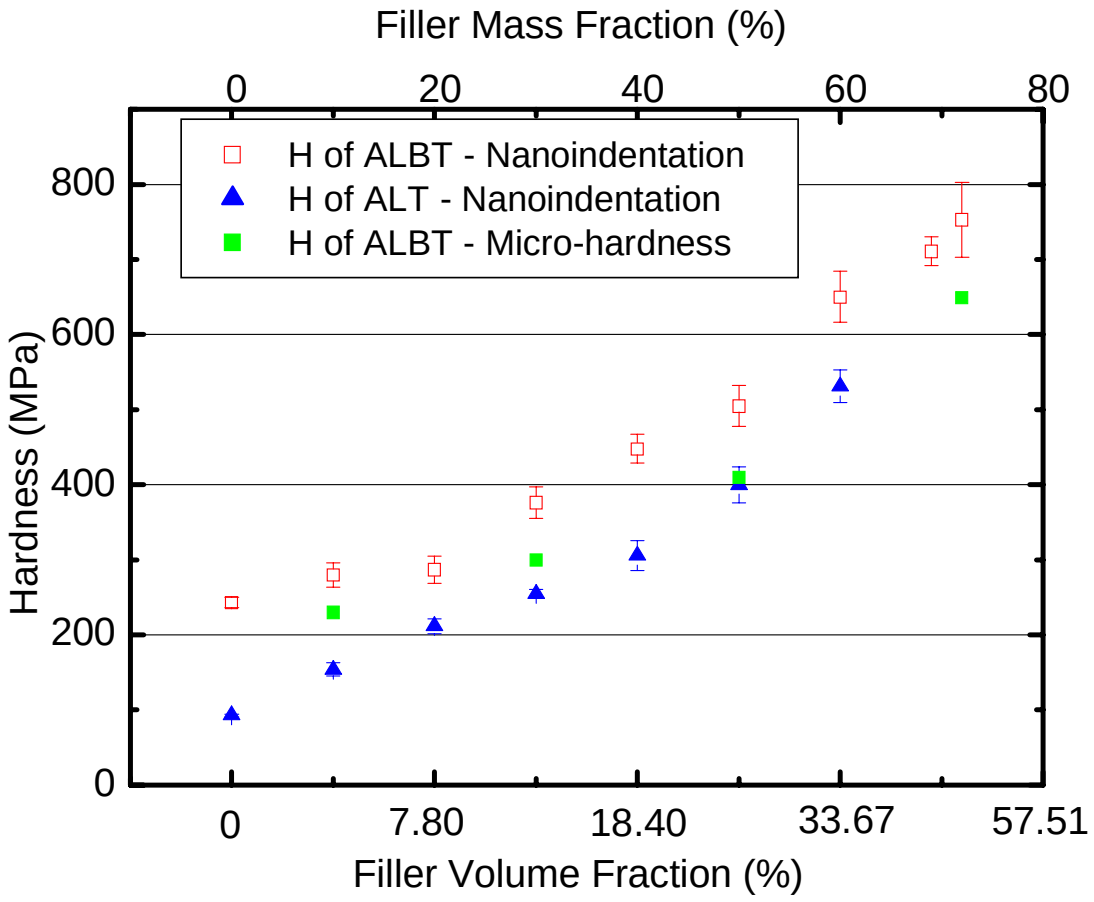

Figure 4.15 Hardness of composites measured using nanoindentation. Values of ALBT and ALT systems are shown with red squares and blue triangles, respectively. Microhardness values are shown with green square symbols. Bottom coordinate and top coordinate are indexed by weight and volume percentage respectively.

This indicates that the nanoindentation hardness test results are representative of the overall mechanical properties of the composites, which is consistent with our expectation from Section 3.4.3. This result highlights the benefit of using a nanoparticle filler phase. The nanoparticles allow a more homogeneous distribution of the filler within the matrix on a finer microstructural scale. (If the filler particles had been larger or the indentation load had been significantly lower, the nano-hardness results would have been subject to a larger variation since the local composition of the indentation region would reflect the influence of an individual particle or the lack of particles in a given area.) Since our composites are being developed as potential adhesives used as joining layers in all-ceramic crowns, the finer microstructural scale will allow thinner join layers to be used in dental restorations. This is particularly important if the geometry of the restoration causes the join layer thickness to vary since it will allow thin areas (~10 μm) to have the same degree of reinforcement as thicker areas (50~100 μm).

The ratio of elastic modulus and hardness is often used to describe the deformation of materials [47, 71-73]. In Fig. 4.16, the red line shows the linear fit of modulus and hardness of composites at various filler levels and unfilled resin. With linear fit through origin and correlation coefficient R of 0.9720, the modulus is very roughly related to hardness by

$$E = 22.4\,H \tag{4.3}$$

However, the linear fit does not describe the relationship of E and H for our sample accurately. Nevertheless, the polynomial fit describes the relation of E and H better.

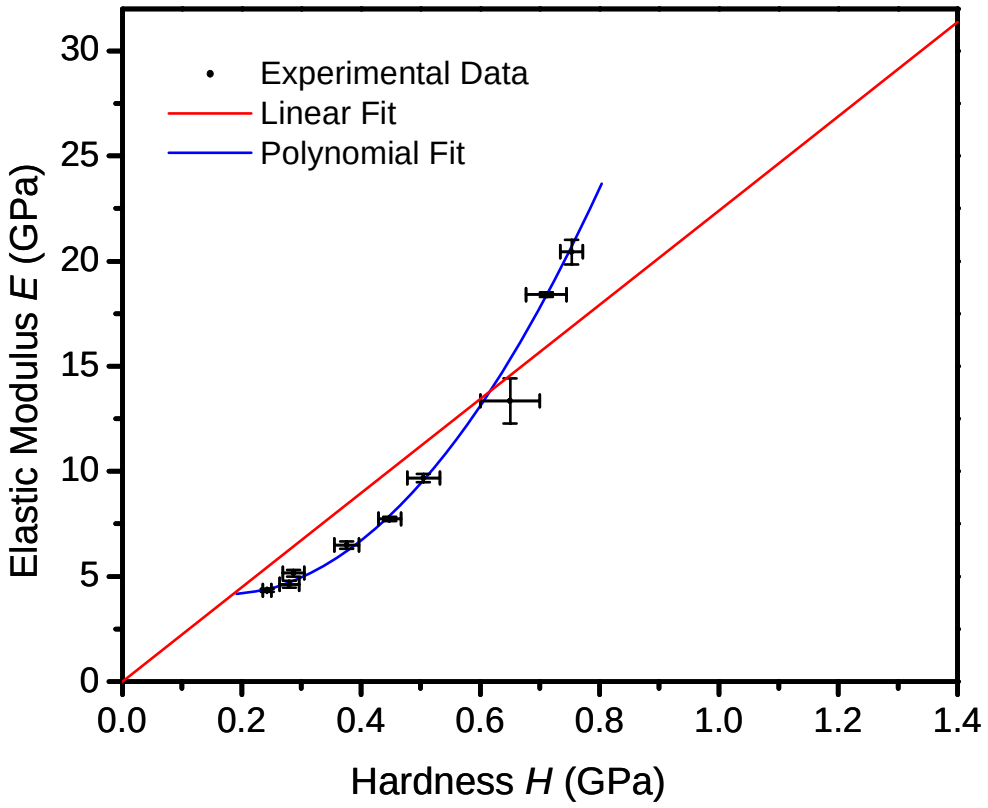

Figure 4.16 Elastic modulus versus hardness for composites at various filler levels. Each datum is the mean with horizontal error bar showing one SD with n=9 in hardness, and vertical error bar showing one SD with n=9 in modulus. Linear regression through the origin provides a correlation coefficient (R-0.9720). The elastic modulus is very roughly linearly related to the hardness by a constant, $E \approx 22.4H$. The polynomial fit is plotted with blue curve.

Elastic modulus and hardness of treated resin composites

I. Phosphate surfactants

The effect of several surfactants on mechanical properties of resin composites is investigated. After getting the highest unmodified filler loading (72 wt%), surfactant is added to assist compounding. The filler loading can be raised up to about 80 wt%, depending on the surfactant and its concentration. All surfactants can increase the maximum filler loading; however, Triton® H66 is the most promising. By using H66, elastic modulus for ALBT systems increases from 20.4±0.6 GPa (72 wt% filler) to 29.2±0.4 GPa (80 wt% filler) as shown in Fig. 4.17. While the elastic modulus for ALT systems increases from 11.9±0.5 GPa (60 wt% filler) to 23.0±3.0 GPa (80 wt% filler). ALBT hardness increases from 753±50 MPa (72 wt% filler) to 949±28 MPa (72 wt% filler) and ALT hardness increases from 531±22 MPa (60 wt% filler) to 760±56 MPa (80 wt% filler) as plotted in Fig. 4.18. For ALBT80 the hardness is 949 MPa for nanoindentation test and 912 MPa for microhardness test. Both the elastic modulus and hardness continue to increase by following the trend of untreated resin composites. Both Fig. 4.17 and 4.18 show the other surfactants, H55, QS-20 and QS-44, are not as effective as H66. At a similar filler fraction level, the elastic modulus and hardness are relatively low for the other surfactants. In addition, the water-like viscous ALT can not hold the filler effectively for higher filler loading samples, which causes the much higher deviation of ALBT (80 wt% filler) in Fig. 4.17 and 4.18 and more open pores inside the cured resin composite (Fig. 4.6).

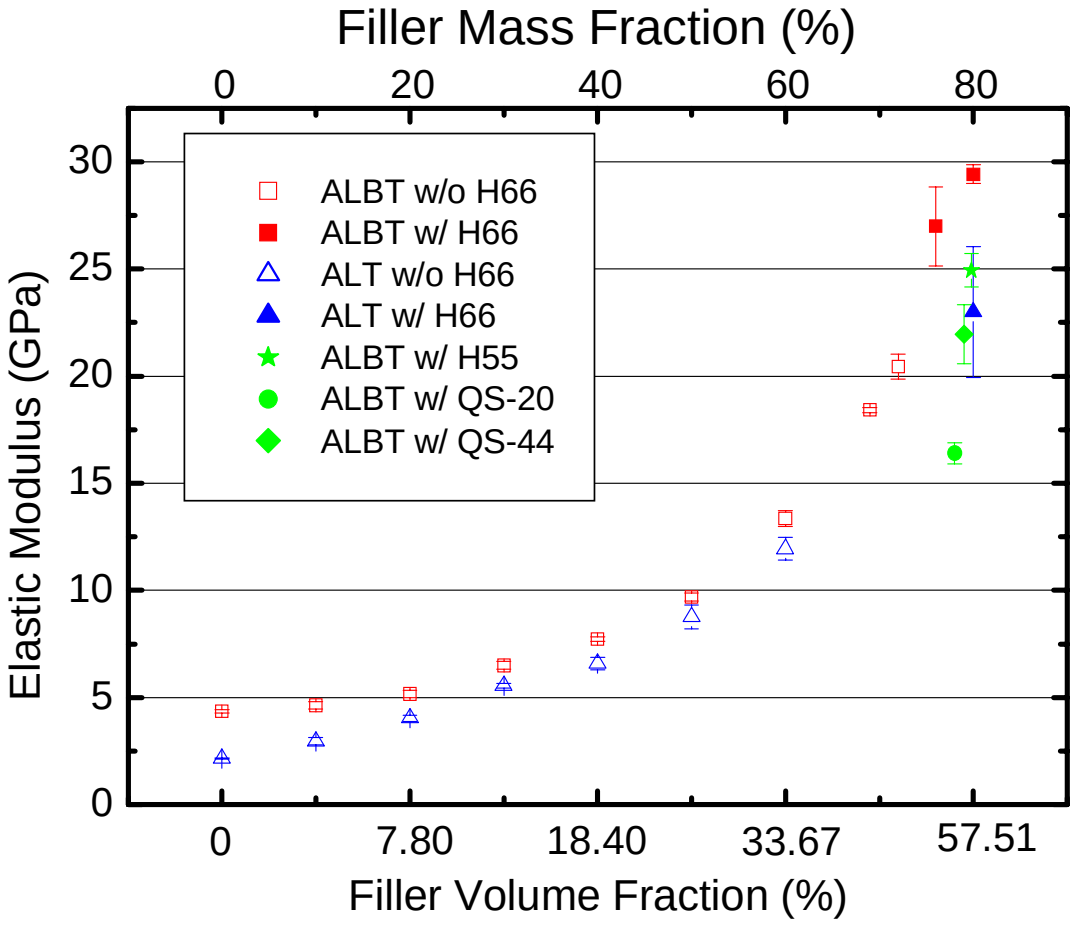

Figure 4.17 Elastic modulus of composites with added surfactant measured using nanoindentation. Values of ALBT and ALT systems are shown with red squares and blue triangles, respectively. Filled symbols represent the composites treated by various surfactants.

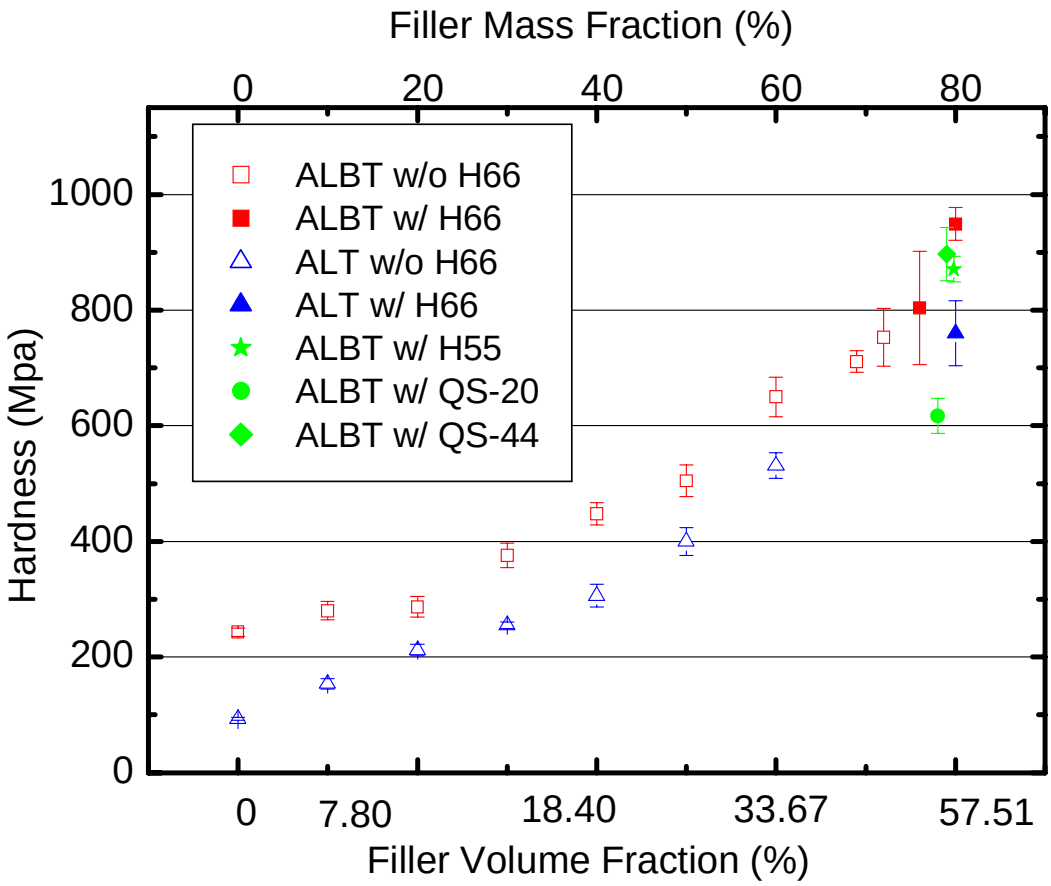

Figure 4.18 Hardness of composites with added surfactant measured using nanoindentation. Values of ALBT and ALT systems are shown with red squares and blue triangles, respectively. Filled symbols represent the composites treated by various surfactants.

II. Thione primers

Because there are no vinyl groups in the above surfactants, they are unable to react chemically with the matrix. We believe that the surfactants act more like plasticizers and do not create any significant bonding between the alumina filler and matrix, even though it decreases the viscosity of paste and eases compounding. Thus, another type of additives, coupling agents, is explored. They are believed to form a bond between alumina filler and matrix. In dentistry, such agents are usually used to provide bonding between ceramics and resin composites. They are called primers. Two types of primers are investigated: Metalprimer II and Metaltite. As shown in Fig. 4.19, the modulus values when they are present basically fall onto the curve of modulus vs. filler loading. However, in Fig. 4.20 the hardness of these specimens is around 20% higher than their counterparts treated by surfactants indicating much stronger bonding.

III. Silane coupling agents

Besides primers, some resin composites are reinforced with silanized alumina powder. The alumina powder is treated with 2 wt%, 4 wt% and 6 wt% of MPTMS. Here the weight percentages are relative to the powder and not the whole resin composites. The weight percentages of filler are finally determined by TGA. The results for elastic modulus are compared with those for composites with and without surfactant, H66, in Fig. 4.21.

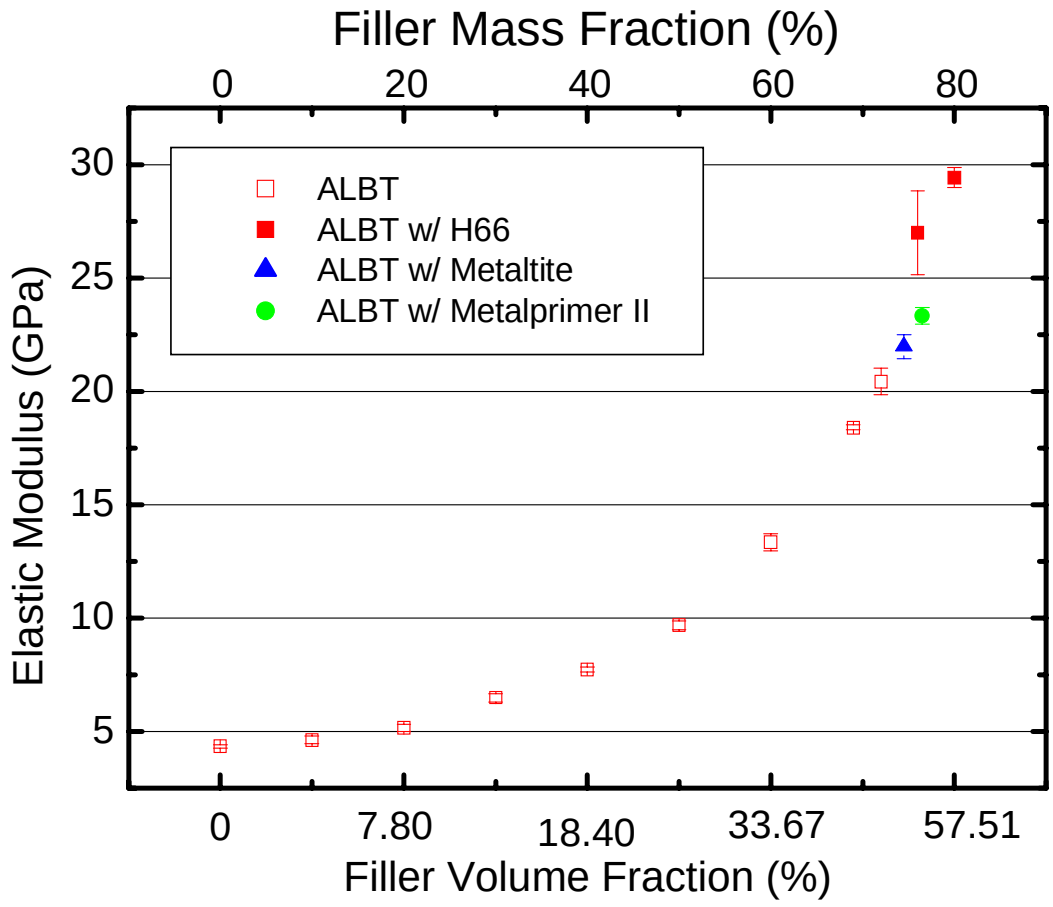

Figure 4.19 Elastic modulus of composites measured using nanoindentation. Filled symbols represent the composites treated by surfactant, H66, (red) and thione primers (blue and green).

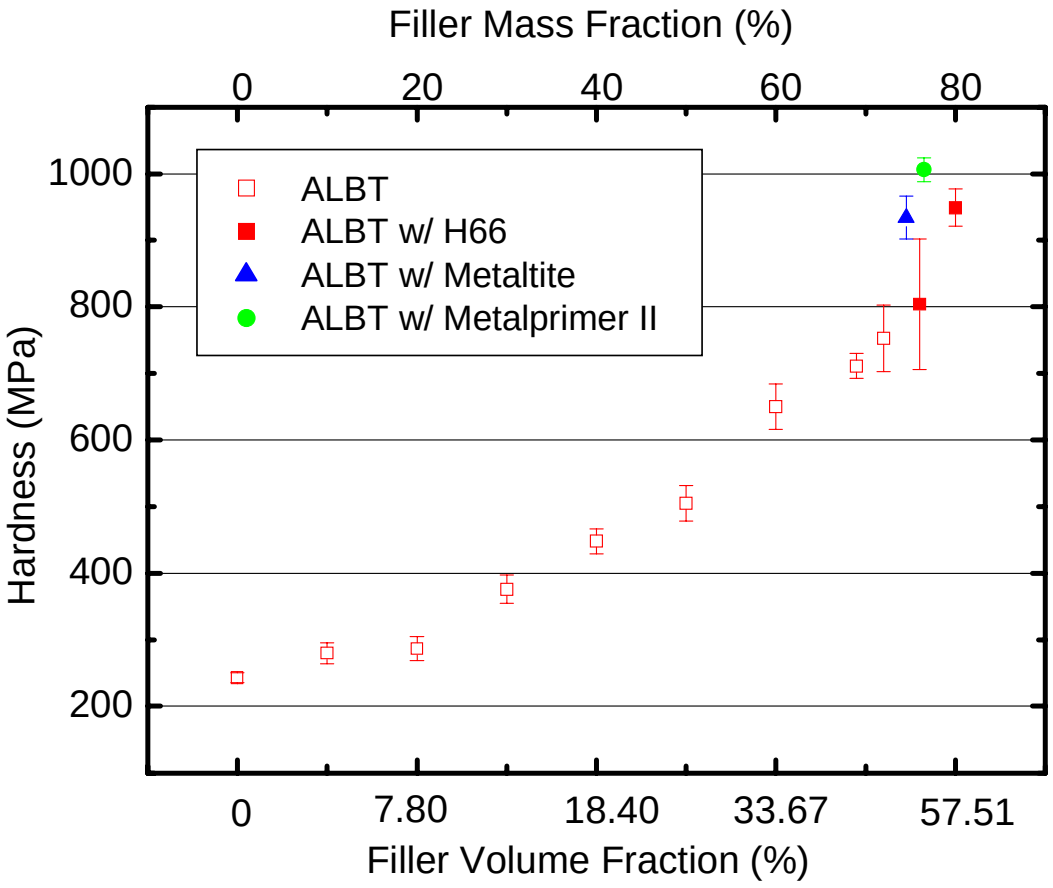

Figure 4.20 Hardness of composites measured using nanoindentation. Filled symbols represent the composites treated by surfactant, H66, (red) and thione primers (blue and green).

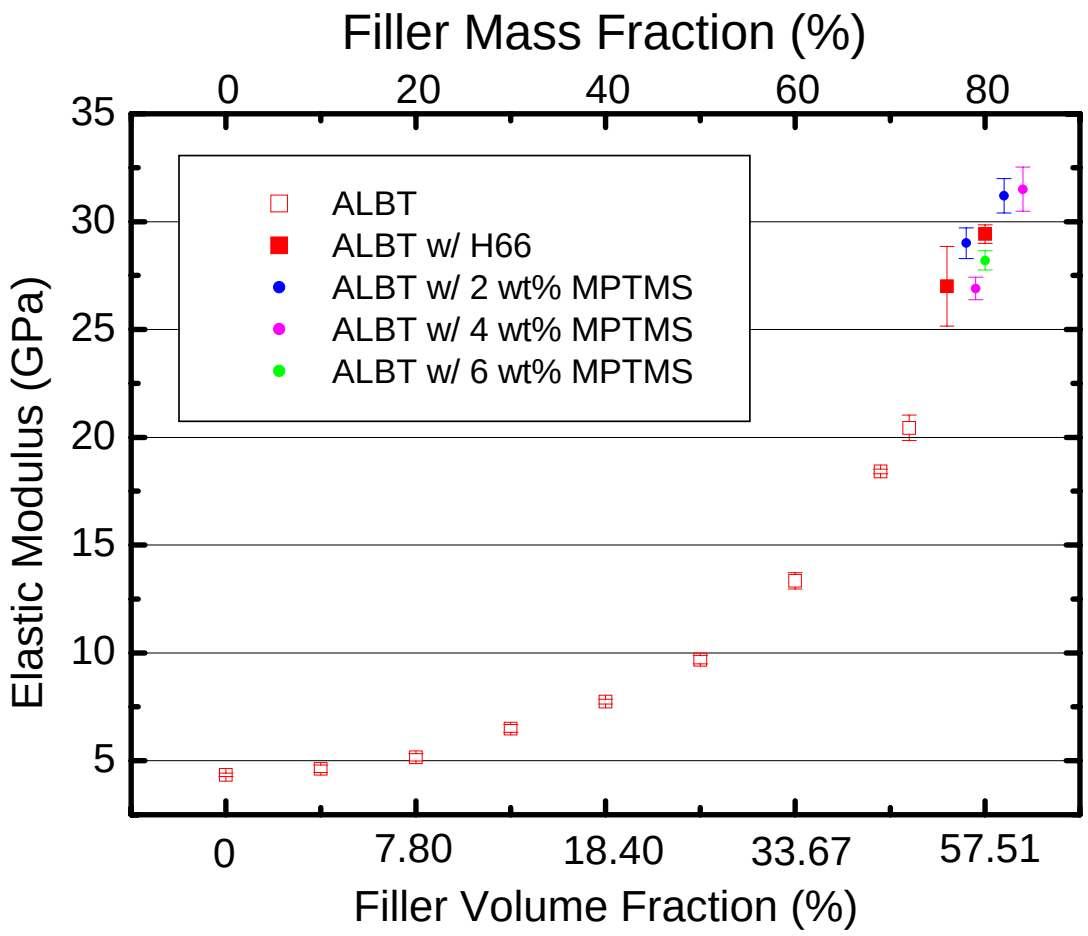

Figure 4.21 Elastic modulus of composites measured using nanoindentation. Filled symbols represent the composites treated by surfactant, H66, and silane (MPTMS).

Apparently, the variation of elastic modulus does not go beyond the tendency of change of elastic modulus for unmodified alumina/resin composites. Applying 2 and 4 wt% of MPTMS increases the maximum of filler fraction up to 83 wt%, which gives us the highest elastic modulus (31.5 GPa) for alumina reinforced resin composites. Fig. 4.22 shows the hardness of these three composites. The samples with 4 wt% of MPTMS have much higher hardness while too much of silane (6 wt%) decreases the hardness.

IV. Organotitanates and zirconates

Organotitanates have drawn great attention in recent years as an interesting class of surface modifier. They are derivatives of orthotitanic acid. The natural chemistry of titanium causes problems in some applications. The organozirconate products that are analogous to the titanates are developed to overcome this. It is generally claimed that organotitanates are effective on a wide variety of particulate mineral surfaces although no comprehensive study has been made. Most of the literature is of a commercial or purely empirical nature and there have been virtually no basic scientific studies [74]. The chemical structures of organotitanates and zirconates are illustrated in Section 3.2.3. Unlike the silicon to carbon bond for silanes, the titanium to carbon bond is very unstable and can not be used to serve as bridging for surface-treatment applications [49]. Thus, the substituents are linked by titanium-oxygen-carbon bonds and their chemistry is dominated by their hydrolytic sensitivity.

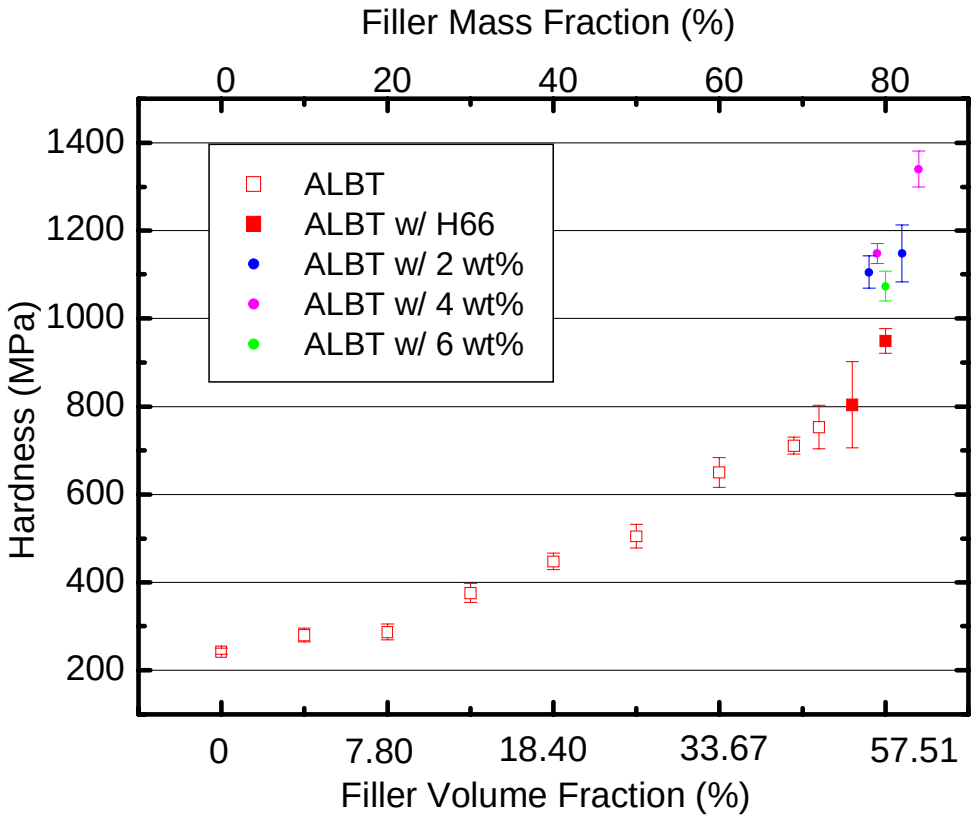

Figure 4.22 Hardness of composites measured using nanoindentation. Filled symbols represent the composites treated by surfactant, H66, and silane (MPTMS).

The effectiveness of two coupling agents, KR55 and NZ33, is examined, as shown in Table 4.1. Although they effectively decrease the viscosity and increase the filler loading to around 80wt% just as the surfactants do, the elastic modulus and hardness of these two resin composites are lower than those treated by other methods. The result is consistent with doubt that has been thrown on these products, i.e. there is better dispersion of the filler due to the presence of the titanate, but no evidence of a chemical bond between filler and matrix [49, 75].

Table 4.1 *E* and *H* of resin composites treated by organotitanates and zirconates

Sample	Modulus (GPa)	Hardness (MPa)
KR55 treated(~79 wt% filler)	28.8±0.9	931±35
NZ33 treated(~78 wt% filler)	27.8±1.3	847±60

4.4.2 Bimodal and micro-sized aluminum oxide as fillers

Relatively larger particles have a smaller specific area for the same mass. Thus, theoretically, they should be easier to compound into the resin matrix. In addition, if the distribution of particle size is broad, or bimodal, the smaller particles could fill in the spaces between the larger particles, yielding higher filler loading for a given amount of matrix. We have done some work in this area. Experimentally, it is easier to compound micro-sized particles than nano-sized particles. For example the maximum filler fraction without surfactant is 80 wt% for 3 micron alumina powder compared to 72

wt% for nanoalumina. As shown in Fig. 4.23, the larger particle reinforced resin composites have similar modulus than nano-particle reinforced ones. However they also have a larger standard deviation for both modulus and hardness. We attribute the effect to the increased influence on the nanoindentation tip by the larger particles. In the case of bimodal particle fillers, we are able to obtain the 80 wt% filler loading by mixing 1:3 (wt%) nano:3-μm without adding surfactant. The modulus of this specimen is 29.4 GPa, which is very close to that of resin reinforced with nanoparticles. However, some non-quantitative work shows that the adhesive join made of micro-sized resin composites is of low toughness because the larger particles could serve as large stress concentrators, which increases the brittleness of resin composites.

4.4.3 Nano-sized silica as fillers

Nano-sized silica is examined as a filler material in control specimens since most of the commercial dental resin composites are reinforced with silica or related materials. The powder is silanized by using 4 wt% of MPTMS and then added directly into the Bis-GMA/TEGDMA:50/50 resin. The elastic modulus is shown in Fig 4.24 with comparison to various fillers, including alumina and diamond. Because of the differences in density among different types of fillers, only volume fraction of filler is used to compare filler loading levels. The silica reinforced resin composites have lower elastic modulus compared to the same filler loading of alumina, and the difference increases as the loading increases. It is attributed to the low stiffness of silica filler.

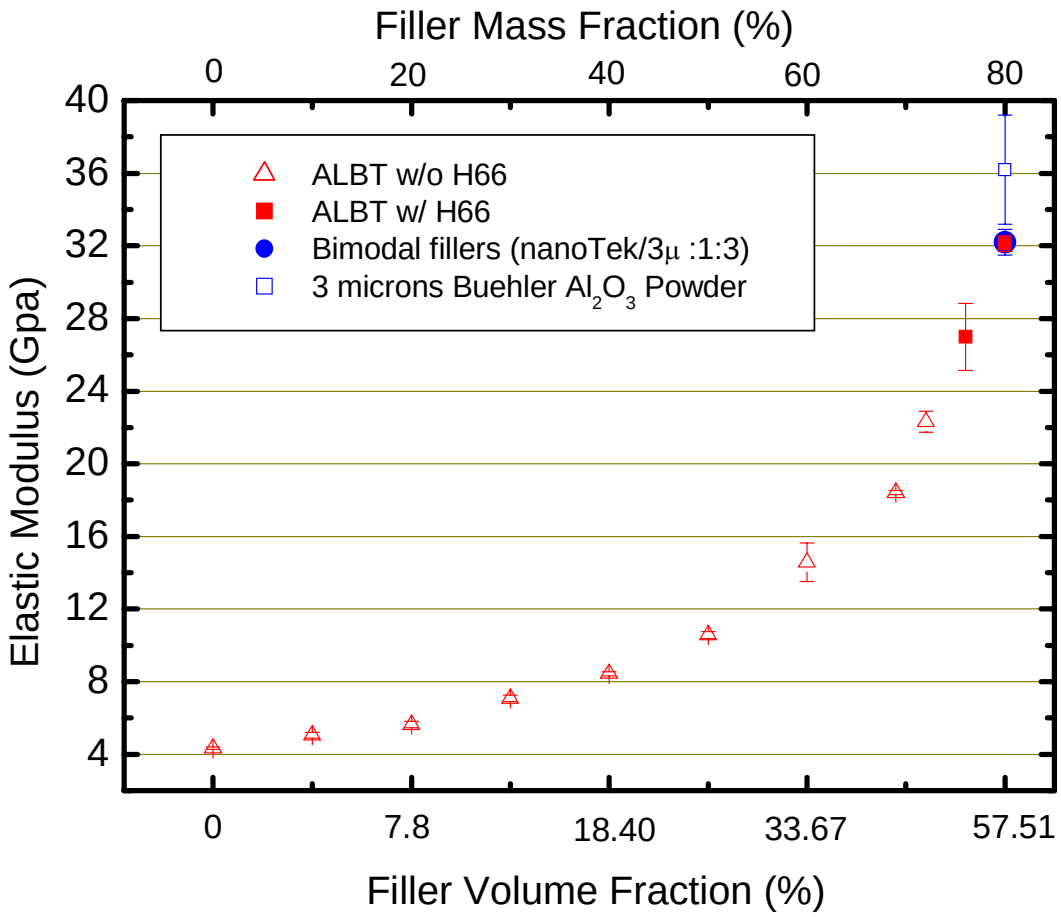

Figure 4.23 Elastic modulus of composites measured using nanoindentation. Resin composites with nanoparticle, bimodal and 3 microns particle are compared.

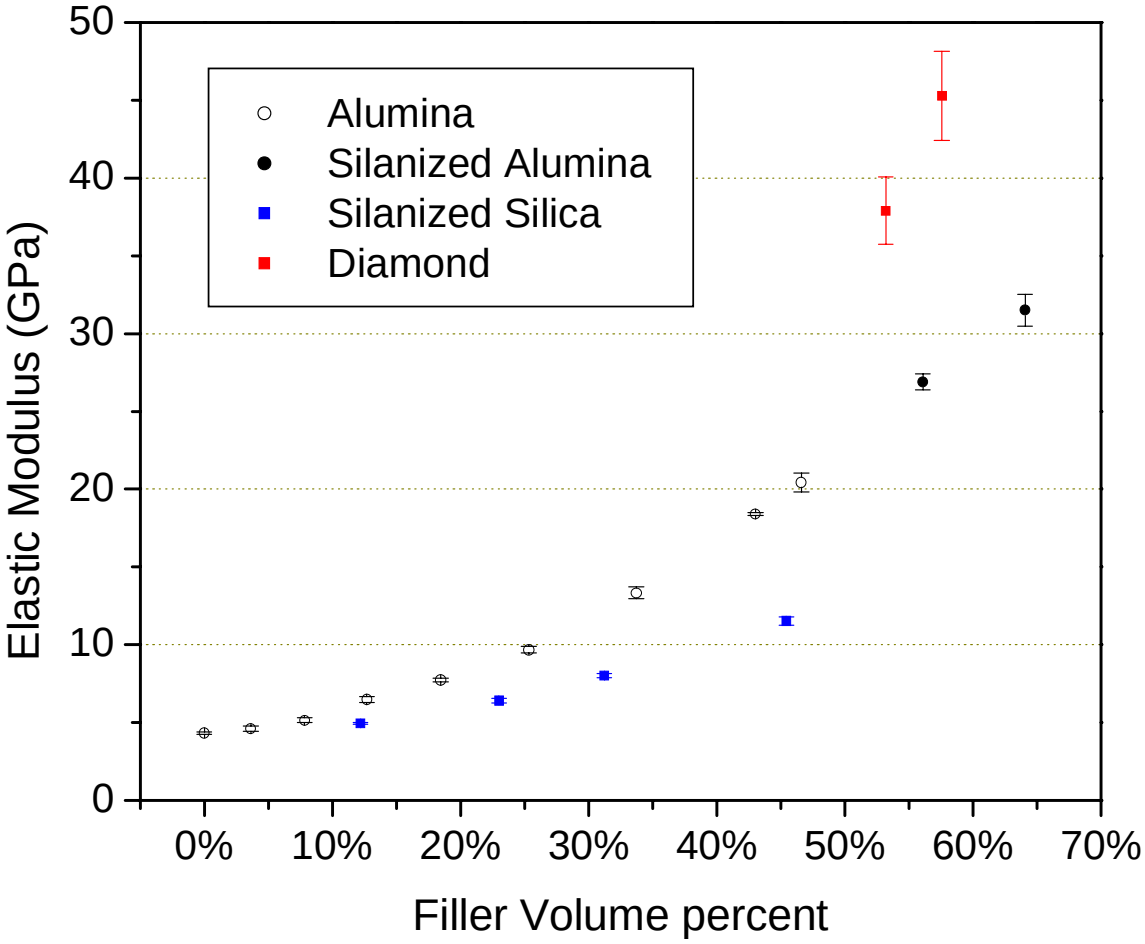

Figure 4.24 Elastic modulus of composites measured using nanoindentation. Resin composites with silanized silica, silanized alumina and diamond filler are compared.

According to the theory of Rules of Mixture, at the same filler loading level, replacing the stiff filler with softer one will decrease the elastic modulus of composites [24, 25]. With the increase of filler portion, the influence of filler on overall properties will increase. It explains why the difference of elastic modulus increases as the loading increases. Another fact that is worth noting is that, even by silanizing silica filler, the volume fraction of filler can not be raised much. This must be related to the larger specific surface area associated with smaller particles and/or frictional retardation during compounding brought by the large amount of chained agglomeration in the silica filler (Fig. 4.4)

4.4.4 Diamond powder as filler

Diamond is the stiffest material in the world. We expected diamond particle reinforced resin composites to possess a much higher modulus for the same volume fraction filler than alumina. We have tested diamond reinforced resin composites with sub-micro-sized diamond powder (375 nm). As shown in Fig. 4.24, the modulus of 375 nm powder filled composite is 37.9±2.2 GPa for 77.7 wt% (53.1 vol%) of filler. By using the surfactant H66, the weight percentage of 375 nm diamond filler gets to 80 wt% (57.5 vol%) and the corresponding elastic modulus is about 45.3±2.9 GPa. Due to the intrinsic high stiffness of the filler, the corresponding resin composite has a higher modulus in comparison with the same filler loading of alumina. The diamond powder is very promising for generating higher modulus composites. However, we have not

identified a good coupling agent for diamond. There are few studies on surfactant or coupling agents for diamond powders, so getting a strong bond between the matrix and diamond filler may be challenging.

4.5 Predictive Models for Elastic Modulus

Our work above has shown that the mechanical properties of dental resin composites are affected by a number of parameters, including the properties of filler, matrix, interface between filler and matrix, and volume fraction of filler. They could also be influenced by the shape, size, and distribution of fillers. A variety of models have been developed to predict the properties of composite materials. When a model works well to predict properties, it may also help to understand the relationship between microstructure and macro-mechanical properties and possibly optimize the properties of a composite. These models usually deal with the blend of two components with close mechanical properties and/or low volume fraction of filler. However, our composites represent a different and important group because of the large modulus mismatch and very high filler loading. Thus, it is valuable to investigate the predictive capabilities of the models for our composites.

4.5.1 Rule of mixtures

The simplest models consider the case where there is either uniform stress or strain. The elastic modulus of composites, E_c, is expressed in terms of elastic modulus,

E_i, Poisson's ratios, υ_i, and volume fractions, V_i, of the constituents (i=1, 2). The overall modulus, E_c, in the direction of loading can be calculated in each case using the relevant so-called Rule of Mixtures (ROM). The uniform strain, Voigt [25] model is given by

$$E^V{}_c = E_1V_1 + E_2V_2 \tag{4.4}$$

For the isostress situation, the Reuss [24] model is given by

$$E^R{}_c = \frac{E_1E_2}{E_1V_2 + E_2V_1} \tag{4.5}$$

where the superscript V and R represent Viogt and Reuss models, respectively.

Since these cases describe ideal situations, it is not possible to make a structure more or less stiff than in these two equations. Thus, the graphs of these functions are actually the upper and lower bounds to the elastic modulus of any composites. In Fig 4.25 and Fig. 4.26, the upper and lower bounds are plotted in blue and experimental data in black for silica and alumina reinforced resin composites, respectively. The experimental data fall into the envelop of the two models for each resin composite. However, the Voigt and Reuss models over-predict and under-predict the experimental data too widely to be useful. This could be caused by several factors. The most important one is the large modulus mismatch. The Voigt and Reuss models work best when the modulus ratio is less than 10. However, the normal E_f/E_m ratio for glass/resin dental composites is around 20 or 30. For alumina resin composites, the ratio is around 80~90.

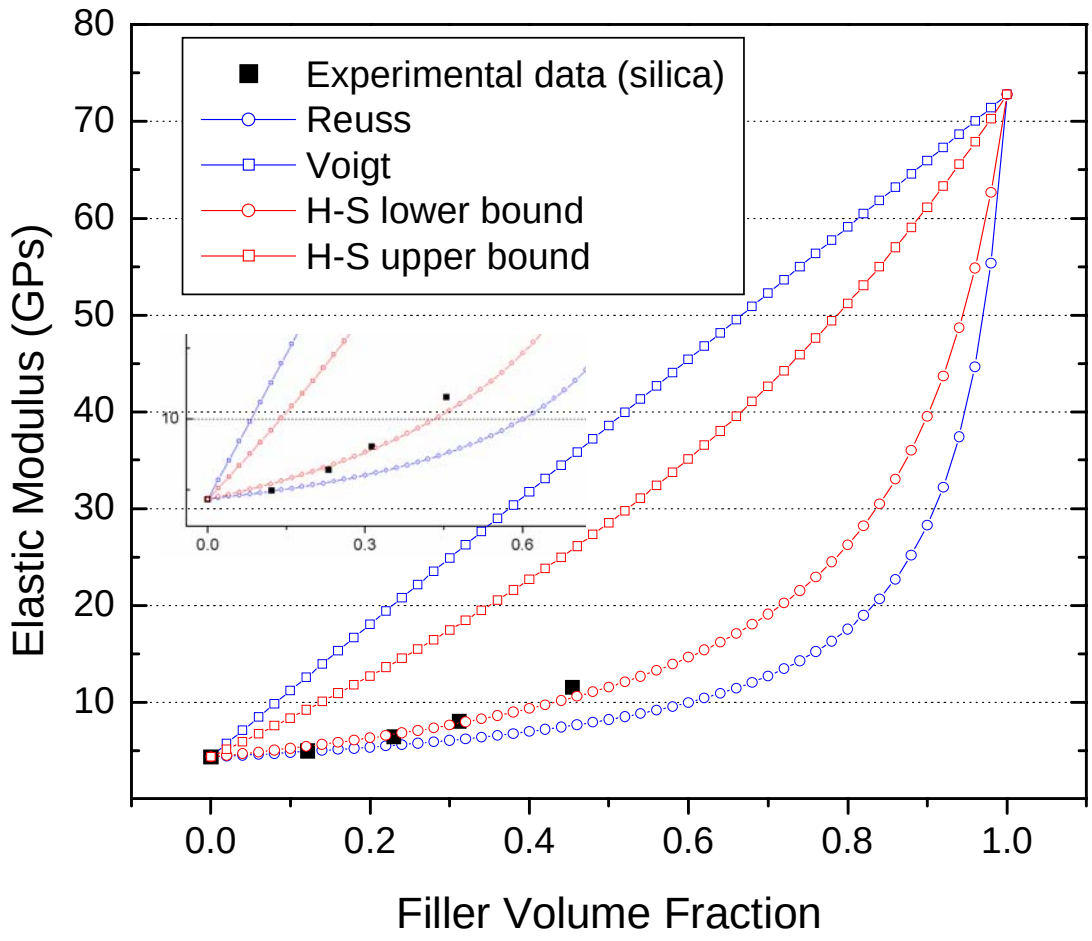

Figure 4.25 The elastic modulus of silica/resin composites from nanoindentation are presented with filled black squares. The modulus prediction from Reuss model, Voigt model and Hashin-Shtrikman model lower bound and upper bound are presented as well. The H-S lower bound is very close to experimental data. The center small picture shows a magnified view of the data.

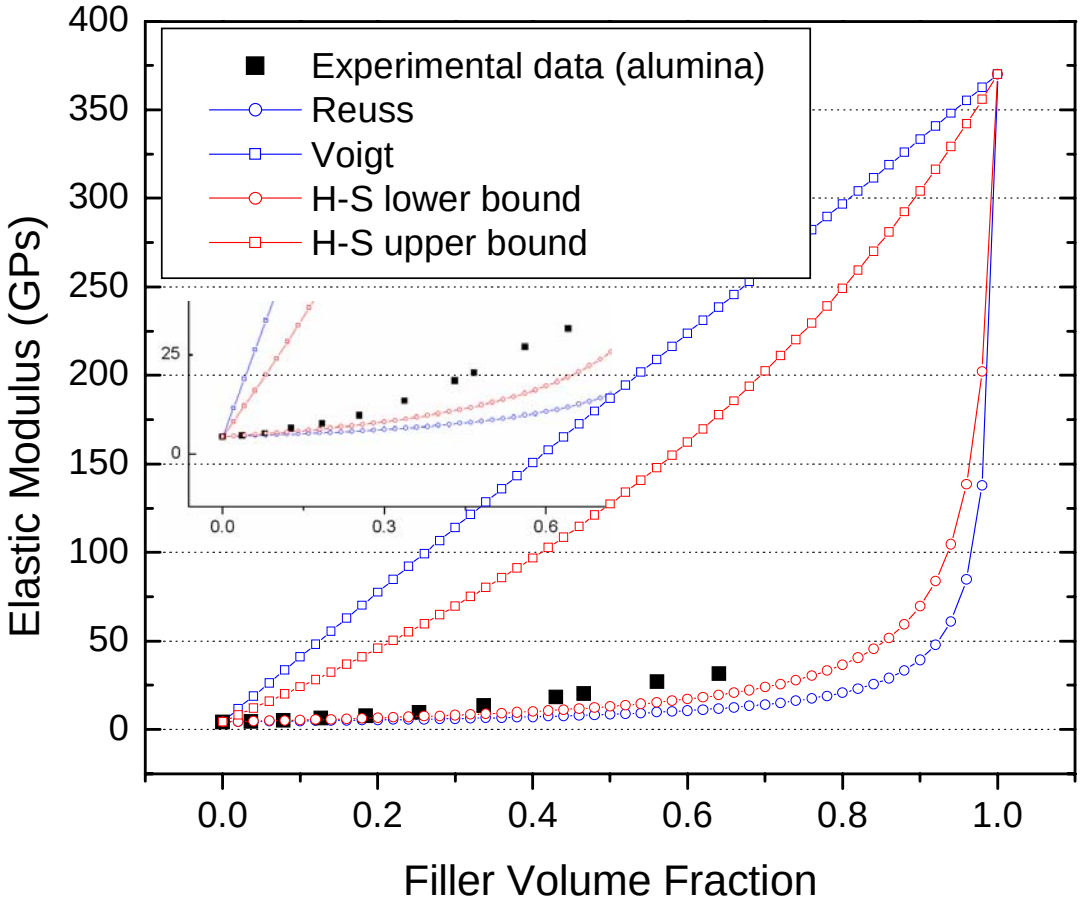

Figure 4.26 The elastic modulus of alumina/resin composites from nanoindentation are presented with filled black squares. The modulus prediction from Reuss model, Voigt model and Hashin-Shtrikman model lower bound and upper bound are presented as well. The Hashin-Shtrikman model lower bound is not very close to experimental data as shown in the magnified insert.

In such cases, it is often seen that the resin composites have a strong matrix influence with the experimental data much closer to the lower bound (Reuss) because it is a two-phase entity with a continuous resin matrix and discontinuous filler [76].

4.5.2 Hashin-Shtrikman model

The Hashin-Shtrikman (H-S) model is an improvement over the Voigt and Reuss models when the elastic modulus of the two phases are relatively widely disparate [77, 78]. The H-S bounds based on minimizing the elastic and complementary elastic energies are more restrictive and are expressed in terms of the shear and bulk moduli, G_i and K_i, and Poisson's ratios, υ_I, respectively, and volume fractions of the constituents (i,j=1,2). The bulk modulus (K) measures a substance's resistance to uniform compression. It is defined as the pressure increase needed for a given relative decrease in volume. Shear modulus (G), is defined as the ratio of shear stress to the shear strain. The shear and bulk moduli of the constituents are given by

$$G_i = \frac{E_i}{2(1+\upsilon_i)} \tag{4.6}$$

and

$$K_i = \frac{E_i}{3(1-2\upsilon_i)} \tag{4.7}$$

Then, the shear and bulk moduli of composite, G_c and K_c, are given by

$$K_c^{\ i} = K_i + \frac{V_j}{\frac{1}{K_j - K_i} + \frac{3V_i}{3K_i + 4G_i}} \tag{4.8}$$

and

$$G_c^{\,i} = G_i + \frac{V_j}{\frac{1}{G_j - G_i} + \frac{6(K_i + 2G_i)V_i}{5G_i(3K_i + 4G_i)}} \tag{4.9}$$

The elastic modulus of a resin composite is then

$$E_c = \frac{9K_cG_c}{3K_c + G_c} \tag{4.10}$$

Since H-S model is a well developed model, the principle and derivation are not presented in detail in this thesis. More information can be found from the book edited by Cristescu et al. [79]. The simulations from these models are shown in Fig 4.25 and 4.26, the upper and lower bounds are obtained by exchanging the subscripts, *i* and *j*. In comparison with Voigt and Reuss, the H-S model has a moderate improvement over the simple models, especially for silica resin composites, which have lower modulus mismatch. However, the fit is still problematic for alumina resin composites, especially at the end of high volume fraction due to the limitation of the model itself. The microstructures are just too complicated to be considered analytically by the simplified models. For advanced models, considering microstructure is necessary. For example, Bush has shown that simulation results become microstructure-dependent if the filler volume fraction is higher than 0.3 [80]. The complexity of developing such models is beyond the scope of this dissertation. However, we have explored phenomenological models for predicting the relationship between elastic modulus and filler volume fraction in the next section.

4.5.3 Phenomenological models

Braem et al. preformed a comprehensive study on 55 different dental composites and developed a model based on the linear mixing of the log of the elastic modulus of the two phases, filler and matrix, of the composites [81]. The expression of the phenomenological model proposed by Braem et al. is given by:

$$E_c = E_m \exp\left[\left(\ln E_f / E_m\right)x\right] = E_m (E_f / E_m)^x \tag{4.11}$$

where E_c, E_m and E_f are elastic modulus of resin composite, matrix and filler; x is the volume fraction of filler. The phenomenological model always lies between the upper and lower bounds of ROM irrespective of what E_m and E_f values are used. However, it is in fact as simple as the ROM. Thus, the improvement is limited, as shown in Fig 4.27 and 4.28. The blue curves indicate the calculation from this model, which fails to give an accurate fitting due to its intrinsic drawbacks for the case of large modulus mismatch between two phases.

Chantler et al. further extended this phenomenological model for cases where the ratio of elastic modulus of filler and matrix is greater than 10, for instance, E(silica)/E(resin)>10 [82]. The idea of extending this model is derived from a study of contact behavior of bilayer structures. A scaling parameter L is introduced to extend the Hertzian theory for bulk monolithic materials to the bilayer structures [83]. Similarly, Chantler et al. introduced a parameter that could bring the importance of the ratio of E_f/E_m into the model [82]. It is expressed by:

$$E_c = E_m (E_f / E_m)^{1-(1-x)^{\beta}} \tag{4.12}$$

where most terms are the same as those in Equation 4.11. The additional β is a function considering the influence of a high modulus mismatch and is restricted to ≤ 1 numerically. It is determined by the following relation:

$$\beta = \frac{2\left\{\left(1-\upsilon_f^2\right)/\left(1-\upsilon_m^2\right)\right\}^{1.7}}{\ln(E_f / E_m)} \tag{4.13}$$

where E_c, E_m and E_f are elastic modulus of resin composite, matrix and filler; υ_f and υ_m are the Poisson's ratio of filler and matrix; x is the volume fraction of filler. The author did not present how the expression of β was obtained in detail. The model fits the silica/resin composites very well as shown in Fig. 4.27 with the red curve, which means that this model works for cases where materials contain relative rigid reinforcement ($E_f/E_m \approx 18$). However, for alumina/resin composites, the elastic modulus ratio is around 190. The red curve in Fig. 4.28 shows the calculated result from the model, indicating that this model works as well as for the case of silica/resin composites. Obviously, the extended phenomenological model modified by Chantler et al. provides better correlation with experimental data. Both models fit the experimental data pretty well for silica/resin composites because of the relatively small elastic modulus mismatch. However, the B-model does not work well for alumina/resin composites because the model overestimates the effect from rigid filler. The C-model considers the influence from large ratio of E_f/E_m, scales it by introducing a parameter β, and provides a reasonable fit for the alumina/resin composites.

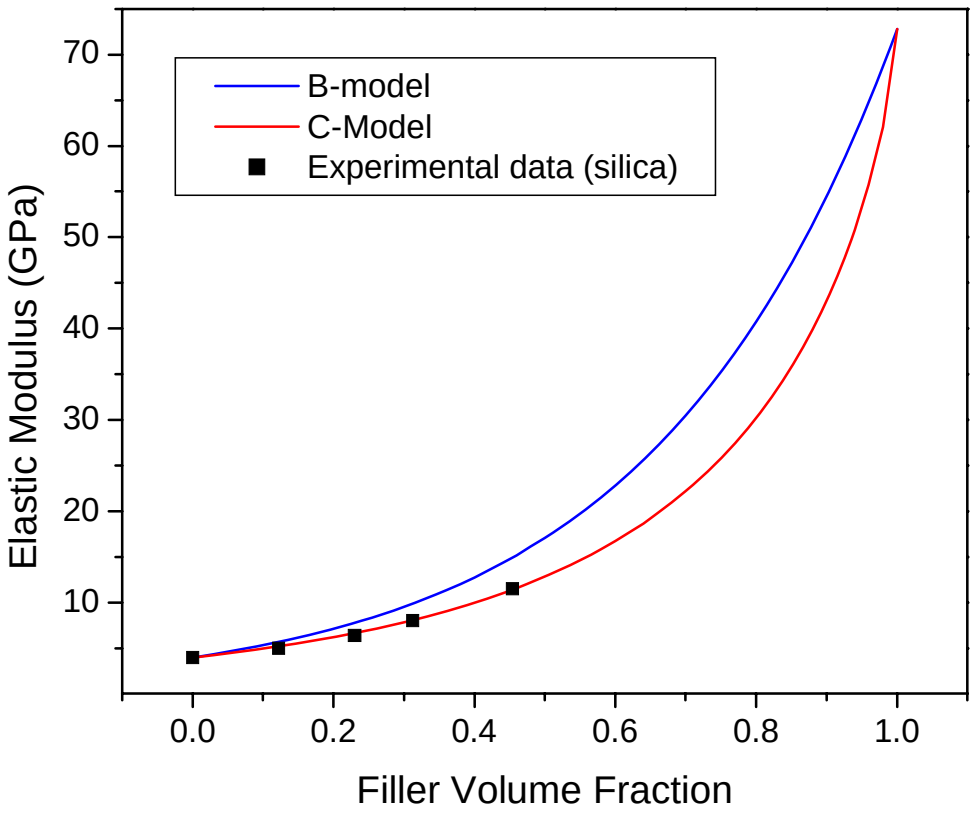

Figure 4.27 The elastic modulus of silica/resin composites from nanoindentation are presented with filled black squares. The modulus prediction from phenomenological models developed by Bream (blue) and Chantler (red).

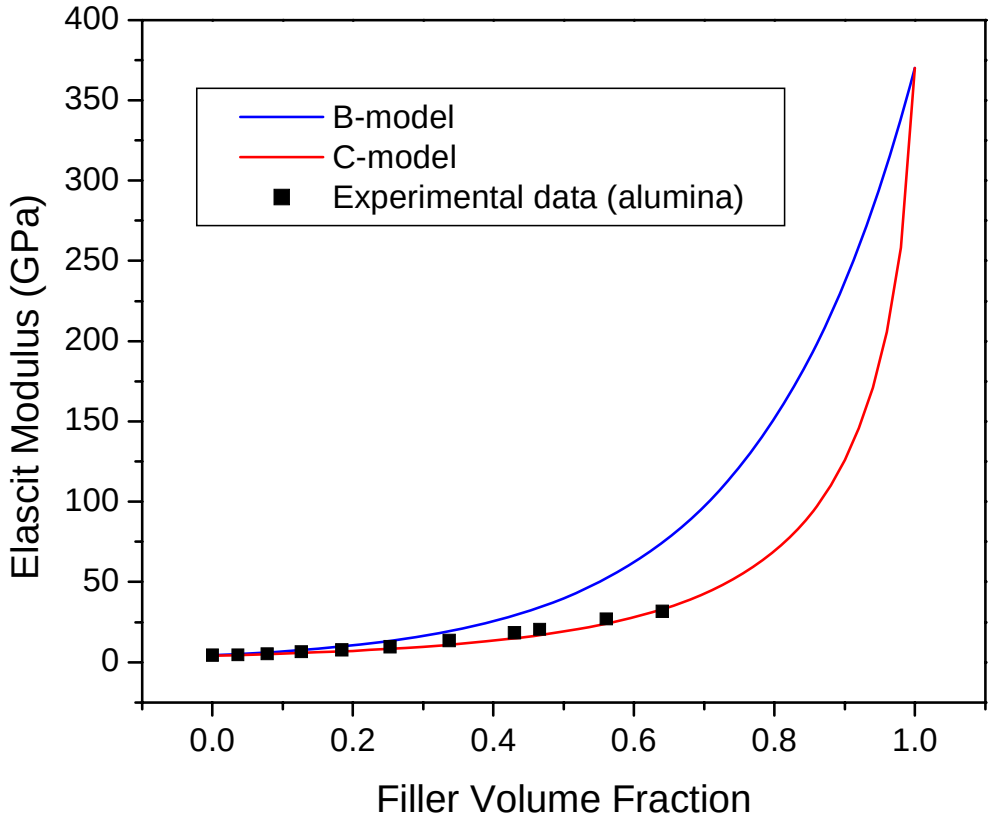

Figure 4.28 The elastic modulus of alumina/resin composites from nanoindentation are presented with filled black squares. The modulus prediction from phenomenological models developed by Bream (blue) and Chantler (red).

The standard deviations of the deviations between experimental data and prediction from models are listed in the Table 4.2.

Table 4.2 Standard deviations of predicted vs. experimental *E* for different models

Model	Silica/resin composites	Alumina/resin composites
B-model*	1.3	14.7
C-model*	0.5	2.1
S-H Low	0.6	4.7
S-H Up	5.4	48.9

** B-model is the model developed by Bream, as shown in Equation 4.11; C-model is the model extended by Chantler et al. as shown in Equation 4.12.*

According to the Fig. 4.28, the B-model starts to depart from the experimental data when the volume fraction of filler is above 0.4, which is consistent with the Bush's conclusion [80]. The microstructure starts to affect the properties when the filler fraction exceeds 0.3. In our case, since the C-model takes into account the effect from the rigid filler appropriately, it has better correlation when the filler fraction exceeds 0.4.

4.5.4 Comparison of models

The application of theoretical models has been presented and comparison has been made. The ROM is a very simple model. It gives a quite broad range which can include all experimental data. In fact, the two situations considered in the ROM are the two ideal cases, iso-strain and iso-stress over two phases. However, the mechanisms

that yield the elastic modulus of composites should be a combination of two cases and the ROM is not capable of specifying the portion of each case for particular materials. The H-S model modifies the ROM model by taking into account the interaction of bulk and shear moduli and thus gives a relatively narrow envelope. However, it is still too broad to be a good predictive model, especially for the case with large ratio of E_f/E_m. In Table 4.2, standard deviations show that S-H works reasonably well for silica/resin (small ratio of E_f/E_m). However, H-S does not deal well with the case of large ratio of E_f/E_m. Although it seems that S-H lower bound is close to experimental data, the deviations between calculations and experimental data increase with increasing volume fraction. This indicates that this model neglects the effect of a stiffer filler.

Phenomenological models give a more accurate prediction since they are developed by fitting the curve into the experimental data. However, this method has limitations when some properties of materials change. The B-model is deficient if the modulus ratio E_f/E_m is higher than 20. The modified C-model keeps the simplicity of the B-model but gives a statistically more reliable prediction. Although the complexity of microstructure is overlooked in this model, it will be welcomed by researchers who need a simple but accurate model to predict elastic modulus for all kinds of composite materials.

4.6 Summary

1) Microstructural investigation confirms that the good dispersion and distribution are achievable for high volume fraction filler reinforced resin composites by our apparatus. The open porosity is below 1.5% for even the 80 wt% alumina/resin composite.
2) Degrees of conversion decrease with increasing filler loading and decreasing curing temperature. They also increase by treating the surface of filler particle with effective coupling agents.
3) Filler loading and filler stiffness have strong impact on *E* and *H* of resin composites. Alumina and diamond powder reinforced resin composites possess much higher *E* and *H* than silica/resin composite that is routine in dentistry. Higher hardness is achieved for the samples with treated surface of filler with coupling agents as compared to the samples of the same filler loading without treatment. Silanes can serve as a good coupling agent.
4) The ROM and Hashin-Shtrikman models give lower and upper boundaries for predicting elastic modulus, which enclose all experimental data. However, the bounds are too separated from each other to be precise predicting methods. An extension of phenomenological model modified by Chantler et al. gives a reliable prediction for elastic modulus by taking into account the effect of large modulus mismatch between filler and matrix.

CHAPTER 5 TIME DEPENDENT BEHAVIOR

5.1 Introduction

The elastic modulus of dental resin composites is a very important parameter for evaluating their performance. The resin composites with low elastic modulus used in dental filling will more readily elastically deform under stresses than the remaining tooth which may result in catastrophic fracture of the surrounding brittle tooth enamel structure, which relies on their support [84]. In addition, excessive elastic deformation induced by low modulus may also disrupt the interface where a restoration is bonded to the remaining tooth structure. This in turn results in the formation of gaps and contributes to microleakage, secondary caries and post-operative sensibility [84, 85]. However, the elastic modulus of dental resin composites is not the only parameter that impacts a dental restoration's performance and lifetime. As we have addressed in the last chapter, resin composites with similar elastic modulus can possess different hardness with variation up to 20% for the same filler loading depending on the particle surface treatment techniques. In such cases, the resin composites with lower hardness undergo more plastic deformation when the applied stress exceeds their elastic limit. In addition, the portion of deformation associated with viscoelasticity of resin composites must be considered when cyclic loading is applied such as in chewing. Both plastic and viscoelastic deformation have a deleterious influence on the performance of dental resin composites, especially when they are exposed to cyclic loading and long term loading. Over time, as

more irreversible plastic and viscoelastic deformation is accumulated within the resin composite, the structures relying on the support of the resin composites would be more likely to undergo catastrophic failure.

The viscoelastic properties of dental resin composites and other polymer composites have been explored by several groups. Mesquita et al. examined the viscoelastic properties of several commercial dental composites using dynamic mechanical analysis under different conditions [43]. In dynamic mechanical analysis, a sinusoidal stress is applied to the specimens. An elastic deformation occurs at the same phase with the stress, indicative of an elastic or storage modulus, while a viscous response occurs with 90 degree behind the stress, indicative of a viscous or loss modulus. The ratio of loss modulus/elastic modulus is the so-called loss tangent, representing the amount of heat lost in the motion. Higher loss tangents mean that more heat is lost and that the deformation of material responds more slowly to the applied stress. Mesquita's values varied from 0.024 to 0.162 depending on filler loading, temperature, frequency and aging conditions [43, 86]. The values increase with decrease of frequency, increase of temperature, and increase of aging time.

Meanwhile, other methods have been developed recently to measure the static elastic modulus and quasi-static viscoelastic properties of other polymer materials by nanoindentation [87-92]. The published work is focused on dynamic viscoelastic testing by measuring the viscoelastic properties over a range of frequencies. Oyen and Cook have published a series of papers concerning nanoindentation behavior and mechanical

properties measurement of polymeric materials based on characteristic load-displacement behaviors (typical examples are shown in Fig. 5.1), and developed a viscous-elastic-plastic (VEP) model to analyze quantitatively the deformation of polymer associated with each mechanism [93-95].

Characteristic load-displacement curves for some typical materials, tested with the triangle-wave loading to fixed peak load (see Section 3.4.4), are shown in Fig. 5.1 [93, 96]. Polyurethane, as an elastomer material, has a predominantly elastic response, as illustrated by an almost completely closed hysteretic loop in Fig. 5.1(a). Fig. 5.1(b) shows a completely open hysteretic loop of the aluminum indicating a predominantly plastic response. In Fig. 5.1(c), the curve shows a partially open hysteretic loop and a considerable elastic recovery on unloading of fused silica indicating a mixed elastic-plastic response. Fig. 5.1(d) shows a fingerprint of another class of typical polymeric material, PMMA, which exhibits an open hysteretic loop. However, the unloading stage is characteristic of a plastic response with the elastic recovery occurring in the latter stage. In addition, in the early unloading stage, there is an increasing displacement and the characteristic forward-displacement termed a "nose," indicative of a viscous response [93, 97]. Fig. 5.1 show 4 typical load-displacement traces for various materials in a non-quantitative way. By analyzing with the VEP model, quantitative inspection of these traces for each material is possible.

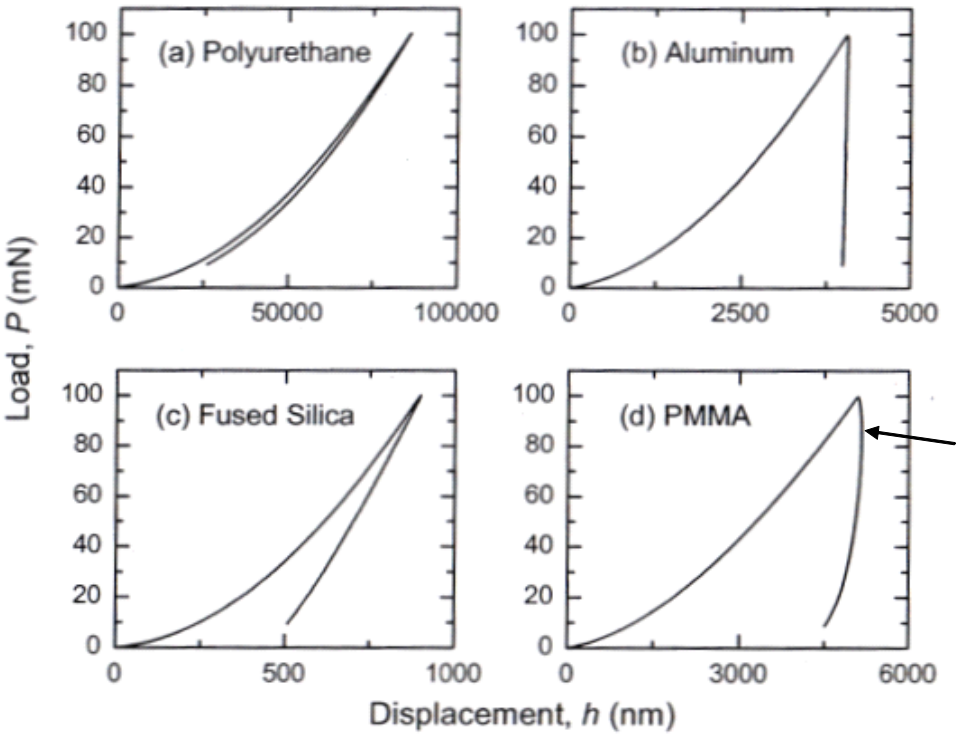

Figure 5.1 Instrumented indentation load (*P*)-displacement (*h*) traces for four different materials by Berkovich indentation: (a) Polyurethane, a predominantly elastic response; (b) Aluminum, a predominantly plastic response; (c) Fused silica, an elastic-plastic response; and (d) polymethylmethacrylate (PMMA), a viscous-elastic-plastic response. Triangle-wave loading, with a rise time of 100 s used for all indentations. [93]. Note the arrow points to the "nose," characteristic of occurrence of viscous flow.

In our studies, we investigate the relation between nanoindentation behavior and mechanical properties for dental resin composites, and then extend the approach to investigate the effect of filler loading and coupling agents on the plastic and viscoelastic properties characterized by indentation behavior. In addition, the viscous-elastic-plastic (VEP) model for polymeric materials developed by Cook and Oyen will be applied to our highly filled, high modulus dental resin composites [93].

5.2 Time Dependent Response of Resin Composites with Alumina and Silica

The experimental procedure as described in Section 3.4.3, is:

- Samples are made using 49.0 wt % Bis-GMA and 49.0 wt % TEGDMA resin system with 2.0 wt % BPO as initiator.
- Samples are made using the same fabrication procedure as those in Chapter 4.
- Samples are polished flat with a 0.5 μm finish.
- The tests are performed at room temperature in the force-control mode of the machine.
- The maximum load is 300 mN.
- The periods of testing time are 30, 100 and 300 seconds, with equal time for loading and unloading, as shown previously in Fig. 3.6 in Chapter 3.

The following sections will focus on the analysis of the changes in the shape of experimental load-displacement curves associated with the composition of various materials, i.e. filler loading and surface treatment, and the testing conditions.

5.2.1 Effect of filler loading

The specimens are termed as following: ***U-1***:74 wt% without additives; ***H-1***:80 wt% w/ H66; ***MP-II***:76.5 wt% w/ MetalPrimer II; ***MT-1***:74.5 wt% w/ Metaltite; ***S-1***,***S-2***,***S-3***:82 wt% w/ 2% Silane, 83 wt% w/ 4% Silane and 80 wt% w/ 6% Silane.

Fig. 5.2 shows the load-displacement curves for (a) pure resin, (b) ***U-1*** and (c) ***Sil-1***. For the same maximum load of 300 mN on the same sample, the penetration depth into the sample varies, depending on how long the indenter takes to reach the peak-load. Pure resin with rise time varying from 15 s to 150 s, in Fig. 5.2(a), exhibits an increasing maximum displacement into the sample. In the 30 s loading-unloading curve, the indentation fingerprint is similar to Fig. 5.1(c), pure elastic-plastic behavior. In the 300 s curve, the resin exhibits a strong viscous response, and like Fig. 5.1(d), the maximum penetration occurs after the load maximum is reached and the unloading slope becomes negative [98]. We believe that the viscoelasticity of polymer is mainly a result of sliding and rearrangement among polymer groups for thermoplastic polymers. For Bis-GMA and TEGDMA, thermoset polymers with a highly crosslinked network, uncrosslinked portion of polymers exists, which can also rearrange and slide. So, even for them, viscous flow still occurs, as shown in Fig. 5.2 (a). The complexity of microstructure of polymer composites makes it almost impossible to identify the mechanisms of fracture or deformation associated with viscous flow quantitatively.

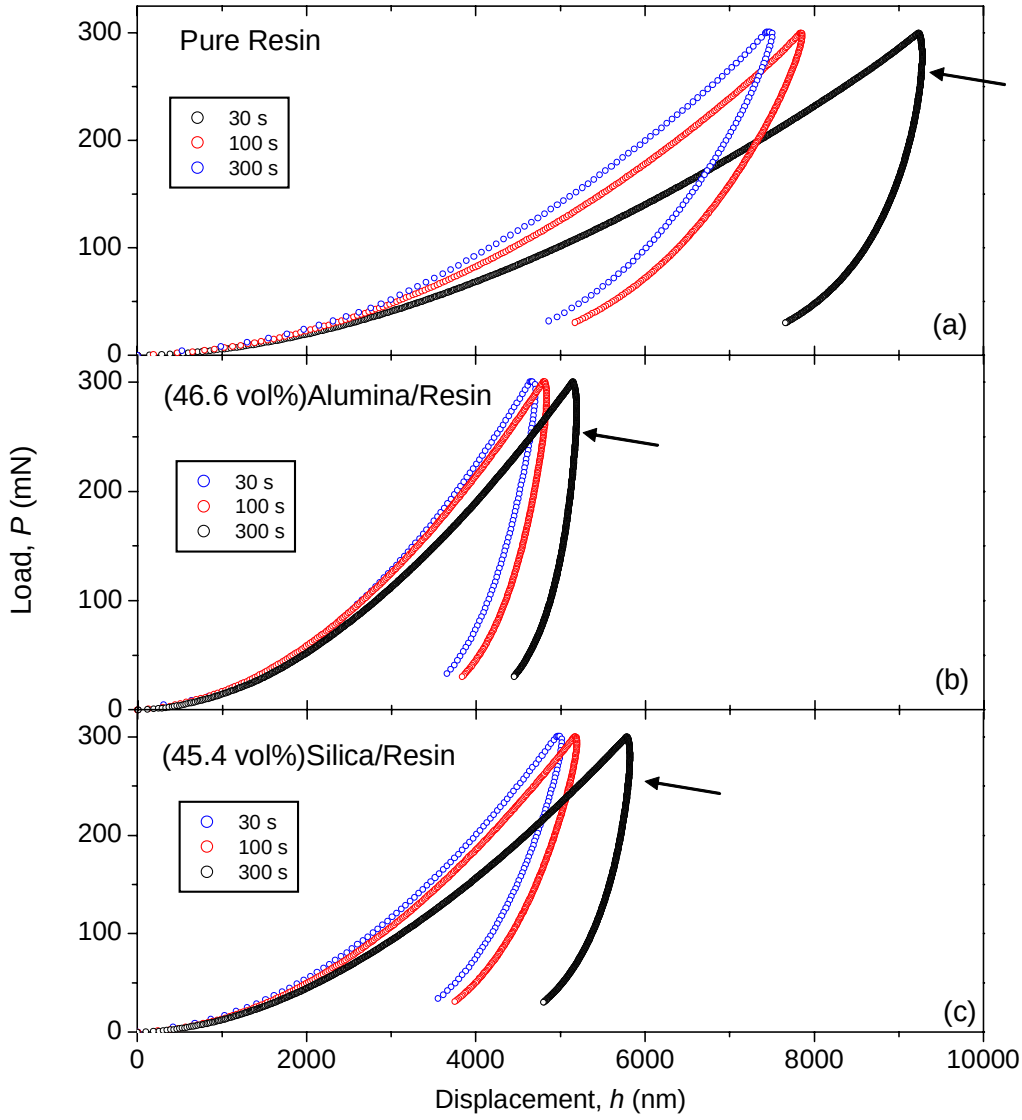

Figure 5.2 Instrumented indentation load (P)-displacement (h) traces for three different materials by Berkovich indentation: (a) pure resin, (b) ***U-1*** (46.6 vol% alumina/resin composite), and (c) ***Sil-1*** (45.4 vol% silica/resin composite). Triangle-wave loading, using a rise time of 15, 50 and 150 s for each indentations, shown in blue, red and black, respectively. Note the arrow points to the "nose," characteristic of occurrence of viscous flow.

However, they basically should be related to two types of mechanisms [93, 94]. First, those occur inside the polymer matrix under stress, which are possibly associated with molecular weight, degree of crosslinking, etc. The other is those occurring along the interface between filler and matrix, which are possibly associated with debonding and sliding along the interface, etc. Compared to polymers, the fillers usually are much stiffer and stronger so that the plastic deformation is less likely to occur in the particles.

Comparing the behaviors of the pure resin and 74 wt% alumina/resin composite in Fig. 5.2(a) and (b), we find that there is much less shift between the three, indicating that there is less viscous flow in the ***U-1***. When the organic fraction of the alumina/resin composite is decreased, the viscous flow associated with the polymer is reduced as well. However, even with about 45 vol% polymer (in ***U-1***), the organic fraction still plays an important role in determining the properties of this alumina/resin composite. On the other hand, without chemical bonding between the alumina and the polymer matrix, sliding may occur along the weak interface between them and contribute to the deformation of the composite. Thus, although the incorporation of filler largely reinforces the composites, the viscoelastic response is still quite pronounced. Fig. 5.2(c) shows the result from the same tests for a silica/resin composite. In comparison with (b), these two samples have similar filler loading (46.6 vs. 45.4 vol%) and similar load-displacement behavior. Thus, the small difference possibly stems from the stiffer alumina filler. Based on these results we hypothesized that if the filler and matrix could be chemically bonded together, the viscous flow would be further attenuated. This is

explored in the following section.

5.2.2 Effect of coupling agents

In this section, the effect of coupling agents on viscous flow is investigated by comparing the composites with close filler loading but different surface treatment. The load-displacement behaviors of three samples are shown in Fig. 5.3, 46.6 vol% non-treated alumina/resin composite (in black), 47.0 vol% (MetalPrimer II treated) alumina/resin composite (in red) and 57.6 vol% (silanized) alumina/resin composite (in blue). They are tested by the same procedure described above. Since they are used for a number of tests, these compositions are named ***U-1***, ***MP-II*** and ***S-2***, respectively. For each sample, from left to right, three curves are obtained from the same testing protocol with the three standard testing times (30, 100 and 300 seconds). ***U-1*** and ***MP-II*** have very close filler fractions (46.6 vs. 47.0 vol%). Besides this small difference, the only difference between them is whether the filler is pretreated by coupling agent. The pretreated composite, ***MP-II***, has less viscous flow under stress in comparison with the untreated composite, ***U-1***, as indicated by less shift between the three curves for different rise times. The reduction of viscous flow is attributed to the attenuation of polymer mobility resulting from the cross-linking between treated filler and matrix and the confinement of polymer segments. The treated sample has smaller displacement depths, indicative of smaller indents imprinted on the surface of ***MP-II***. This means that the treated sample is harder than the untreated one. .

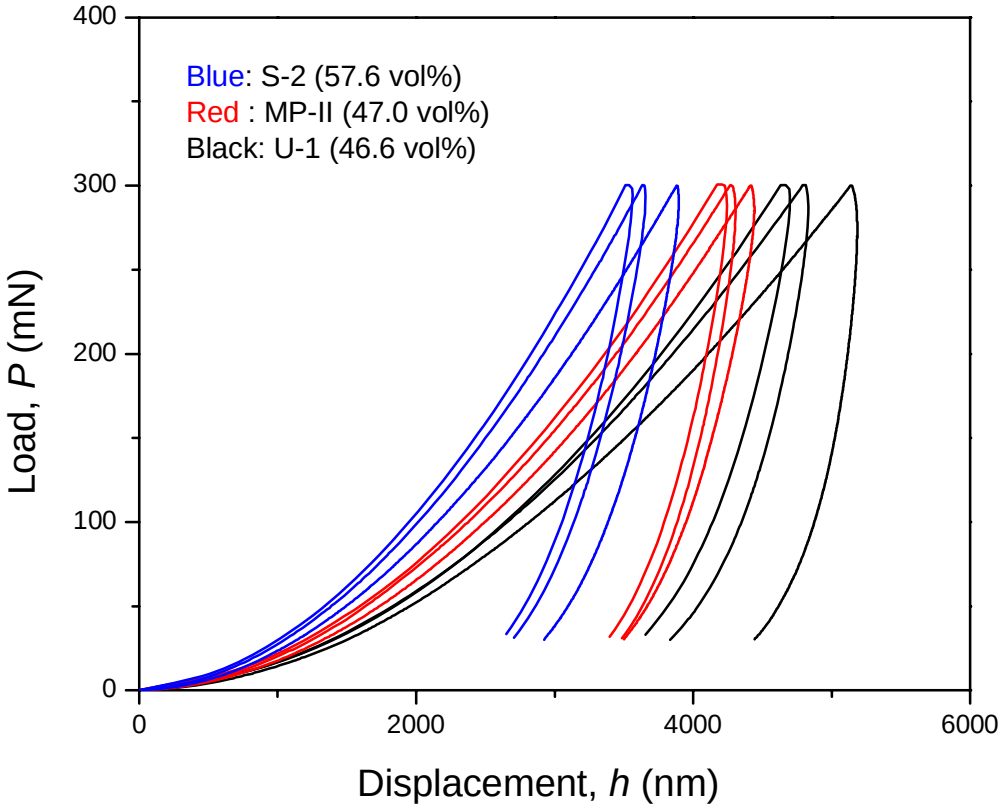

Figure 5.3 Instrumented indentation load (*P*)-displacement (*h*) traces for three different materials by Berkovich indentation: ***U-1*** (46.6 vol% non-treated alumina/resin composite in black), ***MP-II*** (47.0 vol% (MetalPrimer II treated) alumina/resin composite in red and ***S-2*** (57.6 vol% (silanized) alumina/resin composite in blue). Triangle-wave loading is used, for each sample in the same color, from left to right, the three curves are obtained from the same testing protocol but various testing times (30, 100 and 300 seconds), respectively.

Similar behavior was observed for ***S-2*** samples (Fig. 5.3 in blue). Thus, higher filler loading and stronger bonding between filler and matrix mean less viscous flow and plastic deformation under the same stress during the same rise time. These results are consistent with what we found in Section 4.4.1

Besides alumina/resin composites, silica/resin composites are investigated the same way. Load-displacement behaviors of two silica/resin composites are plotted in Fig. 5.4, 45.4 vol% of untreated silica/resin (***Sil-1***) and 46.0 vol% silanized silica/resin (***SS-1***). Viscous flow in ***SS-1*** is reduced in comparison with ***Sil-1***. Note that the three curves for ***SS-1*** are almost collapsed on top of one another, characteristic of an almost time independent behavior. In comparison with ***S-2*** (Fig. 5.3), the effect of silanes in reducing the viscous flow is more pronounced for silanized silica/resin composites (Fig. 5.4).

In summary, by incorporating the harder and stiffer inorganic fillers, silica and alumina, the time-dependent load-displacement behavior of composites, which is largely associated with the polymer resin, is reduced. As a result, less viscous flow and plastic deformation happen during loading and unloading. Moreover, by chemically connecting the filler and matrix, the mobility of polymer and sliding between the two phases, which also contribute to the time-dependent viscoelasticity, are further attenuated.

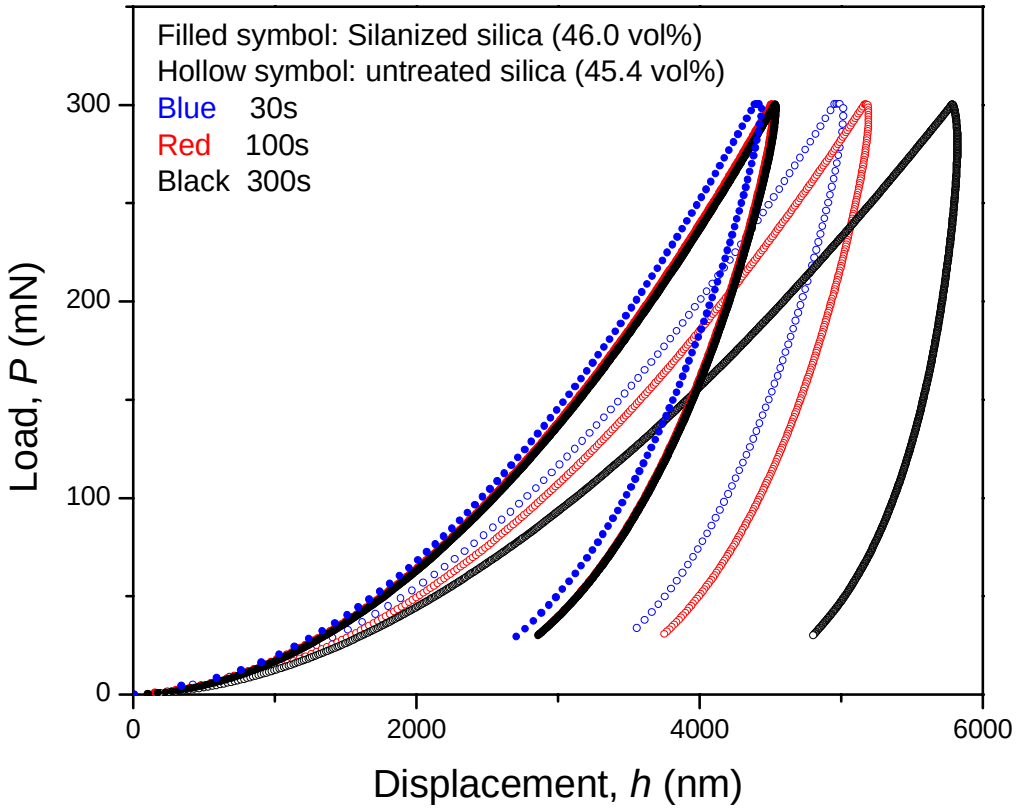

Figure 5.4 Instrumented indentation load (P)-displacement (h) traces for two materials by Berkovich indentation: ***Sil-1*** (45.4 vol% of untreated silica/resin) with hollow symbols and ***SS-1*** (46.0 vol% silanized silica/resin) with filled symbols. Triangle-wave loading, using a rise time of 15, 50 and 150 s for each indentation, shown in blue, red and black, respectively.

5.3 Visco-elastic-plastic Model

The loading-displacement trajectories for pure resin, untreated filler/resin composites and treated filler/resin composites have been explored or evaluated by instrumented indentation testing in a non-quantitative way. It is confirmed that the deformation of polymeric materials consists of three elements during rise time: reversible elastic deformation, instantaneous irreversible plastic deformation and time-dependent irreversible viscous deformation [93]. They stem from different mechanisms that occur in the composites during loading-unloading cycle of indentation. It order to describe the indentation response quantitatively or, in other words, distinguish each deformation from the overall deformation, a visco-elastic-plastic (VEP) model developed by Cook and Oyen is applied [93, 94]. With it, we can assess unambiguously the elastic, plastic and viscoelastic properties (time scales for viscous flow) of our resin composites and further enhance the understanding of deformation mechanisms of resin composites.

5.3.1 Development of VEP model

The development of the VEP model as discussed by Cook et al. is outlined below [93]. A linear viscoelastic mechanical model that consists of a combination of elastic spring elements and time-dependent dashpot elements is used to describe the mechanical behavior of our composites under stress. Conventional expressions for these two elements are that the load on the spring is proportional to the displacement and that

the load on the dashpot is proportional to the displacement rate [99]. Under sharp, conical, or pyramidal indentation conditions, the load-displacement relationship can be expressed by quadratic equations instead of a linear response [50, 51].

Elements

For the elastic element [94]:

$$P_E = k_Q \bullet h_E^2 \tag{5.1}$$

where P_E and h_E are the load and displacement on an elastic spring, and k_Q is a quadratic stiffness. Equation 5.1 can also be reformulated using a plain strain modulus (also termed as indentation modulus for a rigid conical indenter and an isotropic elastic material, Section 3.4.2) of the material, where [100]:

$$E^* = E/(1-\upsilon^2) \tag{5.2}$$

Considering the geometry [51]:

$$k_Q = \alpha_2 E^* \tag{5.3}$$

and

$$\alpha_2 = \pi \tan\psi / 2\beta \tag{5.4}$$

The elastic element is given by

$$P_E = \alpha_2 E^* h_E^2 \tag{5.5}$$

A similar treatment for the viscous constitutive response, for the viscous element, leads to load being proportional to the square of the displacement rate [93, 94]:

$$P_V = \mu_Q \bullet (dh_V / dt)^2 \tag{5.6}$$

where P_V and h_V are the load and displacement in the dashpot, and μ_Q is a quadratic viscosity coefficient. Equation 5.6 can be identified with the time constant for viscous flow, τ, via Equation 5.7 [93, 94].

$$P_V = \alpha_2 E^* \tau^2 (dh_V / dt)^2 \tag{5.7}$$

Besides the elastic and viscous constitutive responses, plastic deformation occurs as well. Under a pyramidal indentation, this element is associated with plastic deformation

$$P_P = \alpha_1 H h_P^2 \tag{5.8}$$

where P_P and h_P are the load and displacement on the plastic element, H is the hardness and $\alpha_1 = \pi \tan^2 \psi$ is a dimensionless geometry parameter for a sharp indenter.

Loading and unloading

All three elements have been identified. Depending on the load-displacement response of materials, an appropriate combination of the elements would be selected. For instance, for an elastic-plastic material, the quadratic elastic and plastic elements are considered in series. Then, the sum of displacements is $h = h_E + h_P$. If we are dealing with a material in which all three elements of deformation are considerable, according to the VEP model the three independent elements are assumed to be in a Maxwell series, where the elastic, plastic and viscous elements are as represented in Fig. 5.5 [93].

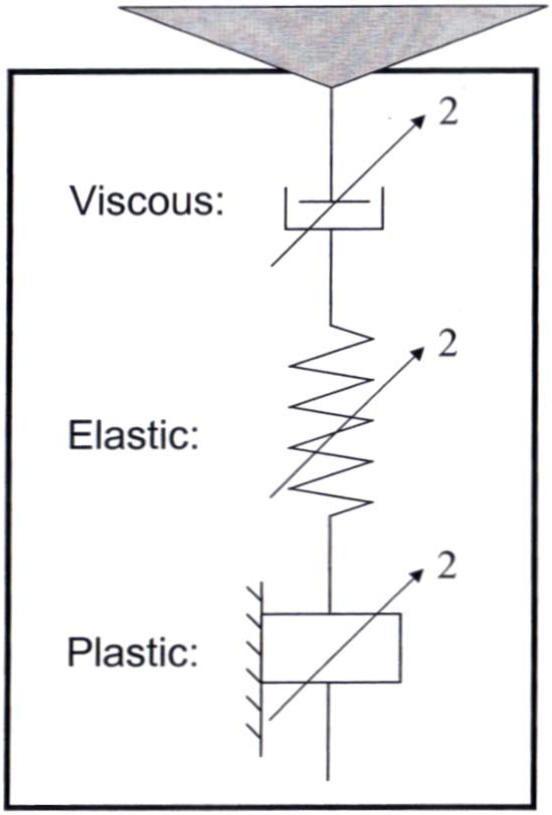

Figure 5.5 Schematic diagram of the series viscous-elastic-plastic quadratic indentation model used. The total deformation due to indentation load is the sum of the deformations in each component and the load is common to all elements [93].

The displacement sum for this model is [93]:

$$h = h_E + h_P + h_V \tag{5.9}$$

and the load is common to all elements,

$$P = P_E = P_P = P_V \tag{5.10}$$

For the triangle-wave load function we use in this study, on loading, the load is expressed as

$$P = P_{\max}(t / t_R), \quad 0 \le t \le t_R \tag{5.11}$$

where t is the time, t_R is the rise time to reach peak load, P_{max}.

On unloading,

$$P = P_{\max}(2 - t / t_R), \quad t_R \le t \le 2t_R \tag{5.12}$$

By substituting the load, P, from Equation 5.11, into Equations 5.5, 5.7 and 5.8, the displacement of each element on loading can be expressed as

$$h_E = \left(\frac{P_{\max} t}{\alpha_2 E^* t_R} \right)^{1/2} \tag{5.13}$$

$$h_V = \frac{2}{3}\left(\frac{P_{\max} t^3}{\alpha_2 E^* \tau^2 t_R} \right)^{1/2} \tag{5.14}$$

and

$$h_P = \left(\frac{P_{\max} t}{\alpha_1 H t_R} \right)^{1/2} \tag{5.15}$$

respectively. And the total displacement on loading is

$$h^R(t) = h_E + h_P + h_V = \left(\frac{P_{\max} t}{\alpha_2 E^* t_R} \right)^{1/2} + \left(\frac{P_{\max} t}{\alpha_1 H t_R} \right)^{1/2} + \frac{2}{3}\left(\frac{P_{\max} t^3}{\alpha_2 E^* \tau^2 t_R} \right)^{1/2} \tag{5.16}$$

At the peak load, $t=t_R$, the displacement is

$$h^{RP} = h_{ER} + h_{PR} + h_{VR} = \left(\frac{P_{\max}}{\alpha_2 E^*}\right)^{1/2} + \left(\frac{P_{\max}}{\alpha_1 H}\right)^{1/2} + \frac{2t_R}{3\tau}\left(\frac{P_{\max}}{\alpha_2 E^*}\right)^{1/2} \quad (5.17)$$

For unloading after loading time t_R, the three displacement components exhibit distinctive behavior: the plastic element remains fixed at constant of its peak-load value $h_{PR} = \left(\frac{P_{\max}}{\alpha_1 H}\right)^{1/2}$; the elastic element recovers back to zero; and the viscous element continues to increase. By substituting the load, P, from Equation 5.12 into the Equation 5.5, 5.7 and 5.8, the displacement of each element on unloading can be expressed as

$$h_E = \left(\frac{P_{\max}(2 - t/t_R)}{\alpha_2 E^*}\right)^{1/2} \quad (5.18)$$

$$h_V = \frac{2t_R}{3\tau}\left(\frac{P_{\max}}{\alpha_2 E^*}\right)^{1/2}\left(2 - (2 - t/t_R)^{3/2}\right) \quad (5.19)$$

and

$$h_P = h_{PR} = \left(\frac{P_{\max}}{\alpha_1 H}\right)^{1/2} \quad (5.20)$$

respectively. And the total displacement on unloading is

$$h^U(t) = h_E + h_P + h_V = \left(\frac{P_{\max}(2 - t/t_R)}{\alpha_2 E^*}\right)^{1/2} + \left(\frac{P_{\max}}{\alpha_1 H}\right)^{1/2} + \frac{2t_R}{3\tau}\left(\frac{P_{\max}}{\alpha_2 E^*}\right)^{1/2}\left(2 - (2 - t/t_R)^{3/2}\right) \quad (5.21)$$

At the end of unloading, $t=2t_R$, the displacement is

$$h^{FP} = h_{EF} + h_{PF} + h_{VF} = 0 + h_{PR} + 2h_{VR} \quad (5.22)$$

Normalization

It is convenient to use the normalized values of displacement, time, and load for

experimental data to explore the validation of the VEP model:

$$\widetilde{h} = h / h_R \qquad \widetilde{t} = t / t_R \qquad \widetilde{P} = P / P_{\max} \tag{5.23}$$

where the denominators are all experimentally measurable.

It is convenient to define some parameters to substitute for others having complex forms:

$$y = \left(\frac{\alpha_1 H}{\alpha_2 E^*} \right)^{1/2} \tag{5.24}$$

$$d = \frac{3\tau}{2t_R} \tag{5.25}$$

$$\frac{1}{e} = 1 + \frac{1}{y} + \frac{1}{d} \tag{5.26}$$

With the normalized coordinators and new parameters in Equations 5.24-26, the load and displacement can be expressed as: on loading, $0 \le \widetilde{t} \le 1$,

$$\left\{ \begin{array}{l} \widetilde{P} = \widetilde{t} \\ \widetilde{h}_P = (e / y)\widetilde{t}^{\,1/2} \\ \widetilde{h}_E = e\widetilde{t}^{\,1/2} \\ h_V = (e / d)\widetilde{t}^{\,3/2} \end{array} \right\} \tag{5.27}$$

and on unloading, $1 \le \widetilde{t} \le 2$,

$$\left\{ \begin{array}{l} \widetilde{P} = 2 - \widetilde{t} \\ \widetilde{h}_P = (e / y) \\ \widetilde{h}_E = e(2 - \widetilde{t})^{1/2} \\ h_V = (e / d)[2 - (2 - \widetilde{t})^{3/2}] \end{array} \right\} \tag{5.28}$$

In both cases

$$\widetilde{h} = \widetilde{h}_E + \widetilde{h}_P + \widetilde{h}_V \tag{5.29}$$

So the parametric sets for $\{\widetilde{P}, \widetilde{h}\}, \{\widetilde{P}, \widetilde{t}\}$ and $\{\widetilde{h}, \widetilde{t}\}$ are connected by Equations 5.24-29.

By fitting the experimental data into any of these sets, the parameters in Equation 5.24-26 can be derived.

Fitting and simulation

The load-displacement behavior of the pure resin in Fig. 5.2 (a) will be used as an example to illuminate the application of VEP model. For a test of 300 seconds, the $\{\tilde{P},\tilde{h}\}$ and $\{\tilde{h},\tilde{t}\}$ trajectories of experimental data are shown in Fig. 5.6 in curve (a) in black and (b) in blue, respectively. The $\{\tilde{h},\tilde{t}\}$ trajectory has a convex shape during loading and there is a discontinuity at the peak load. After the point of discontinuity, the displacement continues increasing, which makes the other convex shape during unloading. On the $\{\tilde{P},\tilde{h}\}$ trajectory, there is hysteresis in $\{\tilde{P},\tilde{h}\}$ indicative of the plastic and viscous deformation components and a characteristic "nose" during unloading, as we have mentioned in Section 5.1. If we held the load at its maximum value for a longer time, then creep would appear. Such results have been presented by other researchers [93-95]. The extent of the convex shape can serve as an index of amount of viscous flow involved. For example, Oyen et al. showed that, for PMMA and HDPE, the elastic recovery was almost compensated by the forwarding viscous flow for t_{rise}=333 seconds [94]. In other words, most of or all points on unloading curve of $\{\tilde{P},\tilde{h}\}$ would be located on the right side of line $\tilde{t}=1$ if it were plotted on Fig. 5.6. In contrast, our resin possesses less viscosity, characterized by a small "nose". Viscous flow does not play as dominant a role in our composites as in the PMMA and HDPE above.

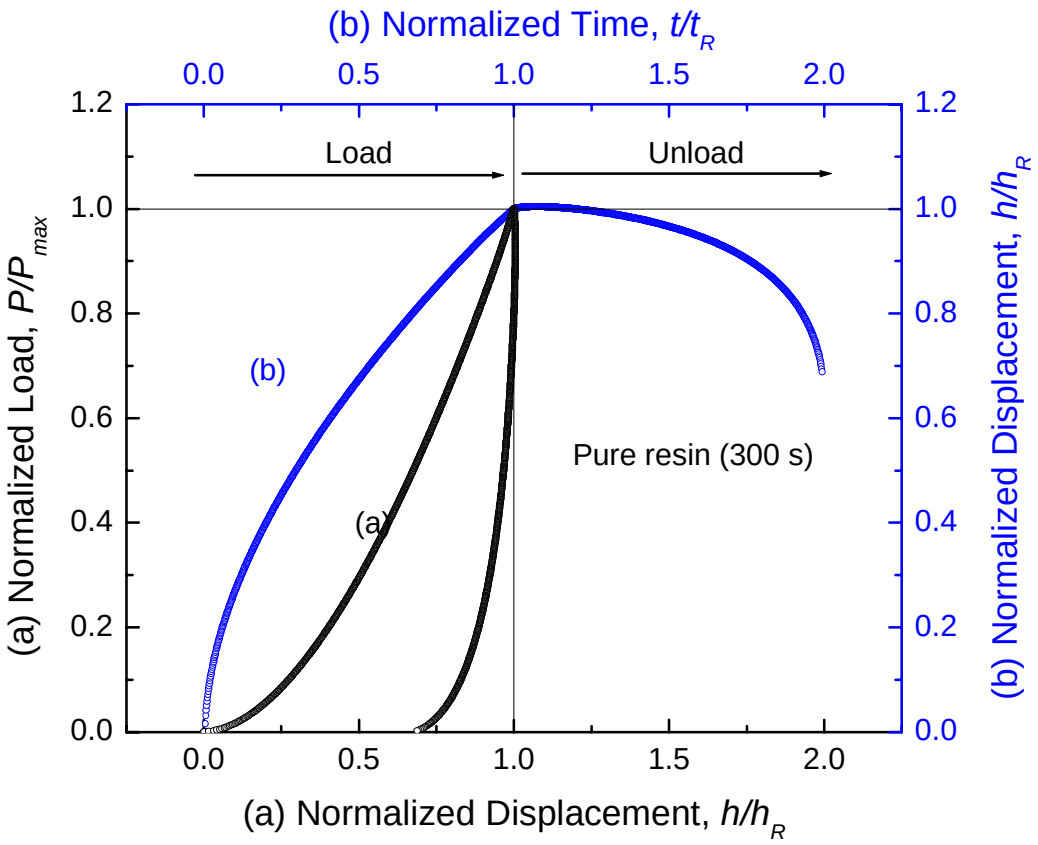

Figure 5.6 Normalized displacement-normalized time response (in blue) and normalized load-normalized displacement response (in black) with 300 s loading-unloading procedure for pure resin.

The following paragraph introduces how to analyze the deformations from each component, elastic, plastic and viscous, quantitatively by employing VEP model. It is based on the treatment by Cook et al. [93].

It is convenient to determine the parameters, *y*, *d* and *e* by fitting data to the normalized unloading $\{\tilde{h}, \tilde{t}\}$ trajectory. Also note that only two of the three parameters are independent. In Fig. 5.7, the normalized $\{\tilde{h}, \tilde{t}\}$ from unloading experimental data are plotted with black hollow circles and the curve fit from the VEP model is represented by the red curve. The fitting work is done by computer software, Microcal Origin, (Microcal Software Inc., Northampton, MA) according to the formulas in Equation 5.28 and 5.29. By fitting the experimental data, the values of *y* and *d* are obtained. The third parameter, *e*, is calculated using Equation 5.26. Then the material properties are deconvoluted using

$$\left\{\begin{array}{l} \tau = \dfrac{2dt_R}{3} \\ E^* = \dfrac{P_{\max}}{\alpha_2 h_R^2 e^2} \\ H = \dfrac{P_{\max} y^2}{\alpha_1 h_R^2 e^2} \end{array}\right\} \tag{5.30}$$

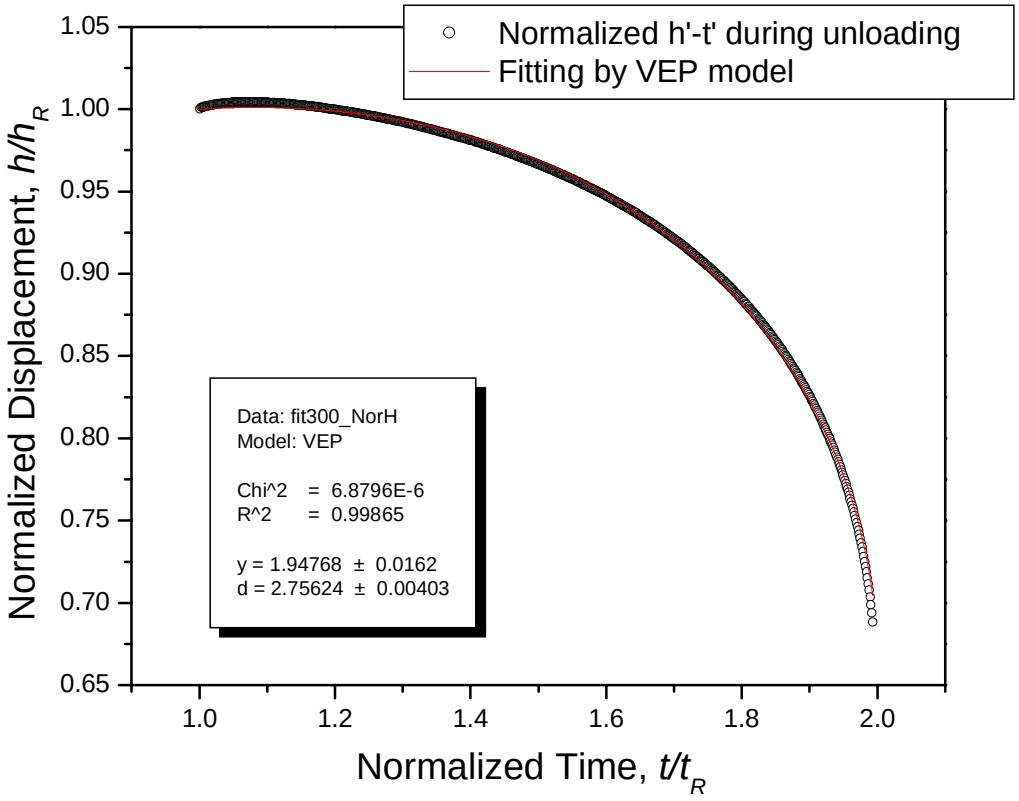

Figure 5.7 The unloading part of normalized displacement-normalized time response (black circles) and fitting by program, Microcal® Origin, for pure resin. The whole triangle-wave, loading and unloading , takes 300 seconds. Constitutive parameters, y and d, are given by fitting according to Equation 5.23.

5.3.2 Application of VEP model

By putting back all parameters we have extracted into Equation 5.27 and 5.28 for a loading-unloading event of 300 seconds, we calculate the normalized displacements from each element, as shown in Fig. 5.8. During loading, the elastic, plastic, and viscous components all increase with the increasing load, in a convex manner for elastic and plastic and in a concave manner for viscous deformation, to their maximum. At $\tilde{t} = 1$, there is a discontinuity as the curve switches from loading to unloading. Correspondingly, there is a discontinuity in the derivative of their $\{\tilde{h}, \tilde{t}\}$ trajectories for elastic and plastic components, while there is no such point for viscous components. During unloading, the plastic component remains fixed value of the peak load, while the elastic component recovers to zero. Meanwhile, the viscous component keeps increasing in a convex manner, associated with the decreasing load. Overall, the elastic component consists of about one half of deformation during loading and at the initial stage of unloading, indicative of relatively brittle mechanical behavior in comparison with other thermoplastic materials [93-95].

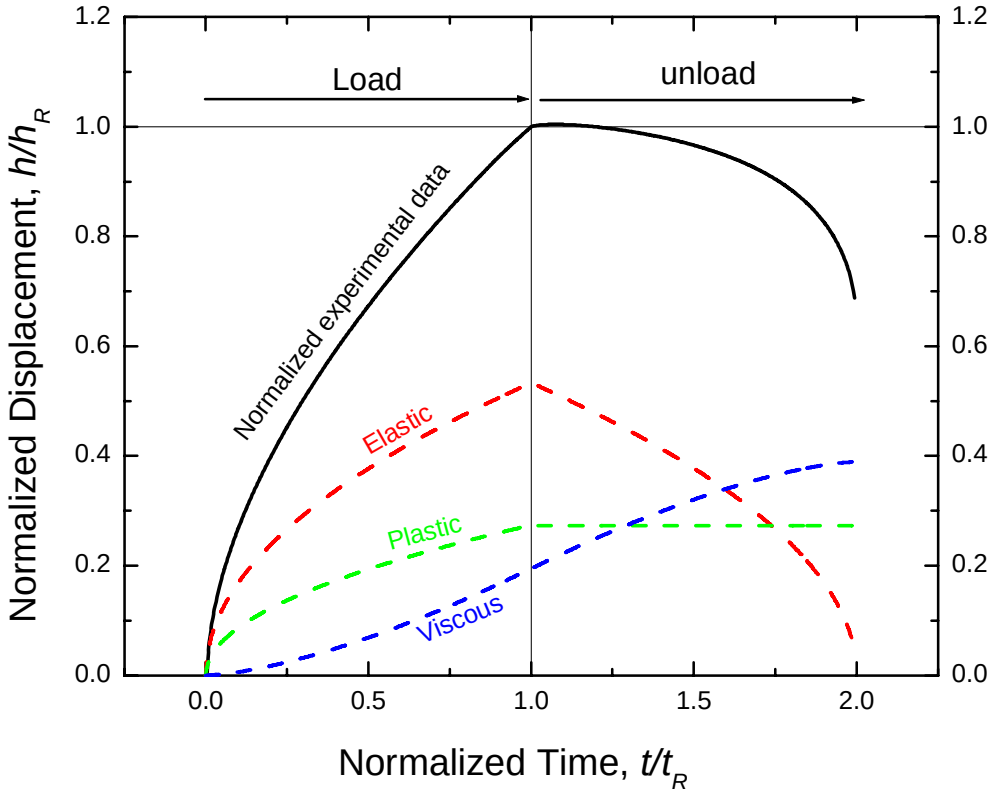

Figure 5.8 Normalized displacement-normalized time response with 300 s loading-unloading procedure for pure resin. Colorful dashed lines represent the component (elastic, plastic and viscous) deformations in red, green and blue, respectively. The total deformation is represented by black solid line.

In addition, we can also use these parameters to predict responses for the same loading protocols but various loading-unloading times, using the constitutive Equations 5.5, 5.7, 5.8, 5.9 and 5.10. In Fig. 5.9, the $\{\tilde{P}, \tilde{h}\}$ responses are plotted according to the prediction from VEP models with colorful lines. The parameters are extracted by fitting unloading data of the test of 300 seconds. The experimental data for various testing times, 30, 100, and 300 seconds, are also plotted with grey hollow circles. For the test of 300 seconds, the prediction and experimental data almost overlap except for a part of the curve during loading. It is not surprising, since the prediction is deconvoluted from $\{\tilde{h}, \tilde{t}\}$ during unloading. For the test of 100 seconds, as we still use those parameters from the fitting of 300 seconds, the prediction line matches the experimental data quite well, indicative of the ability and accuracy of the VEP model. For the 30-second test, the prediction is a little further off from experimental data.

It can be explained by Deborah number effect, which is the fact that apparent time constant describing material flow behavior varies with the observation time of the test [93]. Briefly, there are various flow mechanisms involved during the loading-unloading event and they have different time constants. For the total displacement, when the loading-unloading time changes, the contribution from each mechanism changes as well. Due to the complexity of the polymer, it is hard to predict the situation for each mechanism.

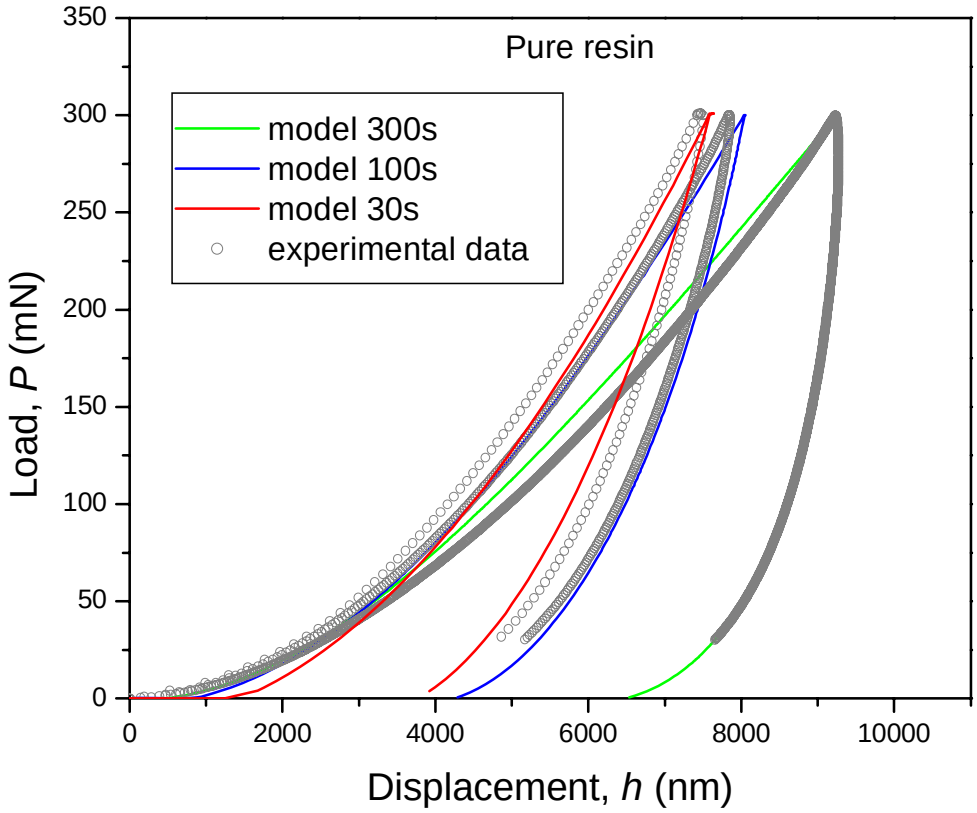

Figure 5.9 Instrumented indentation load (P)-displacement (h) traces for pure resin, displaying the experimental responses from Fig. 5.2 (a) with grey hollow circles. The solid lines are fits to each response using the VEP model for various observation times, 30, 100 and 300 seconds, in red, blue and green, respectively.

However, it should be noted that for longer rise times, more mechanisms are involved and make more contributions to the displacement. In other words, as the observation time is increased, the slower flow mechanisms start to make their contribution in overall displacement. As a result, since the parameters that we use for prediction are from the single 300-second test, more mechanisms should contribute to the displacement than in 30- and 100-second tests. Thus, the VEP model predicts displacements from each mechanism which works for 300-second case. However, for the cases of shorter rise time, there are fewer mechanisms actually involved so the VEP model over predicts the displacement. Thus, the limitation of the model stems from not only the simplicity of the VEP model, but the nature of material flow with various time constants. For a single time constant model, it is hard to predict mechanical behavior that stems from different mechanisms with different time scales. For the extreme cases with very long rise time, its prediction will be significantly off [93]. Another limitation of the VEP model is associated with the selection of tests. The 300-second case is selected as the subject for fitting to include as many mechanisms as possible. If 30- or 100-second tests were used to extract parameters, not enough mechanisms would be included. As a result, the prediction would substantially differ from the experimental data (see figures in appendix). So, it is necessary to choose an appropriate observation time, where all three components make a significant contribution, to get a reasonable prediction. The VEP model is also applied to other samples fabricated by different procedures (or with different coupling agents). The prediction

for an ***MP-II*** sample is presented in Fig. 5.10, very similar to the one in Fig. 5.9. See the appendix for the additional curves for samples with different surfactants or coupling agents. Table 5.1 summarizes the elastic modulus, hardness and time constants extracted from data using the VEP model.

5.3.3 Mechanical properties derived from VEP model

Table 5.1 E, H and τ of various resin composites.

Samples	***R-1***	***U-1***	***MP-II***	***S-1***	***S-3***	***Sil-1***	***SS-1***
E (GPa)	4.7(4.6)	21.0(20.4)	25.1(23.3)	28.4(31.2)	25.9(28.2)	11.9(11.4)	9.3(11.5)
H (GPa)	0.97 (0.244)	2.50 (0.753)	3.69 (1.006)	5.68 (1.148)	6.16 (1.074)	2.51 (0. 542)	4.00 (0.667)
τ (s)	156	259	333	420	402	331	535

Alumina filled composites: R-1: *pure resin;* ***U-1****:72 wt% without additives;* ***MP-II****: 76.5 wt% w/ MP II;* ***S-1*** *and* ***S-3****:82 wt% w/ 2% Silane and 80 wt% w/ 6% Silane;* ***Silica filled composites: Sil-1:*** *59.5 wt% of silica w/o additives;* ***SS-1:*** *60 wt% w/ 4% Silane; Inside the brackets, numbers are E and H obtained from direct testing by nanoindentation while outside, the values are E and H obtained from VEP modeling (the H is also called true hardness).*

In the VEP model, Equation 5.30 gives a way to calculate the mechanical properties of materials, i.e. E*, H, and τ. Note here $E^* = E/(1-\upsilon^2)$. The Poisson ratio, υ, in this paper is set to be 0.33 to simplify the calculation. The table shows that calculated elastic modulus match very well with data obtained from direct tests of nanoindentation, except for ***S-1***, ***S-3***, and ***SS-1.***

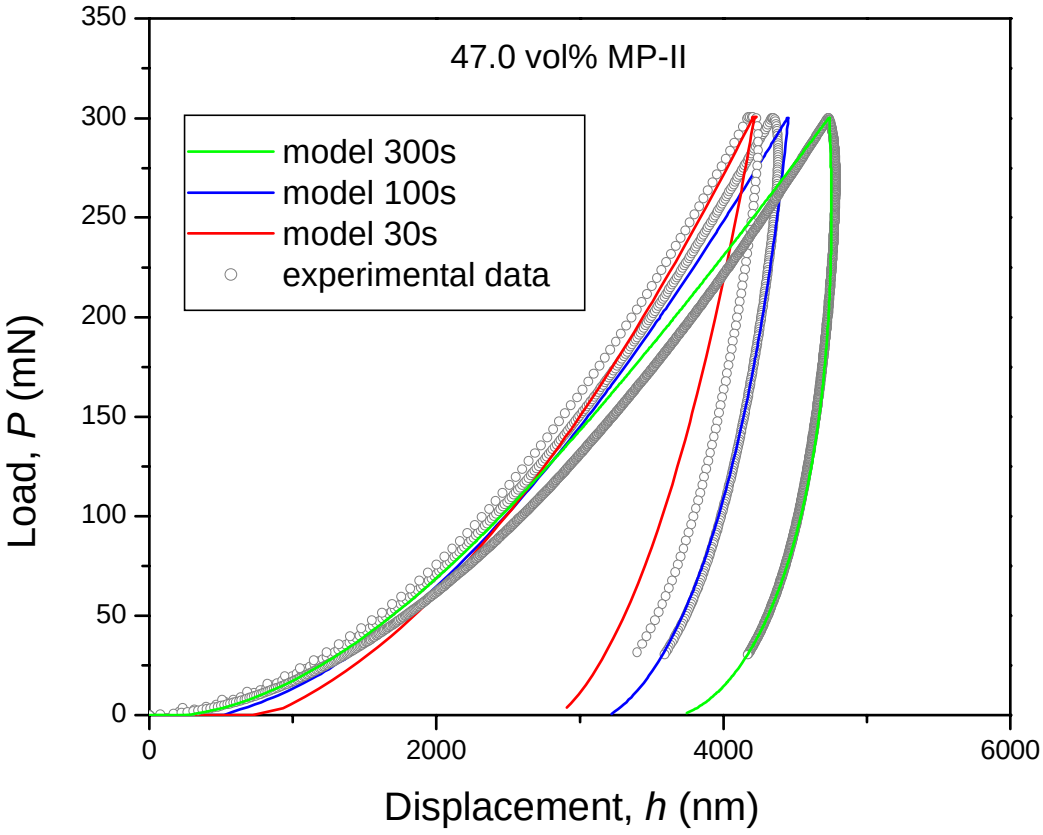

Figure 5.10 Instrumented indentation load (P)-displacement (h) traces for ***MP-II***, displaying the experimental responses (Fig. 5.3 in red line) with grey hollow circles. The solid lines are fits to each response using the VEP model for various observation times, 30, 100 and 300 seconds, in red, blue and green, respectively.

These three exceptional samples all have strong bonding between filler and matrix, as we have addressed in Section 4.4.1. Stronger bonding usually leads to less viscous flow in the sample. In this case, the VEP model does not work as well as for cases where all three components contribute more equally to the overall deformation.

Calculated hardness (true hardness) data are much greater than those obtained from direct tests. In the VEP model, the total irreversible deformation consists of two parts: plastic and viscous deformations. The true hardness from the model is only determined from the plastic deformation by excluding the viscous one. For direct testing, the total irreversible deformation is considered to determine the hardness, which makes the values lower than true hardness from the VEP model. Moreover, besides the influence from time-dependent behavior, the true hardness is different from the conventional hardness, which stems from the definition used to constitute the elements in Equations 5.8 [101]. Even for elastic-plastic materials, the true hardness values (determined using model of Maxwell combination of the elastic and plastic components) are found to be about 3 to 4 times larger than the conventional hardness values. So, the hardness value is not well defined for various types of materials and the physical meaning of hardness is under debate [101, 102].

Besides E and H, the VEP model also gives a way to estimate the relaxation time of the resin composite materials. The relaxation times, τ, are presented in Table 5.1. As expected, the materials with less viscous flow possess greater relaxation time. For pure resin, the τ is determined to be about 156 seconds while the unloading times (15 s,

50 s and 150 s) correspond to about 1/10, 1/3 and 1/1 of the τ. The viscous flow is activated especially for the last two cases. For ***SS-1*** sample, the τ is about 535 seconds, unloading times correspond to about 1/35, 1/10 and 1/3.5 of the τ and hence, viscous flow does not play as dominant a role as for pure resin sample. The τ can also be used to explain why the 30- and 100-second curves of $\{\tilde{P}, \tilde{h}\}$ are closer and there is relatively greater distance between 100- and 300-second curves, in Fig. 5.2 and 5.3. For example, when the observation times are about 1/28 (15 s) and 1/9 (50 s) of τ for ***S-2*** sample in Fig. 5.3 in blue, the unloading time is almost negligible as compared to the relaxation time of this material and hence, the two curves are very close. However, 150 seconds are about 1/3 of the τ, so viscous flow does happen during unloading and leads to more viscous deformation. Therefore, a relatively greater shift to the right is observed.

5.4 Summary

1. The time-dependent response of resin composites has a potential effect on the performance of joining adhesives and cements when they undergo cyclic and long-term loading.
2. The time-dependent response of our resin composites is affected by filler loading and coupling agents. Increasing filler loading and strong bonding between filler and matrix can reduce the viscous flow effectively.
3. The VEP model is based on a combination of three quadratic deformation elements connected in a pseudo-Maxwell series, representing the elastic, plastic, and viscous

elements. The load-displacement trajectories and their components are reasonably well predicted by the model, validating the model for highly crosslinked resin/inorganic filler composites.

4. The VEP model also calculates the values of E, H and τ. The elastic modulus obtained from the VEP matches the values from direct testing very well, which confirms our mechanical testing of nanoindentation. In addition, τ is an important parameter characteristic of the time scale of viscous flow.

CHAPTER 6 CONCLUSION

The fabrication and mechanical testing of the new elastic modulus dental resin nanocomposites are presented. This composite is promising for applications that require high stiffness to limit flexure of brittle ceramic structures. In this thesis, the significance associated with the optimizing the fabrication and properties of all-ceramic crowns, and providing stiff support for crown implanting is discussed. In order to achieve a high elastic modulus resin composite across a small section, high stiffness materials, nano-sized alumina and sub-micron-sized diamond are used as filler materials. Their microstructures are investigated by various methods and mechanical properties with respect to the type, size and loading of the fillers, and chemical additives are explored mainly by nanoindentation. In addition, the time-dependent behaviors of the resin composites are also investigated via analyzing load-displacement trajectories by nanoindentation.

In this dissertation:

i. A new family of high modulus dental composites where the elastic modulus can be tailored by varying the volume fraction of filler and the modulus of the filler is developed. Compared to the silica/resin composites with elastic modulus less than 15 GPa currently used in dentistry, our nanoalumina/resin composites have elastic modulus as high as 31.5 GPa, while our diamond/resin composites have elastic

modulus as high as 45.3 GPa. These composites with higher elastic modulus have the potential to enhance the lifetime of all ceramic crowns when used to adhere them to remaining tooth structures, as well as to allow development of laminar structures when they are used as joining layers.

ii. Nanoindentation is used to characterize the resin composites. Besides obtaining the elastic modulus and hardness on the small area, time-dependent viscous properties are also investigated. It is found for the first time that viscous flow is directly related to surface treatment (coupling agents) of the filler and this can be characterized by nanoindentation. By achieving strong bonding between filler and matrix, viscous flow in the resin composites is greatly reduced due to attenuating the mobility of polymer.

iii. Several models are employed to predict the modulus of our composites that are specifically valuable because of the large modulus mismatch of filler and matrix and high filler loading. The results show that the predicted modulus boundaries given by ROM (Rule of Mixtures) and Hashin-Shtrikman model do not fit our composites very well [24, 25, 79]. An extension of the phenomenological model modified by Chantler et al. gives a reliable prediction for elastic modulus by taking into account the effect of large modulus mismatch between filler and matrix.

iv. We are the first to confirm that the VEP model works well with highly crosslinked, highly filled resin composite systems, which is very valuable to evaluate dental resin composites in the future [93]. The VEP model is based on a combination of three

quadratic deformation elements connected in a pseudo-Maxwell series, representing the elastic, plastic and viscous elements for instrumented indentation tests. We find that it gives reasonable predictions for the load-displacement behaviors and also calculates the E, H, and τ for various resin composites. The calculated E matches the result from direct testing. In addition, τ is an important parameter characteristic of the time scale of viscous flow, which will be valuable for fatigue characterization.

v. From the above discussion we know that the filler loading is the most critical factor related to the elastic modulus of the composites for the same filler. One challenge is to achieve high filler loading with a very viscous system and uniform mechanical properties of a very small area (<50 μm). Our own developed apparatus provides a good means by combining the shear force and vibration. In addition, the surface treatment of the filler is also very important in increasing the filler loading and enhancing compatibility of filler and matrix. Through microstructural characterization, we confirm that the resin composites with uniformly distributed filler and low porosity are achieved using the apparatus. The resin composites have uniform mechanical properties even when observed in a small section down to about 50 μm or even lower, which is critical for our applications.

CHAPTER 7 FUTURE WORK

Current work has been concentrating on the improvement of the performance of layered structures against static mechanical testing of composite joining layers. But, for applications in real crowns, the resin composites are supposed to work in the wet environment subject to millions of times of chewing. Fatigue testing should be the focus in the near future. And in this case, the impact of deformation of resin composites associated with viscous flow on the fracture modes of layer structures can be investigated.

Natural teeth and bone are layered structures. Usually they consist of functional graded layer, like elastic modulus graded layered structures. In natural tooth enamel, the elastic modulus decreases through surface to the dentin junction area. If we go back to have a look at the elastic modulus vs. filler loading curve (Fig. 4.24), it shows us a modulus graded tendency with the control of the filler loading or even by controlling the filler type. If the cement layers are modulus graded structures, they provide a cushion layer for crowns and it might be able to improve the performance of crowns and lengthen their service life.

Higher elastic modulus polymer composite also have some other applications in biomedical fields, like bone cement. Compared to conventional bone cement material, such as polyethylene and PMMA, the bioactive filler reinforced polymer composites are expected to have better mechanical properties and stronger adhesion to bones. Their

static mechanical properties are superior to those resin composites filled with hydroxyapatite powder. Some preliminary work has shown that graded porosity structures of the composites are achievable by salt leaching technique. This is valuable for bone interlock and vascular growth.

APPENDIX

Fig. A.1 shows a simulation in which the parameters are calculated from fitting to 100-second test. As we have stated in Section 5.3.2, they lead to a prediction from the VEP model that is significantly off from experimental data, which proves that the selection of fitting subject is important. Besides the *P-h* simulation, the *E* and *H* also have much greater difference from direct testing (not shown here).

Other figures in this appendix are the simulations from VEP model for various resin composites. Fig. A.2, A.3, A.4 and A.5 show the simulation for sample: ***U-1***, ***S-2***, ***Sil-1*** and diamond/resin composites based on fitting to 300-second test. They all give quite close prediction indicating the effectiveness of the VEP model for all types of composites. The mechanical properties obtained from modeling have been shown in Table 5.1. In addition, it is worth noting that all predictions underestimate the displacements compared to experimental data. The cause is under investigation.

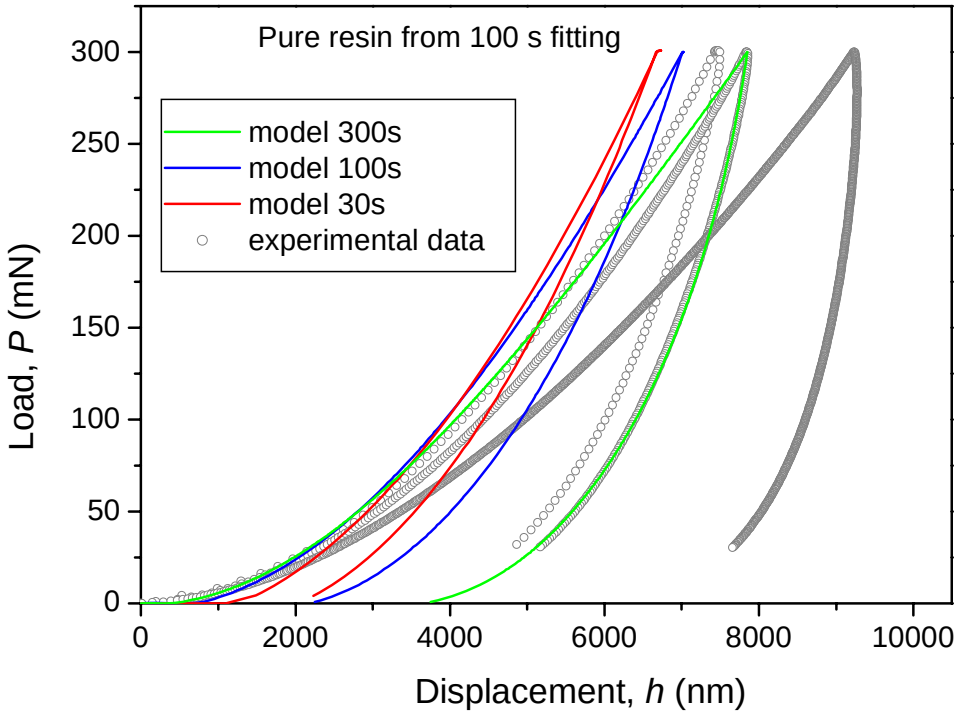

Figure A.1 Instrumented indentation load (P)-displacement (h) traces for pure resin, displaying the experimental responses with grey hollow circles. The solid lines are fits to each response using the VEP model for various observation times, 30, 100 and 300 seconds, in red, blue and green, respectively. Note the parameters are obtained from fitting to a 100-second test.

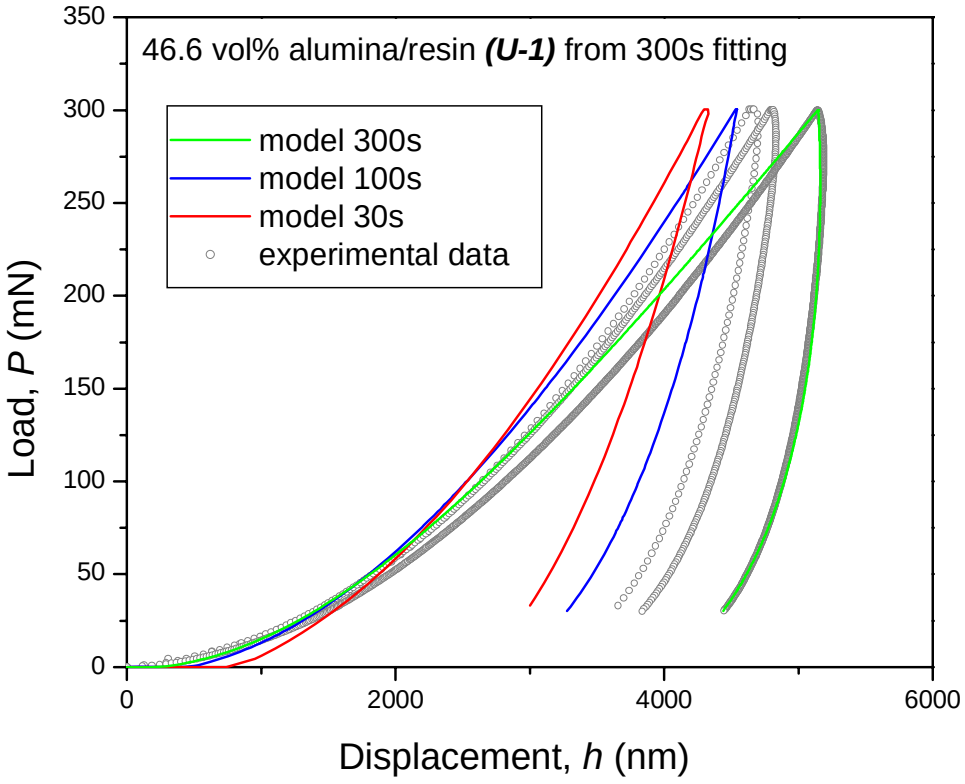

Figure A.2 Instrumented indentation load (P)-displacement (h) traces for ***U-1***, displaying the experimental responses with grey hollow circles. The solid lines are fits to each response using the VEP model for various observation times, 30, 100 and 300 seconds, in red, blue and green, respectively.

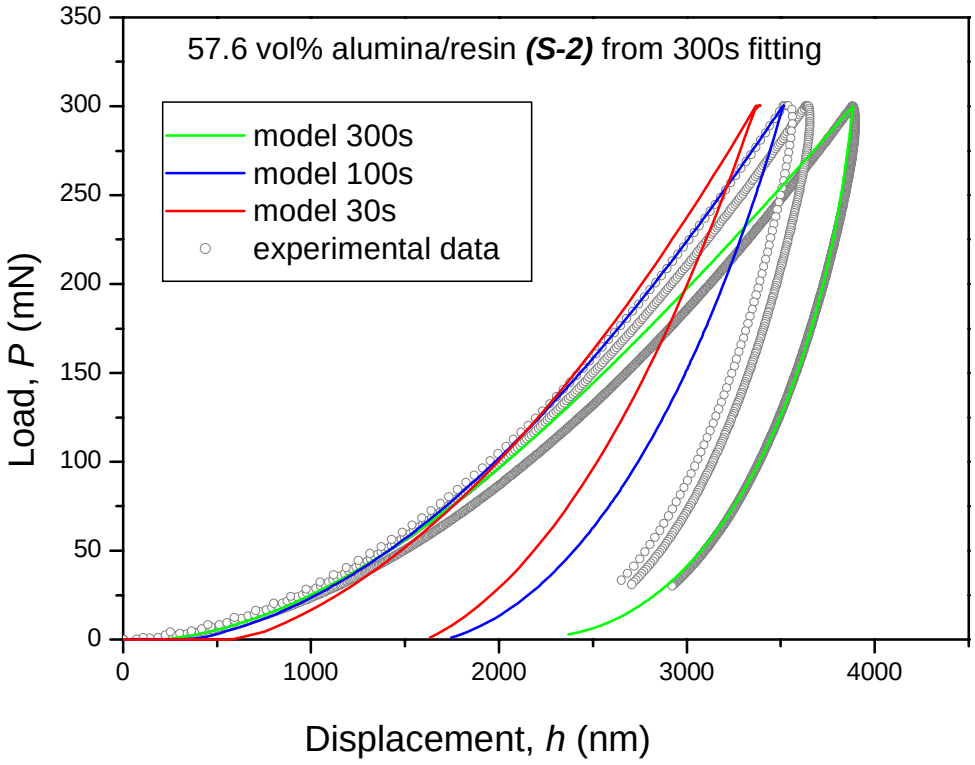

Figure A.3 Instrumented indentation load (P)-displacement (h) traces for ***S-2***, displaying the experimental responses with grey hollow circles. The solid lines are fits to each response using the VEP model for various observation times, 30, 100 and 300 seconds, in red, blue and green, respectively.

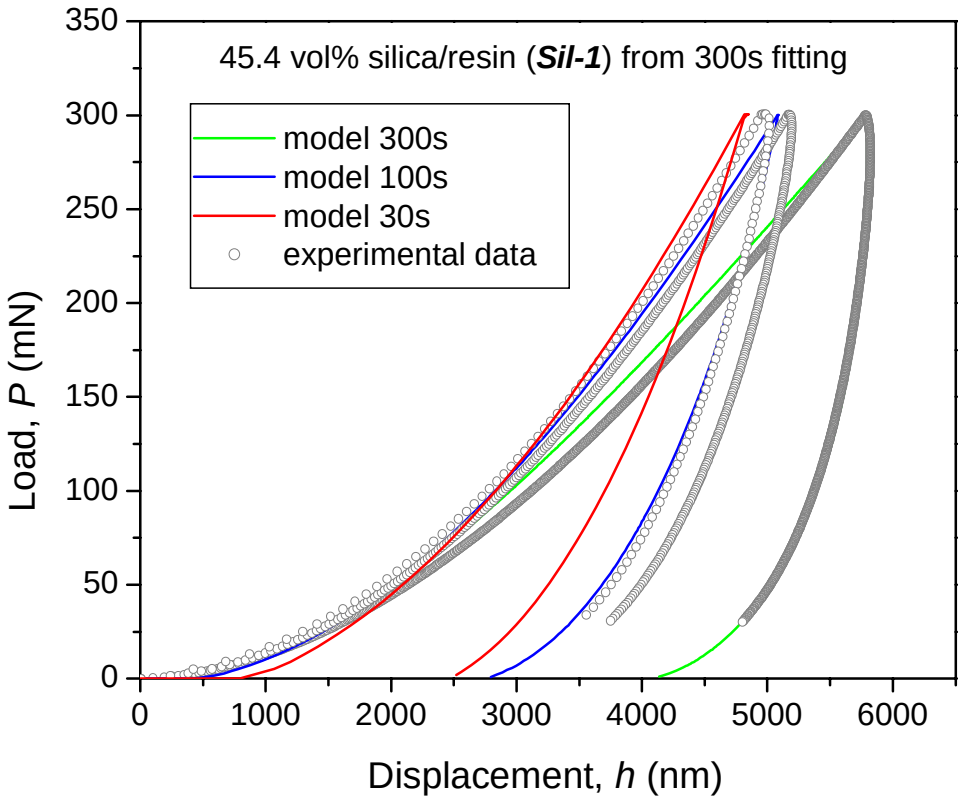

Figure A.4 Instrumented indentation load (P)-displacement (h) traces for ***Sil-1***, displaying the experimental responses with grey hollow circles. The solid lines are fits to each response using the VEP model for various observation times, 30, 100 and 300 seconds, in red, blue and green, respectively.

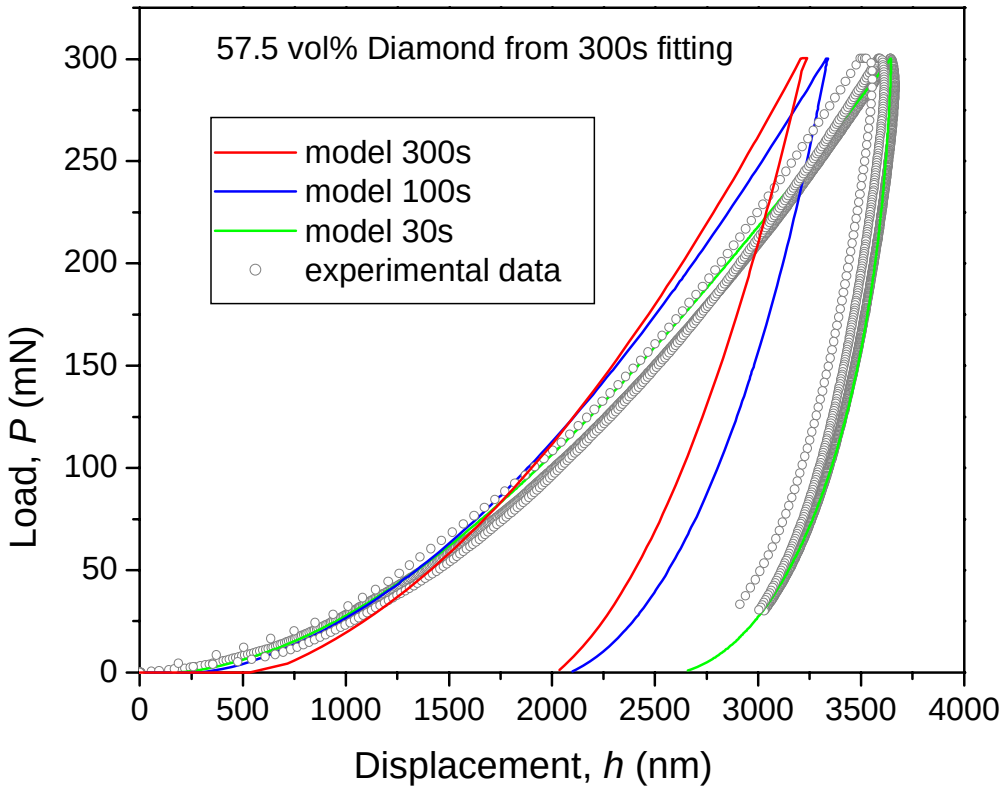

Figure A.5 Instrumented indentation load (P)-displacement (h) traces for diamond/resin composite, displaying the experimental responses with grey hollow circles. The solid lines are fits to each response using the VEP model for various observation times, 30, 100 and 300 seconds, in red, blue and green, respectively.

REFERENCES

[1] D. F. Williams and J. Cunningham, *Materials in Clinical Dentistry*. Oxford, UK: Oxford University, 1979.

[2] S. Ramakrishna, J. Mayer, E. Wintermantel, and K. W. Leong, "Biomedical applications of polymer-composite materials: a review," *Composites Science and Technology*, vol. 61, pp. 1189-1224, 2001.

[3] D. E. Rekow and V. P. Thompson, "Engineering long term clinical success of advanced ceramic prostheses," *Journal of Materials Science-Materials in Medicine*, vol. 18, pp. 47-56, 2007.

[4] D. F. Williams, *Williams Dictionary of Biomaterials*: Liverpool University Press, 1999.

[5] E. Wintermantel and J. Mayer, *Anisotropic biomaterials strategies and developments for bone implants*. Marcel Dekker: New York, 1995.

[6] K. P. Baidya, S. Ramakrishna, A. Ritchie, and M. Rahman, "design and evaluation of composite external fracture fixation device," presented at Proc. ICCM-12, Paris, France.

[7] J. L. Cuy, A. B. Mann, K. J. Livi, M. F. Teaford, and T. P. Weihs, "Nanoindentation mapping of the mechanical properties of human molar tooth enamel," *Archives of Oral Biology*, vol. 47, pp. 281-291, 2002.

[8] B. W. Darvell, *Materials Science for Dentistry*, 2002.

[9] K. Kvam, "Fracture-Toughness Determination of Ceramic and Resin-Based Dental Composites," *Biomaterials*, vol. 13, pp. 101-104, 1992.

[10] N. Tanaka, A. M. Khan, H. Shintani, M. Taira, K. Wakasa, and M. Yamaki, "Dental High-Speed Cutting of Porous-Machinable-Ceramic Resin Composites and Bovine Enamel," *Journal of Materials Science-Materials in Medicine*, vol. 4, pp. 71-75, 1993.

[11] H. H. K. Xu, J. B. Quinn, D. T. Smith, J. M. Antonucci, G. E. Schumacher, and F. C. Eichmiller, "Dental resin composites containing silica-fused whiskers - effects of whisker-to-silica ratio on fracture toughness and indentation properties," *Biomaterials*, vol. 23, pp. 735-742, 2002.

[12] C. P. Turssi, J. L. Ferracane, and L. L. Ferracane, "Wear and fatigue behavior of nano-structured dental resin composites," *Journal of Biomedical Materials Research Part B-Applied Biomaterials*, vol. 78B, pp. 196-203, 2006.

[13] L. G. Hanu, G. P. Simon, and Y. B. Cheng, "Thermal stability and flammability of silicone polymer composites," *Polymer Degradation and Stability*, vol. 91, pp. 1373-1379, 2006.

[14] H. L. Qin, S. M. Zhang, C. G. Zhao, M. Feng, M. S. Yang, Z. J. Shu, and S. S. Yang, "Thermal stability and flammability of polypropylene/montmorillonite composites," *Polymer Degradation and Stability*, vol. 85, pp. 807-813, 2004.

[15] S. Jesse, M. A. Guillorn, I. N. Ivanov, A. A. Puretzky, J. Y. Howe, P. F. Britt, and D. B. Geohegan, "In situ electric-field-induced contrast imaging of electronic

transport pathways in nanotube-polymer composites," *Applied Physics Letters*, vol. 89, pp. -, 2006.

[16] S. Musikhin, L. Bakueva, E. H. Sargent, and A. Shik, "Luminescent properties and electronic structure of conjugated polymer-dielectric nanocrystal composites," *Journal of Applied Physics*, vol. 91, pp. 6679-6683, 2002.

[17] H. Takele, U. Schurmann, H. Greve, D. Paretkar, V. Zaporojtchenko, and F. Faupel, "Controlled growth of Au nanoparticles in co-evaporated metal/polymer composite films and their optical and electrical properties," *European Physical Journal-Applied Physics*, vol. 33, pp. 83-89, 2006.

[18] T. Erb, U. Zhokhavets, G. Gobsch, S. Raleva, B. Stuhn, P. Schilinsky, C. Waldauf, and C. J. Brabec, "Correlation between structural and optical properties of composite polymer/fullerene films for organic solar cells," *Advanced Functional Materials*, vol. 15, pp. 1193-1196, 2005.

[19] M. Sumita, Y. Tsukumo, K. Miyasaka, and K. Ishikawa, "Tensile Yield Stress of Polypropylene Composites Filled with Ultrafine Particles," *Journal of Materials Science*, vol. 18, pp. 1758-1764, 1983.

[20] P. B. Messersmith and E. P. Giannelis, "Synthesis and Characterization of Layered Silicate-Epoxy Nanocomposites," *Chemistry of Materials*, vol. 6, pp. 1719-1725, 1994.

[21] R. L. Bowen, "Use of Epoxy Resins in Restorative Materials," *Journal of Dental Research*, vol. 35, pp. 360-369, 1956.

[22] F. Lutz and R. W. Phillips, "A Classification and Evaluation of Composite Resin Systems," *Journal of Prosthetic Dentistry*, vol. 50, pp. 480-488, 1983.

[23] J. K. Anusavice, *Phillips' Science of Dental Materials*, 11 ed: Saunders, 2003.

[24] A. Reuss and Z. Angew, "Berechnung der fliessgrenze von Mishkristallen auf Grund der Plastizitatsbeding fur Einkristalle," *Math Mech*, vol. 9, pp. 49-58, 1929.

[25] W. Voigt, "Uber Die Bezichungen zwischen den beiden Elastizitaskonstanen iostroper Korper," *Wied Ann*, vol. 38, pp. 573-587, 1889.

[26] S. Shinzato, M. Kobayashi, K. Choju, T. Kokubo, and T. Nakamura, "Bone-bonding behavior of alumina bead composite," *Journal of Biomedical Materials Research*, vol. 46, pp. 287-300, 1999.

[27] M. Kobayashi, S. Shinzato, K. Kawanabe, M. Neo, M. Matsushita, T. Kokubo, T. Kikutani, and T. Nakamura, "Alumina powder/Bis-GMA composite: Effect of filler content on mechanical properties and osteoconductivity," *Journal of Biomedical Materials Research*, vol. 49, pp. 319-327, 2000.

[28] B. J. Ash, R. W. Siegel, and L. S. Schadler, "Glass-transition temperature behavior of alumina/PMMA nanocomposites," *Journal of Polymer Science Part B-Polymer Physics*, vol. 42, pp. 4371-4383, 2004.

[29] P. Somasundaran, T. Y. Chen, and D. Sarkar, "A novel processing scheme for core-shell nano composites using controlled polymer adsorption," *Materials Research Innovations*, vol. 2, pp. 325-327, 1999.

[30] L. T. Drzal, M. J. Rich, M. F. Koenig, and P. F. Lloyd, "Adhesion of Graphite

Fibers to Epoxy Matrices .2. The Effect of Fiber Finish," *Journal of Adhesion*, vol. 16, pp. 133-152, 1983.

[31] W. D. Hergeth, U. J. Steinau, H. J. Bittrich, G. Simon, and K. Schmutzler, "Polymerization in the Presence of Seeds .4. Emulsion Polymers Containing Inorganic Filler Particles," *Polymer*, vol. 30, pp. 254-258, 1989.

[32] A. Oden, M. Andersson, I. Krystek-Ondracek, and D. Magnusson, "Five-year clinical evaluation of Procera AllCeram crowns," *Journal of Prosthetic Dentistry*, vol. 80, pp. 450-456, 1998.

[33] K. A. Malament and S. S. Socransky, "Survival of Dicor glass-ceramic dental restorations over 14 years: Part I. Survival of Dicor complete coverage restorations and effect of internal surface acid etching, tooth position, gender, and age," *Journal of Prosthetic Dentistry*, vol. 81, pp. 23-32, 1999.

[34] F. J. Burke, G. J. Fleming, D. Nathanson, and P. M. Marquis, "Are adhesive technologies needed to support ceramics? An assessment if the current evidence.," *Journal of Adhesive Dentistry*, vol. 4, pp. 7-22, 2002.

[35] B. R. Lawn, A. Pajares, Y. Zhang, Y. Deng, M. A. Polack, I. K. Lloyd, E. D. Rekow, and V. P. Thompson, "Materials design in the performance of all-ceramic crowns," *Biomaterials*, vol. 25, pp. 2885-2892, 2004.

[36] J. J. Lee, Y. J. Wang, I. K. Lloyd, and B. R. Lawn, "Joining Veneers to Ceramic Cores and Dentition with Adhesive Interlayers," *Journal of Dental Research*, vol. In press, 2007.

[37] K. A. Malament and S. S. Socransky, "Survival of Dicor glass-ceramic dental restorations over 14 years. Part II: Effect of thickness of Dicor material and design of tooth preparation," *Journal of Prosthetic Dentistry*, vol. 81, pp. 662-667, 1999.

[38] V. P. Thompson and D. E. Rekow, "Dental ceramics and the molar crown testing ground," *J Appl Oral Sci*, vol. 12, pp. 26-36, 2004.

[39] J. H. Kim, P. Miranda, D. K. Kim, and B. R. Lawn, "Effect of an adhesive interlayer on the fracture of a brittle coating on a supporting substrate," *Journal of Materials Research*, vol. 18, pp. 222-227, 2003.

[40] D. K. Kim, Y. G. Jung, I. M. Peterson, and B. R. Lawn, "Cyclic fatigue of intrinsically brittle ceramics in contact with spheres," *Acta Materialia*, vol. 47, pp. 4711-4725, 1999.

[41] M. Huang, X. Niu, P. Shrotriya, V. Thompson, D. Rekow, and W. O. Soboyejo, "Contact damage of dental multilayers: Viscous deformation and fatigue mechanisms," *Journal of Engineering Materials and Technology-Transactions of the Asme*, vol. 127, pp. 33-39, 2005.

[42] L. Musanje and B. W. Darvell, "Effects of strain rate and temperature on the mechanical properties of resin composites," *Dental Materials*, vol. 20, pp. 750-765, 2004.

[43] R. V. Mesquita, D. Axmann, and A. Geis-Gerstorfer, "Dynamic visco-elastic properties of dental composite resins," *Dental Materials*, vol. 22, pp. 258-267, 2006.

[44] W. R. Krause, S. H. Park, and R. A. Straup, "Mechanical-Properties of Bis-Gma Resin Short Glass-Fiber Composites," *Journal of Biomedical Materials Research*, vol. 23, pp. 1195-1211, 1989.

[45] H. H. K. Xu, "Dental composite resins containing silica-fused ceramic single-crystalline whiskers with various filler levels," *Journal of Dental Research*, vol. 78, pp. 1304-1311, 1999.

[46] H. H. K. Xu, T. A. Martin, J. M. Antonucci, and F. C. Eichmiller, "Ceramic whisker reinforcement of dental resin composites," *Journal of Dental Research*, vol. 78, pp. 706-712, 1999.

[47] H. H. K. Xu, D. T. Smith, G. Schumacher, F. C. Eichmiller, and J. M. Antonucci, "Indentation modulus and hardness of whisker-reinforced heat-cured dental resin composites," *Dental Materials*, vol. 16, pp. 248-254, 2000.

[48] H. K. H. K. Xu, F. C. Eichmiller, D. T. Smith, G. E. Schumacher, A. A. Giuseppetti, and J. M. Antonucci, "Effect of thermal cycling on whisker-reinforced dental resin composites," *Journal of Materials Science-Materials in Medicine*, vol. 13, pp. 875-883, 2002.

[49] R. Rothon, *Particulate-filled Polymer Composites*: Longman Scientific & Technical, 1995.

[50] W. C. Oliver and G. M. Pharr, "An Improved Technique for Determining Hardness and Elastic-Modulus Using Load and Displacement Sensing Indentation Experiments," *Journal of Materials Research*, vol. 7, pp. 1564-1583, 1992.

[51] I. N. Sneddon, "The relation between load and penetration in the axisymmetric boussinesq problem for a punch of arbitrary profile," *International Journal of Engineering Science*, vol. 3, pp. 47-57, 1965.

[52] M. F. Doerner and W. D. Nix, "A method for interpreting the data from depth-sensing indentation instruments," *Journal of Materials Research*, vol. 1, pp. 601-609, 1986.

[53] S. I. Bulychev and V. P. Alekhin, *Zavod. Lab.*, vol. 53, pp. 76, 1987.

[54] S. I. Bulychev, V. P. Alekhin, M. K. Shorshorov, A. P. Ternovskii, and G. D. Shnyrev, *Zavod. Lab.*, vol. 41, pp. 1137, 1975.

[55] M. R. Vanlandingham, J. S. Villarrubia, W. F. Guthrie, and G. F. Meyers, "Nanoindentation of polymers: an overview," *Macromol. Symp.*, vol. 167, pp. 15-43, 2001.

[56] E. Baumgarten, R. Wagner, and C. Lenteswagner, "Quantitative-Determination of Hydroxyl-Groups on Alumina by Ir Spectroscopy," *Fresenius Zeitschrift Fur Analytische Chemie*, vol. 334, pp. 246-251, 1989.

[57] M. Abboud, M. Turner, E. Duguet, and M. Fontanille, "PMMA-based composite materials with reactive ceramic fillers .1. Chemical modification and characterisation of ceramic particles," *Journal of Materials Chemistry*, vol. 7, pp. 1527-1532, 1997.

[58] J. Lee and A. F. Yee, "Inorganic particle toughening I: micro-mechanical deformations in the fracture of glass bead filled epoxies," *Polymer*, vol. 42, pp.

577-588, 2001.

[59] F. Heutling, H. E. Franz, and K. Friedrich, "Microfractographic analysis of delamination growth in fatigue loaded carbon fibre thermosetting matrix composites," *Materialwissenschaft Und Werkstofftechnik*, vol. 29, pp. 239-253, 1998.

[60] B. Wetzel, F. Haupert, and M. Q. Zhang, "Epoxy nanocomposites with high mechanical and tribological performance," *Composites Science and Technology*, vol. 63, pp. 2055-2067, 2003.

[61] T. H. Yoon, Y. K. Lee, B. S. Lim, and C. W. Kim, "Degree of polymerization of resin composites by different light sources," *Journal of Oral Rehabilitation*, vol. 29, pp. 1165-1173, 2002.

[62] S. Imazato, J. F. McCabe, H. Tarumi, A. Ehara, and S. Ebisu, "Degree of conversion of composites measured by DTA and FTIR," *Dental Materials*, vol. 17, pp. 178-183, 2001.

[63] J. L. Keddie, R. A. L. Jones, and R. A. Cory, "Size-Dependent Depression of the Glass-Transition Temperature in Polymer-Films," *Europhysics Letters*, vol. 27, pp. 59-64, 1994.

[64] J. Mattsson, J. A. Forrest, and L. Borjesson, "Quantifying glass transition behavior in ultrathin free-standing polymer films," *Physical Review E*, vol. 62, pp. 5187-5200, 2000.

[65] I. M. Peterson, A. Pajares, B. R. Lawn, V. P. Thompson, and E. D. Rekow,

"Mechanical characterization of dental ceramics by hertzian contacts," *Journal of Dental Research*, vol. 77, pp. 589-602, 1998.

[66] R. W. Wassell, J. F. Mccabe, and A. W. G. Walls, "Subsurface Deformation Associated with Hardness Measurements of Composites," *Dental Materials*, vol. 8, pp. 218-223, 1992.

[67] B. Vanmeerbeek, G. Willems, J. P. Celis, J. R. Roos, M. Braem, P. Lambrechts, and G. Vanherle, "Assessment by Nano-Indentation of the Hardness and Elasticity of the Resin-Dentin Bonding Area," *Journal of Dental Research*, vol. 72, pp. 1434-1442, 1993.

[68] H. H. K. Xu, D. T. Smith, S. Jahanmir, E. Romberg, J. R. Kelly, V. P. Thompson, and E. D. Rekow, "Indentation damage and mechanical properties of human enamel and dentin," *Journal of Dental Research*, vol. 77, pp. 472-480, 1998.

[69] M. Hahn, D. Pleul, M. Nitschke, G. Frens, G. Bundel, S. Prause, and F. Simon, "Plasma modification of diamond surfaces," *Journal of Adhesion Science and Technology*, vol. 19, pp. 1039-1052, 2005.

[70] M. E. J. Dekkers and D. Heikens, "The Effect of Interfacial Adhesion on the Tensile Behavior of Polystyrene Glass-Bead Composites," *Journal of Applied Polymer Science*, vol. 28, pp. 3809-3815, 1983.

[71] B. R. Lawn and V. R. Howes, "Elastic Recovery at Hardness Indentations," *Journal of Materials Science*, vol. 16, pp. 2745-2752, 1981.

[72] V. Lorenzo, J. M. Perena, J. G. Fatou, J. A. Mendezmorales, and J. A. Aznarez,

"Delayed Elastic Recovery of Hardness Indentations in Polyethylene," *Journal of Materials Science*, vol. 23, pp. 3168-3172, 1988.

[73] D. B. Marshall, T. Noma, and A. G. Evans, "A Simple Method for Determining Elastic-Modulus-to-Hardness Ratios Using Knoop Indentation Measurements," *Journal of the American Ceramic Society*, vol. 65, pp. C175-C176, 1982.

[74] S. J. Monte, "Ken React Reference Manual," Bayonne, NJ.

[75] Y. N. Sharma, R. D. Patel, I. H. Dhimmar, and I. S. Bhardwaj, "Studies of the Effect of Titanate Coupling Agent on the Performance of Polypropylene Calcium-Carbonate Composite," *Journal of Applied Polymer Science*, vol. 27, pp. 97-104, 1982.

[76] J. L. Katz, "Modelling the Young's moduli of dental composites," *Journal of Materials Science Letters*, vol. 7, pp. 133-134, 1988.

[77] Z. Hashin and S. Shtrikman, "Note on a Variational Approach to the Theory of Composite Elastic Materials," *Journal of the Franklin Institute-Engineering and Applied Mathematics*, vol. 271, pp. 336-&, 1961.

[78] R. L. Sakaguchi, B. D. Wiltbank, and C. F. Murchison, "Prediction of composite elastic modulus and polymerization shrinkage by computational micromechanics," *Dental Materials*, vol. 20, pp. 397-401, 2004.

[79] N. D. Cristescu, E.-M. Cracuim, and C. D. Cristescu, *Mechanics of Elastic Composites*: Chapman & Hall/CRC, 2003.

[80] M. B. Bush, "An Investigation of 2-Dimensional and 3-Dimensional Models for

Predicting the Elastic Properties of Particulate-Reinforced and Whisker-Reinforced Composite-Materials," *Materials Science and Engineering a-Structural Materials Properties Microstructure and Processing*, vol. 154, pp. 139-148, 1992.

[81] M. Braem, V. E. Vandoren, P. Lambrechts, and G. Vanherle, "Determination of Young Modulus of Dental Composites - a Phenomenological Model," *Journal of Materials Science*, vol. 22, pp. 2037-2042, 1987.

[82] P. M. Chantler, X. Hu, and N. M. Boyd, "An extension of a phenomenological model for dental composites," *Dental Materials*, vol. 15, pp. 144-149, 1999.

[83] X. Z. Hu and B. R. Lawn, "A simple indentation stress-strain relation for contacts with spheres on bilayer structures," *Thin Solid Films*, vol. 322, pp. 225-232, 1998.

[84] D. W. Jones and A. S. Rizkalla, "Characterization of experimental composite biomaterials," *Journal of Biomedical Materials Research*, vol. 33, pp. 89-100, 1996.

[85] W. T. Nakayama, D. R. Hall, D. E. Grenoble, and J. L. Katz, "Elastic Properties of Dental Resin Restorative Materials," *Journal of Dental Research*, vol. 53, pp. 1121-1126, 1974.

[86] J. Sabbagh, J. Vreven, and G. Leloup, "Dynamic and static moduli of elasticity of resin-based materials," *Dental Materials*, vol. 18, pp. 64-71, 2002.

[87] C. Klapperich, K. Komvopoulos, and L. Pruitt, "Nanomechanical properties of polymers determined from nanoindentation experiments," *Journal of Tribology-Transactions of the Asme*, vol. 123, pp. 624-631, 2001.

[88] H. Lu, B. Wang, J. Ma, G. Huang, and H. Viswanathan, "Measurement of creep compliance of solid polymers by nanoindentation," *Mechanics of Time-Dependent Materials*, vol. 7, pp. 189-207, 2003.

[89] M. Nowicki, A. Richter, B. Wolf, and H. Kaczmarek, "Nanoscale mechanical properties of polymers irradiated by UV," *Polymer*, vol. 44, pp. 6599-6606, 2003.

[90] G. M. Odegard, T. Gates, and H. M. Herring, "Characterization of viscoelastic properties of polymeric materials through nanoindentation," *Experimental Mechanics*, vol. 45, pp. 130-136, 2005.

[91] K. Park, S. Mishra, G. Lewis, J. Losby, Z. F. Fan, and J. B. Park, "Quasi-static and dynamic nanoindentation studies on highly crosslinked ultra-high-molecular-weight polyethylene," *Biomaterials*, vol. 25, pp. 2427-2436, 2004.

[92] L. Cheng, X. Xia, W. Yu, L. E. Scriven, and W. W. Gerberich, "Flat-punch indentation of viscoelastic material," *Journal of Polymer Science Part B-Polymer Physics*, vol. 38, pp. 10-22, 2000.

[93] R. F. Cook and M. L. Oyen, "Nanoindentation behavior and mechanical properties measurement of polymeric materials," *International Journal of Materials Research*, vol. In press, 2007.

[94] M. L. Oyen and R. F. Cook, "Load-displacement behavior during sharp indentation of viscous-elastic-plastic materials," *Journal of Materials Research*, vol. 18, pp. 139-150, 2003.

[95] M. L. Oyen, R. F. Cook, J. A. Emerson, and N. R. Moody, "Indentation responses of time-dependent films on stiff substrates (vol 19, pg 2487, 2004)," *Journal of Materials Research*, vol. 19, pp. 3120-3121, 2004.

[96] M. L. Oyen, "Analytical techniques for indentation of viscoelastic materials," *Philosophical Magazine*, vol. 86, pp. 5625-5641, 2006.

[97] B. J. Briscoe, L. Fiori, and E. Pelillo, "Nano-indentation of polymeric surfaces," *Journal of Physics D-Applied Physics*, vol. 31, pp. 2395-2405, 1998.

[98] B. Tang and A. H. W. Ngan, "Accurate measurement of tip-sample contact size during nanoindentation of viscoelastic materials," *Journal of Materials Research*, vol. 18, pp. 1141-1148, 2003.

[99] W. N. Findley, J. S. Lai, and K. Onaran, *Creep and Relaxation of Nonlinear Viscoelastic materials*. New York: Dover Publications, 1989.

[100] J. J. Vlassak and W. D. Nix, "Indentation Modulus of Elastically Anisotropic Half-Spaces," *Philosophical Magazine a-Physics of Condensed Matter Structure Defects and Mechanical Properties*, vol. 67, pp. 1045-1056, 1993.

[101] F. Mammeri, E. Le Bourhis, L. Rozes, C. Sanchez, A. Huignard, and D. Lefevre, "Time, dependence of the indentation behavior of hybrid coatings," *Journal of Non-Crystalline Solids*, vol. 345-46, pp. 610-614, 2004.

[102] M. Sakai, "The Meyer hardness: A measure for plasticity?," *Journal of Materials Research*, vol. 14, pp. 3630-3639, 1999.

CURRICULUM VITAE

YIJUN WANG

EDUCATION

2002—2007	University of Maryland, College Park, MD, USA
Ph.D.	Materials Science and Engineering
1999—2002	Nanjing University, Nanjing, China
M.S.	Materials Science and Engineering
1995—1999	Nanjing University, Nanjing, China
B.S..	Materials Science and Engineering

PUBLICATIONS

1 **Yijun Wang**, James J. Lee, Isabel K. Lloyd, Otto C. Wilson Jr., Marc. Rosenblum and Van Thompson. High Modulus Nanopowder Reinforced Dimethacrylate Matrix Composites, J. of Biomed. Res. Part A. (2006) 10.1002/jbm.a.31029

2 James Lee, **Yijun Wang**, Isabel K Lloyd, Brian Lawn. Joining Veneers to Ceramic Cores and Dentition with Adhesive Interlayers. J. of Dental Res. 86(2007) 745-748

3 **Yijun Wang**, Ai-Dong Li, Di Wu, Hui-Qing Ling, Nai-Ben Ming. Electrical Properties of $Bi_{3.25}La_{0.75}Ti_3O_{12}/LaAlO_3/Si$ Structures for Ferroelectric Field Effect Transistor Applications. J. Phys. D: Appl. Phys. 37 (2004) 832–835.

4 X.S.Wang, **Yijun Wang**, J.Yin and Z.G.Liu. Enhanced Ferroelectric Properties of $Pb(Zr_{0.52}Ti_{0.48})O_3$ films on $Pt/TiO_2/SiO_2/Si(001)$ using ZnO Buffer Layer. Scripta materialia. 46 (2002) 783-788

5 D. Li, Q. Y. Shao, **Yijun Wang**, C.L. Mak, K. H. Wong, D. Wu, and Naiben Ming, Epitaxial Growth of $(PbZr)TiO_3$ Films on $LaAlO_3$ by Sol-gel Method using Inorganic Zirconium Source. B. Mater. Res. Bull.(2001)

6 Yue-feng Tang, Ai-dong Li, **Yijun Wang**, Qi-yue Shao, Yi-nong Lu, Zhi-da Ling. Fabrication of Ultrafine Mullite Powders. Mater. Chem. and Phys. 87 (2002) 301-304.

7 Qiyue Shao, Aidong Li, Huiqin Ling, Di wu, **Yijun Wang**, Naiben Ming. Growth and Ferroelectric Properties of Sol-gel Derived $Pb(Zr,Ti)O_3$ using Inorganic Zirconium Precursor. Materials letters 50(2001) 32-35

8 Yue-feng Tang, Zhi-da Ling, Yi-nong Lu, Ai-dong Li, Hui-qin Ling, **Yijun Wang**, Qi-yue Shao. Preparation of Composite Coating Particles of a-Al_2O_3-SiO_2 by the Heterogeneous Nucleation-and-growth Processing. Mater. Lett., 56 (2002) 446-449.

9 Yue-feng Tang, Zhi-da Ling, Yi-nong Lu, Ai-dong Li, Hui-qin Ling, **Yijun Wang**, Qi-yue Shao. Study on Densification of Composite Coating Particles of a-Al_2O_3-SiO_2. Mater. Chem. and Phys. 75 (2001) 265-269.

CONFERENCE PRESENTATIONS

1 "Layered Structures Joined with Novel Resin Composite", 35th AADR/IADR International Association for Dental Research & American Association for Dental Research, Orlando, FL, March 8, 2006

2 "Processing of Dental Composites with a High Modulus using Nanosized Alumina Oxide" 107th American Ceramic Society Annual Meeting & Exposition, Bioceramics session, Baltimore, Maryland, April 12, 2005

3 "High Modulus Nanocomposites", MS&T Materials Science and Technology 2005 Annual Meeting & Exhibition, Session: Nanocomposites, Pittsburgh, PA, September 27, 2005

4 "High Elastic Modulus Dental Composites", 83rd IADR/AADR/CADR, Baltimore, Maryland, March 9, 2005

5 "Ambient and Thermal Approaches to Joining Laminar Dental Restoration Materials", 106th American Ceramic Society Annual Meeting & Exposition, the Bioceramics symposium, Indianapolis, Illinois, April 19, 2004

6 "Progress on Glassy Joins for Laminar Dental All-Ceramic Restorations", 35th AADR/IADR International Association for Dental Research & American Association for Dental Research, Orlando, FL, March 8, 2006

PROFESSIONAL AFFILIATION

- Materials Research Society
- The International and American Associations for Dental Research
- The American Ceramic Society